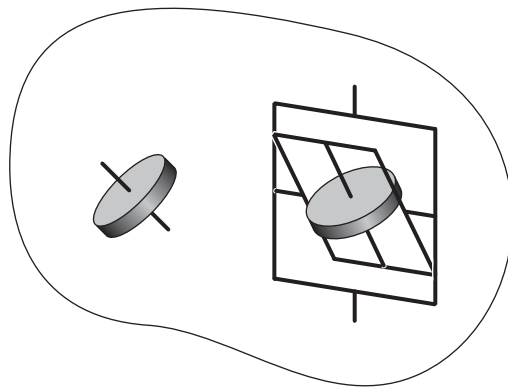


# Dynamics and Control of Attitude, Power, and Momentum for a Spacecraft Using Flywheels and Control Moment Gyroscopes

*Carlos M. Roithmayr  
Langley Research Center, Hampton, Virginia*

*Christopher D. Karlgaard, Renjith R. Kumar, Hans Seywald, and David M. Bose  
Analytical Mechanics Associates, Inc., Hampton, Virginia*



## The NASA STI Program Office ... in Profile

Since its founding, NASA has been dedicated to the advancement of aeronautics and space science. The NASA Scientific and Technical Information (STI) Program Office plays a key part in helping NASA maintain this important role.

The NASA STI Program Office is operated by Langley Research Center, the lead center for NASA's scientific and technical information. The NASA STI Program Office provides access to the NASA STI Database, the largest collection of aeronautical and space science STI in the world. The Program Office is also NASA's institutional mechanism for disseminating the results of its research and development activities. These results are published by NASA in the NASA STI Report Series, which includes the following report types:

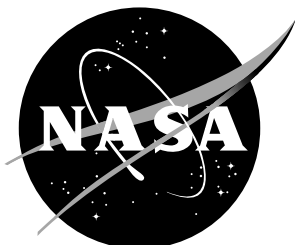
- **TECHNICAL PUBLICATION.** Reports of completed research or a major significant phase of research that present the results of NASA programs and include extensive data or theoretical analysis. Includes compilations of significant scientific and technical data and information deemed to be of continuing reference value. NASA counterpart and peer-reviewed formal professional papers, but having less stringent limitations on manuscript length and extent of graphic presentations.
- **TECHNICAL MEMORANDUM.** Scientific and technical findings that are preliminary or of specialized interest, e.g., quick release reports, working papers, and bibliographies that contain minimal annotation. Does not contain extensive analysis.
- **CONTRACTOR REPORT.** Scientific and technical findings by NASA-sponsored contractors and grantees.
- **CONFERENCE PUBLICATION.** Collected papers from scientific and technical conferences, symposia, seminars, or other meetings sponsored or co-sponsored by NASA.
- **SPECIAL PUBLICATION.** Scientific, technical, or historical information from NASA programs, projects, and missions, often concerned with subjects having substantial public interest.
- **TECHNICAL TRANSLATION.** English-language translations of foreign scientific and technical material pertinent to NASA's mission.

Specialized services that complement the STI Program Office's diverse offerings include creating custom thesauri, building customized databases, organizing and publishing research results... even providing videos.

For more information about the NASA STI Program Office, see the following:

- Access the NASA STI Program Home Page at <http://www.sti.nasa.gov>
- E-mail your question via the Internet to [help@sti.nasa.gov](mailto:help@sti.nasa.gov)
- Fax your question to the NASA STI Help Desk at (301) 621-0134
- Phone the NASA STI Help Desk at (301) 621-0390
- Write to:  
NASA STI Help Desk  
NASA Center for Aerospace Information  
7121 Standard Drive  
Hanover, MD 21076-1320

NASA/TP-2003-212178



# Dynamics and Control of Attitude, Power, and Momentum for a Spacecraft Using Flywheels and Control Moment Gyroscopes

*Carlos M. Roithmayr  
Langley Research Center, Hampton, Virginia*

*Christopher D. Karlgaard, Renjith R. Kumar, Hans Seywald, and David M. Bose  
Analytical Mechanics Associates, Inc., Hampton, Virginia*

National Aeronautics and  
Space Administration

Langley Research Center  
Hampton, Virginia 23681-2199

---

April 2003

## Acknowledgment

The research described herein was conducted as part of the Langley Research Center Creativity and Innovation initiative, and the authors are sincerely appreciative of all the support we received. The first author is especially grateful to the management of the Aerospace Systems Concepts and Analysis Competency, and the Spacecraft and Sensors Branch for their encouragement. Special thanks are due to Anne Costa for creating the illustrations that appear on the cover and in Chapter 2.

Cover art depicts a spacecraft containing a typical flywheel and double-gimbal control moment gyroscope.

---

Available from:

NASA Center for AeroSpace Information (CASI)  
7121 Standard Drive  
Hanover, MD 21076-1320  
(301) 621-0390

National Technical Information Service (NTIS)  
5285 Port Royal Road  
Springfield, VA 22161-2171  
(703) 605-6000

# Contents

<b>1</b>	<b>Introduction</b>	<b>1</b>
1.1	International Space Station Flywheels . . . . .	2
1.2	Existing Control Laws . . . . .	2
1.3	Overview . . . . .	3
<b>2</b>	<b>Equations of Motion for Spacecraft with Flywheels and CMGs</b>	<b>5</b>
2.1	Derivation of Dynamical Equations . . . . .	5
2.1.1	Generalized Speeds . . . . .	6
2.1.2	Generalized Active Forces . . . . .	7
2.1.3	Generalized Inertia Forces . . . . .	8
2.1.4	General Vector-Dyadic Equations . . . . .	11
2.2	Dynamical Equations for A Complex Gyrostat . . . . .	12
2.3	Dynamical Equations for Spacecraft with CMGs . . . . .	18
2.4	Approximate Equations for a Spacecraft with Flywheels and CMGs . . . . .	21
2.5	Linearized Equations for Control Law Design . . . . .	23
2.6	Nondimensional Equations for Control Law Design . . . . .	24
2.7	Nonlinear Equations used in Simulations . . . . .	27
<b>3</b>	<b>Flywheel Steering Laws</b>	<b>29</b>
<b>4</b>	<b>Linear Controllers</b>	<b>33</b>
4.1	Weighting . . . . .	33
4.2	Simulation Parameters . . . . .	35
4.3	Energy Feedback . . . . .	35
4.4	Control System Block Diagram . . . . .	36
4.5	TEA Seeking . . . . .	37
4.5.1	Undamped Flywheel Rotors . . . . .	39
4.5.2	Damped Flywheel Rotors . . . . .	43
4.5.3	Counteracting Damping with Kinetic Energy Error Feedback . . . . .	46
4.5.4	Comparison of Steering Laws . . . . .	48
4.6	Attitude Hold . . . . .	50
4.6.1	Attitude Hold without Momentum Management . . . . .	50
4.6.2	Attitude Hold with Flywheel Momentum Management . . . . .	55
4.6.3	Attitude Hold with Thrusters . . . . .	58
4.6.4	Fuel Savings for Attitude-Hold Command . . . . .	60

<b>5</b>	<b>Nonlinear Controllers</b>	<b>65</b>
5.1	Global Asymptotically Stable Reorientation . . . . .	65
5.2	Large-Angle Reorientation with CMGs . . . . .	68
5.3	Large-Angle Reorientation with CMGs and Flywheels . . . . .	71
5.4	Large-Angle Reorientation with CMGs, Flywheels, and Flywheel Momentum Feedback	71
<b>6</b>	<b>Summary of Results</b>	<b>76</b>
	<b>References</b>	<b>78</b>

# Chapter 1

## Introduction

Flywheels offer great promise for reducing the mass and extending the life of spacecraft; they store more energy per unit of mass and last significantly longer than chemical batteries. Moreover, flywheels can simultaneously store energy and exert torque on a spacecraft, making it possible for one system of flywheels to replace two separate systems typically used for energy storage and attitude control. When the mass of the two conventional systems is taken into account, the specific energy of flywheel systems is expected to be 5 to 10 times greater, according to Ref. [1]. The attitude control system typically represents 11% of the mass of a spacecraft, and batteries make up 6% of the mass; replacing 17% of a spacecraft's mass with a flywheel system whose mass is 1.7% would lead to a 15% reduction in total spacecraft mass. Secondary benefits occur as well; since flywheels have higher system level efficiencies than batteries, a reduction in solar array size and mass becomes possible, and reboost propellant can be reduced because the smaller arrays produce less drag. Flywheel systems are expected to last 15 years (Ref. [1]) or more whereas typical batteries last only 5 years. The greatest advantage of flywheels over batteries accrues in low earth orbit where eclipse happens more frequently and for larger fractions of an orbit than in higher orbits; repeated charge and discharge cycles, and high depth of discharge significantly degrade batteries over time.

Flywheel energy storage technology can be employed in the transportation, utility, and manufacturing industries; potential NASA applications include spacecraft, launch vehicles, aircraft power systems, uninterruptable power supplies, and planetary rovers. Flywheels are recognized as a critical space technology in NASA's recent Advanced Cross-Enterprise Technology Development research announcement, Ref. [2], which called for "high-risk, high-payoff technology advances." The Advanced Power and On-Board Propulsion section of the announcement requested proposals for "energy storage . . . techniques that dramatically reduce spacecraft bus mass, volume, and cost"; specifically, "flywheel energy storage system component improvements . . . that enhance their . . . integration with spacecraft attitude control functions." To date, flywheel energy storage devices have not yet been flown onboard an actual spacecraft.

The Agency's interest in flywheel technology spans several decades, including two workshops devoted to flywheels in 1983 and 1984, two workshops dealing with magnetic suspension held at Langley Research Center (LaRC) in 1988 and 1990, and flywheel workshops in 1997, 1998, 1999, 2000, and 2002 co-sponsored by Glenn Research Center (GRC), where an active development program exists. Under contracts administered by LaRC, Integrated Power and Attitude Control Systems (IPACS) were evaluated in the mid 1970's as reported in Ref. [3], and considered for the Space Station in the mid 1980's as summarized in Ref. [4].

## 1.1 International Space Station Flywheels

For several years the International Space Station (ISS) Payloads Office funded a program at GRC to develop flywheel energy storage technology. The project would have added significantly to the capacity for energy storage onboard the Station, and reduced or eliminated the cost and time required to replace chemical batteries.

Each device in the ISS Flywheel Energy Storage System (FESS) was to consist of two counter-rotating rotors placed in vacuum housings, and levitated with magnetic bearings. Motor-generators would connect the rotors to the existing electrical power system so that they could store energy when available from the photovoltaic arrays, and supply energy when needed. Each rotor, made up of a metallic hub and a rim of composite material, would spin at angular speeds ranging between 18,000 and 60,000 rev/min. The FESS could have been made up of as many as 48 flywheel pairs, replacing all of the batteries on the Assembly Complete configuration of ISS. Unfortunately, plans called for FESS to be used only for energy storage, not for attitude control.

The attitude of ISS is controlled with 4 Control Moment Gyroscopes (CMGs), together with a Reaction Control System (RCS). The CMGs were activated following installation of the laboratory module Destiny in February, 2001, and 1 CMG experienced a bearing failure in June, 2002, after less than 16% of the expected  $8\frac{1}{2}$  year performance life. CMGs are able to control attitude without requiring expenditure of RCS propellant most of the time; however, in certain situations such as Orbiter rendezvous and docking, the CMGs will become saturated. Desaturation with the RCS consumes propellant, which must then be resupplied from Earth at a cost of \$10,000 to \$20,000 per pound.

Forty-eight pairs of FESS flywheels would have possessed a total useable angular momentum (Ref. [5]) of approximately 120,000 N-m-s; only 50% to 75% of this figure would have been required for energy storage, leaving 30,250 to 60,500 N-m-s available for attitude control, or 1.5 to 3 times the amount available from the current set of 4 CMGs. The FESS, or a similar system, could thus provide a backup system for momentum exchange that could serve even in the event of failure of all CMGs. Used to assist the CMGs, a flywheel system could allow attitude maneuvers that are faster or of larger excursions than would be possible with the CMGs alone, and better accommodation of activities that require CMG momentum, such as Remote Manipulator System operations with large payloads, centrifuge spin-up and spin-down, and the Alpha Magnetic Spectrometer experiment with its strong permanent magnets. Steady-state attitude motion could be reduced, thus improving the quasi-steady microgravity environment. It may even be possible to reduce or eliminate expenditure of propellant required occasionally to desaturate the CMGs.

## 1.2 Existing Control Laws

A numerical investigation of the merits of using the FESS to assist the CMGs requires a feedback control law designed for CMGs and flywheels used together as an integrated set of effectors. The current CMG control law was originally developed by Wie et al. in Ref. [6] and refined by Harduvel as described in Ref. [7]; it minimizes a cost function involving spacecraft attitude and angular speed, and CMG angular momentum. A CMG steering law, such as the one developed by Kennel in Ref. [8], determines the speeds of the two gimbals (in which each constant speed CMG rotor is mounted) needed to produce the torque requested by the control law. As a natural extension of the present approach, we seek a new control law derived from a cost function that includes flywheel angular momentum in addition to the aforementioned quantities. Also needed is a “flywheel steering law,” a counterpart to the CMG steering law that will determine the motor-generator torque to be

applied to each member of a flywheel pair such that rotational kinetic energy is stored or discharged in the required manner, and the net torque requested by the control law is produced simultaneously.

A review of the literature does not reveal any existing three-axis control laws for earth-pointing spacecraft using flywheels and CMGs together, or even flywheels alone, where attitude control, momentum management, and power management are addressed in a unified way. As mentioned earlier, the current ISS attitude control system is designed only for use of CMGs (and CMG desaturation with RCS); no provisions exist for using flywheels or other momentum exchange devices. In Ref. [3], Notti, Cormack, and Klein give a sketch of a control law and an energy distribution law; however, this work is not applicable primarily because each flywheel rotor is assumed to be supported by two gimbals and the ISS FESS did not contain any gimbals. In addition, the control law lacks flywheel angular momentum as a feedback parameter. Recent work on control laws for integrated power and attitude control systems deals either with sets of four or more flywheels whose spin axes are non-collinear (Refs. [9]–[11]), or with sets of variable-speed, single-gimbal control moment gyroscopes (Refs. [12]–[14]); neither of these types of configurations are directly applicable to the counter-rotating flywheel pair arrangement of the FESS. Varatharajoo and Fasoulas develop control laws in Ref. [15] for a spacecraft using a counter-rotating flywheel configuration; however, they only consider a pitch-axis controller.

Hall’s control law, proposed in Ref. [9], is an open-loop scheme (rather than a feedback law) for performing large-angle attitude maneuvers. It does not account for gravitational and aerodynamic torques which have a significant effect on the motion of ISS, and therefore can not be used for maintaining torque equilibrium attitude, the primary job of the CMGs. Hall introduces a flywheel steering law based on a matrix pseudo-inverse; it is applied in each of Refs. [10]–[14]. Tsiotras, Shen, and Hall employ Lyapunov stability theory in Ref. [10] to develop a feedback control law which performs well in simulations involving disturbance torques; however, flywheel momentum is managed by expenditure of propellant. Costic et al. develop in Ref. [11] a nonlinear controller which includes an adaptive scheme for estimating the mass distribution of the spacecraft, but they do not address momentum management.

In Ref. [12], Fausz and Richie extend the work of Hall to a nonlinear feedback controller applicable to a set of variable-speed, single-gimbal control moment gyroscopes. Together with Tsiotras, they continue their discussion in Ref. [13] and present simulation results, but momentum management is not addressed in either of the two papers. Yoon and Tsiotras develop an adaptive nonlinear control law in Ref. [14], and incorporate wheel-speed equalization to reduce the possibility of singularities and keep the wheel speeds within acceptable limits. Numerical simulation results show that attitude and power profiles can be tracked even when the spacecraft inertia properties are unknown. Of all the papers mentioned heretofore, Ref. [14] is the only one in which attitude control, momentum management, and power management for flywheels is considered in an integrated fashion.

It is important to note that Refs. [9]–[15] fail to take into account damping torque exerted by the spacecraft and a flywheel rotor on each other; in practice, this will cause the actual rotational kinetic energy possessed by the flywheels to differ from the required amount. None of these works include any feedback of errors in flywheel power or kinetic energy, something which must be done under realistic conditions.

### 1.3 Overview

As a prerequisite for the design of laws for controlling attitude and managing angular momentum of flywheels and CMGs, one must have in hand equations of motion for a spacecraft containing

these devices. In Chapter 2 of the material that follows, a complete, nonlinear set of equations of motion for such a system is derived in vector-dyadic form, and subsequently compared to some others existing in the literature. Two configurations of special interest are then examined. In the absence of CMGs, the system forms a complex gyrostap; scalar equations of motion are given for the case of three orthogonally mounted pairs of flywheels where the spin axes of the members of each pair are parallel. Another special case occurs when flywheels are absent; under certain assumptions, the equations are shown to correspond to those used by Wie et al. in Ref. [6] for a spacecraft with CMGs. These assumptions made in connection with the CMGs are then applied to the full system, resulting in approximate equations which are subsequently linearized about an Earth-pointing motion, and nondimensionalized for use in control law design.

Two flywheel “steering laws” are developed in Chapter 3 such that torque commanded by an attitude control law is achieved while energy is stored or discharged at the required rate. The first law is based upon a suggestion by Hall in Ref. [9]. It requires the formation of a matrix pseudo-inverse; the total power requirement is provided by the entire flywheel system, with no assumptions regarding the distribution of the requirement among the three flywheel pairs. The second steering law follows from the assumption that the power requirement is divided evenly among the three flywheel pairs, and does not require construction of a pseudo-inverse.

In Chapter 4 designs are given for control laws, obtained with the Linear Quadratic Regulator technique, that allow CMGs and flywheels to be used as an integrated set of effectors for maintaining torque equilibrium attitude and managing momentum, or for holding a specified attitude until momentum saturation occurs. The control algorithms compensate for damping torque, exerted by the flywheel bearings, through feedback of error in rotational kinetic energy, that is, the difference between actual energy of the flywheels and the energy they should have based on the required power. In numerical simulations of nonlinear motion, several variations of the linear control laws are seen to perform well in achieving torque equilibrium attitude when initial conditions of the spacecraft differ from the steady-state conditions, and the spacecraft is subject to gravity-gradient torque together with a prescribed time history of aerodynamic torque. Angular momentum of flywheels and CMGs is minimized, flywheels store or discharge energy as commanded, and flywheel angular speeds are kept within appropriate limits.

Instead of continuously varying the spacecraft attitude to manage angular momentum, the controllers can be requested to keep the spacecraft in a specified orientation until the angular momentum capacity of the actuators is exceeded, at which time thrusters can be used for the remainder of the operation. Hence, the controllers designed for momentum exchange devices have been supplemented with a minimum-fuel jet selection scheme that enables thrusters to provide the required torque. Flywheels can be used to aid the CMGs in holding attitude, resulting in a delay for the time of CMG momentum saturation and onset of thruster firings, and thus in a reduction of the propellant expended. Simulation results indicate a certain amount of propellant can be saved during operations leading up to docking between ISS and another spacecraft.

Nonlinear control algorithms for performing large-angle reorientations or slew maneuvers are presented in Chapter 5. These control algorithms are based on feedback linearization and Lyapunov stability theory, and they take into account constraints such as slew rate limits and maximum control torques. Good performance is observed in simulations; however, the momentum capacity of ISS CMGs, together with the expected capacity of ISS flywheels, would be insufficient to perform most Space Station maneuvers without expending propellant.

Chapter 6 concludes the report with a summary of the results, as well as some suggestions for future research.

## Chapter 2

# Equations of Motion for Spacecraft with Flywheels and CMGs

One must have in hand equations governing the motion of a spacecraft possessing flywheels and CMGs if laws for controlling the motion are to be crafted, and subsequently exercised in numerical simulations. Kane's method is used in Sec. 2.1 to derive a set of nonlinear dynamical equations in vector-dyadic form; they are general with regard to the number and orientation of flywheel rotors, and the number of CMG rotors and gimbals. Certain terms of the equations are shown to be in agreement with work previously published by others. In Sec. 2.2 a set of twelve scalar equations is obtained by applying the generic relationships to the special case of a complex gyrostat consisting of a base body and three pairs of flywheels mounted in orthogonal directions. When only one flywheel is present the system becomes a simple gyrostat, and the resulting equations for rotational motion are shown to correspond to expressions given by Kane, Likins, and Levinson in Ref. [16]. A second configuration of particular interest arises when CMGs are the only spacecraft appendages; the equations used by Wie et al. in Ref. [6] are shown in Sec. 2.3 to follow from the general ones given in Sec. 2.1, along with several reasonable, clearly stated assumptions. The exact and approximate relationships presented in Secs. 2.2 and 2.3 respectively are combined in Sec. 2.4 to form approximate equations for a spacecraft with flywheels and CMGs, which are linearized in Sec. 2.5 and nondimensionalized in Sec. 2.6 in preparation for design of linear control laws. Finally, the approximate nonlinear equations are modified to account for damping of flywheel rotors, and presented in Sec. 2.7 together with all other differential equations employed in numerical simulations of nonlinear motion.

### 2.1 Derivation of Dynamical Equations

The system of interest,  $S$ , is composed of a rigid body  $B$  moving in an inertial or Newtonian reference frame  $N$ , and several rigid axisymmetric rotors  $R_1, \dots, R_\rho$  whose mass centers are fixed in  $B$ . A subset of the rotors  $R_1, \dots, R_{\mathcal{F}}$  have spin axes fixed in  $B$  so that these rotors represent non-gimbaled flywheels or reaction wheels. Each of the remaining rotors  $R_{\mathcal{F}+1}, \dots, R_\rho$  are attached to  $B$  with one or more massless gimbals which permit the direction of the spin axis to change relative to  $B$ ; these rotors thus represent a number of CMGs,  $\mathcal{C} = \rho - \mathcal{F}$ . (The latter subset could contain gimbaled flywheel rotors as well as CMGs, but we concern ourselves in this work only with non-gimbaled flywheels.) This system is illustrated in Fig. 2.1, with rotors  $R_2, \dots, R_{\rho-1}$  omitted for the sake of clarity.

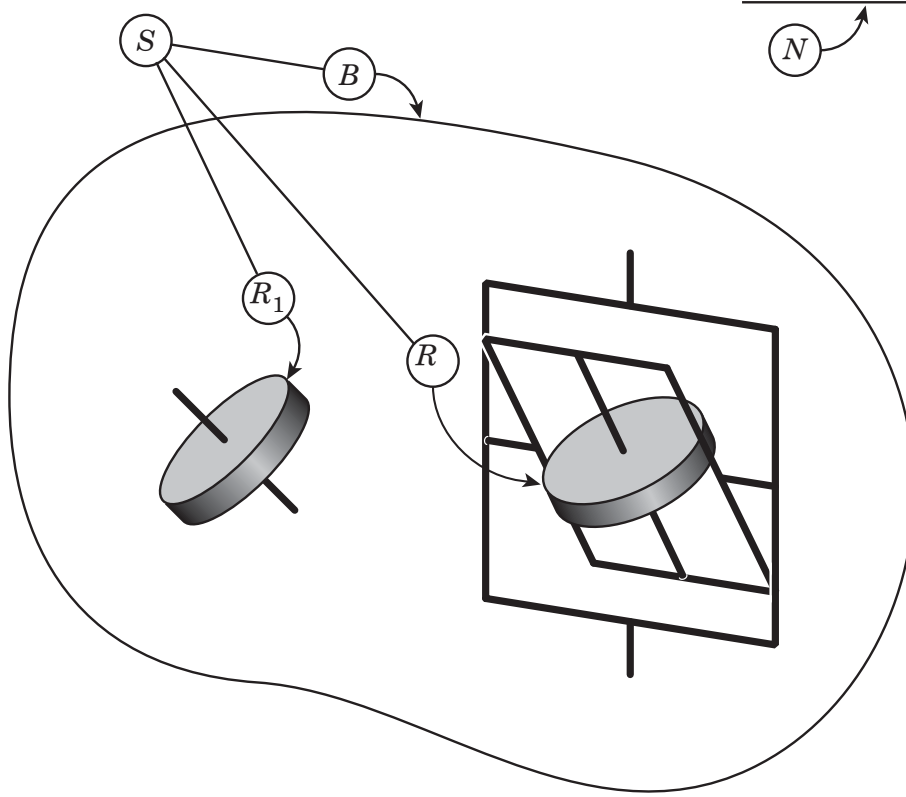


Figure 2.1: Spacecraft with Flywheel and CMG

The equations of motion are derived using Kane's equations (Eqs. (6.1.2), Ref. [17])

$$F_r + F_r^* = 0 \quad (r = 1, \dots, n) \quad (2.1)$$

where  $F_r$  are generalized active forces for  $S$  in  $N$ ,  $F_r^*$  are generalized inertia forces for  $S$  in  $N$ , and  $n$  is the number of degrees of freedom of  $S$  in  $N$ .

### 2.1.1 Generalized Speeds

The system  $S$  is holonomic and therefore a complete description of the motion of  $S$  in  $N$  requires  $n$  generalized speeds  $u_1, \dots, u_n$ , conveniently chosen as follows.

$${}^N\boldsymbol{\omega}^B = u_1 \hat{\mathbf{b}}_1 + u_2 \hat{\mathbf{b}}_2 + u_3 \hat{\mathbf{b}}_3 \quad (2.2)$$

where  ${}^N\boldsymbol{\omega}^B$  is the angular velocity of  $B$  in  $N$ , and  $\hat{\mathbf{b}}_1$ ,  $\hat{\mathbf{b}}_2$ , and  $\hat{\mathbf{b}}_3$  are a set of mutually orthogonal, right-handed unit vectors fixed in  $B$ .

We introduce unit vectors  $\hat{\boldsymbol{\beta}}_i$  fixed in  $B$  such that they are each parallel to the spin axis of a flywheel rotor  $R_i$ , and therefore to the angular velocity  ${}^B\boldsymbol{\omega}^{R_i}$  of  $R_i$  in  $B$ . Generalized speeds  $u_4, \dots, u_{\mathcal{F}+3}$  associated with the flywheels can then be used to write the angular velocities as

$${}^B\boldsymbol{\omega}^{R_i} = u_{i+3} \hat{\boldsymbol{\beta}}_i \quad (i = 1, \dots, \mathcal{F}) \quad (2.3)$$

The inner gimbal of each CMG is fastened to  $B$  with a revolute joint in a single-gimbal configuration, whereas a double-gimbal CMG has the inner gimbal attached with a revolute joint to

an outer gimbal, which is in turn mounted in  $B$  with a second revolute joint. The axis of each revolute joint is assumed to pass through the mass center of the rotor, which is thus fixed in  $B$ . In order to maintain generality with regard to the number of CMG rotors and gimbals, the angular velocities  ${}^B\boldsymbol{\omega}^{R_{\mathcal{F}+1}}, \dots, {}^B\boldsymbol{\omega}^{R_\rho}$  of the rotors relative to  $B$  are not written explicitly, but they must be functions of the generalized speeds  $u_{\mathcal{F}+4}, \dots, u_{n-3}$ , where one generalized speed is required for every gimbal.

The final three generalized speeds are associated with the velocity of the mass center  $S^*$  of  $S$  in  $N$ ,

$${}^N\mathbf{v}^{S^*} = u_{n-2}\hat{\mathbf{n}}_1 + u_{n-1}\hat{\mathbf{n}}_2 + u_n\hat{\mathbf{n}}_3 \quad (2.4)$$

where  $\hat{\mathbf{n}}_1$ ,  $\hat{\mathbf{n}}_2$ , and  $\hat{\mathbf{n}}_3$  are a set of mutually orthogonal, right-handed unit vectors fixed in  $N$ .

### 2.1.2 Generalized Active Forces

Let  $\sigma$  be the set of forces exerted on  $S$  *except* those exerted by  $B$  and  $R_i$  on each other ( $i = 1, \dots, \rho$ ). The forces in  $\sigma$  acting on  $B, R_1, \dots, R_\rho$  are equivalent to single forces  $\mathbf{F}_B, \mathbf{F}_1, \dots, \mathbf{F}_\rho$  applied at the mass centers  $B^*, R_1^*, \dots, R_\rho^*$  of bodies  $B, R_1, \dots, R_\rho$ , respectively, together with couples whose torques are  $\mathbf{M}_B, \mathbf{M}_1, \dots, \mathbf{M}_\rho$ .

To account for the forces exerted by  $B$  on  $R_i$ , we regard them as equivalent to a single force  $\mathbf{F}^{B/R_i}$  applied at  $R_i^*$ , together with a couple whose torque is  $\mathbf{M}^{B/R_i}$ . Since  $R_i^*$  is fixed in  $B$ ,  $\mathbf{F}^{B/R_i}$  contributes nothing to  $F_r$  ( $i = 1, \dots, \rho; r = 1, \dots, n$ ).

Body  $B$  makes a contribution  $(F_r)_B$  to the  $r$ th generalized active force, given by Eq. (4.6.1) of Ref. [17]. Likewise, each rotor makes a contribution denoted by  $(F_r)_{R_i}$ . Accounting for contributions from all bodies in the system, the law of action and reaction, and discounting the noncontributing forces,

$$\begin{aligned} F_r &= (F_r)_B + \sum_{i=1}^{\rho} (F_r)_{R_i} \\ &= {}^N\mathbf{v}_r^{B^*} \cdot \mathbf{F}_B + {}^N\boldsymbol{\omega}_r^B \cdot \left( \mathbf{M}_B - \sum_{i=1}^{\rho} \mathbf{M}^{B/R_i} \right) \\ &\quad + \sum_{i=1}^{\rho} \left[ {}^N\mathbf{v}_r^{R_i^*} \cdot \mathbf{F}_i + {}^N\boldsymbol{\omega}_r^{R_i} \cdot \left( \mathbf{M}_i + \mathbf{M}^{B/R_i} \right) \right] \quad (r = 1, \dots, n) \end{aligned} \quad (2.5)$$

where  ${}^N\mathbf{v}_r^{B^*}$  is known as the  $r$ th partial velocity of  $B^*$  in  $N$ ,  ${}^N\boldsymbol{\omega}_r^B$  is the  $r$ th partial angular velocity of  $B$  in  $N$ , and so forth.

Since the mass centers of all bodies belonging to  $S$  are fixed in  $B$ , the system mass center  $S^*$  is also fixed in  $B$ , and the velocities of  $B^*$  and  $R_i^*$  in  $N$  can be written in terms of the velocity of  $S^*$  in  $N$ ,

$${}^N\mathbf{v}^{B^*} = {}^N\mathbf{v}^{S^*} + {}^N\boldsymbol{\omega}^B \times \mathbf{r}^{S^*B^*} \quad (2.6)$$

$${}^N\mathbf{v}^{R_i^*} = {}^N\mathbf{v}^{S^*} + {}^N\boldsymbol{\omega}^B \times \mathbf{r}^{S^*R_i^*} \quad (i = 1, \dots, \rho) \quad (2.7)$$

where  $\mathbf{r}^{S^*B^*}$  is the position vector from  $S^*$  to  $B^*$ , and  $\mathbf{r}^{S^*R_i^*}$  is the position vector from  $S^*$  to  $R_i^*$ . Thus, the partial velocities can be written as

$${}^N\mathbf{v}_r^{B^*} = {}^N\mathbf{v}_r^{S^*} + {}^N\boldsymbol{\omega}_r^B \times \mathbf{r}^{S^*B^*} \quad (r = 1, \dots, n) \quad (2.8)$$

$${}^N\mathbf{v}_r^{R_i^*} = {}^N\mathbf{v}_r^{S^*} + {}^N\boldsymbol{\omega}_r^B \times \mathbf{r}^{S^*R_i^*} \quad (i = 1, \dots, \rho; r = 1, \dots, n) \quad (2.9)$$

The angular velocities in  $N$  of the rotors can be written in terms of the angular velocity of  $B$  in  $N$ ,

$${}^N\boldsymbol{\omega}^{R_i} = {}^N\boldsymbol{\omega}^B + {}^B\boldsymbol{\omega}^{R_i} \quad (i = 1, \dots, \rho) \quad (2.10)$$

and therefore their partial angular velocities can be written as

$${}^N\boldsymbol{\omega}_r^{R_i} = {}^N\boldsymbol{\omega}_r^B + {}^B\boldsymbol{\omega}_r^{R_i} \quad (i = 1, \dots, \rho; r = 1, \dots, n) \quad (2.11)$$

Substitution from Eqs. (2.11), (2.9), and (2.8) into (2.5) yields

$$\begin{aligned} F_r &= \left( {}^N\mathbf{v}_r^{S^*} + {}^N\boldsymbol{\omega}_r^B \times \mathbf{r}^{S^*B^*} \right) \cdot \mathbf{F}_B + {}^N\boldsymbol{\omega}_r^B \cdot \left( \mathbf{M}_B + \sum_{i=1}^{\rho} \mathbf{M}_i \right) \\ &\quad + \sum_{i=1}^{\rho} \left[ \left( {}^N\mathbf{v}_r^{S^*} + {}^N\boldsymbol{\omega}_r^B \times \mathbf{r}^{S^*R_i^*} \right) \cdot \mathbf{F}_i + {}^B\boldsymbol{\omega}_r^{R_i} \cdot \left( \mathbf{M}_i + \mathbf{M}^{B/R_i} \right) \right] \\ &= {}^N\mathbf{v}_r^{S^*} \cdot \left( \mathbf{F}_B + \sum_{i=1}^{\rho} \mathbf{F}_i \right) + {}^N\boldsymbol{\omega}_r^B \cdot \left[ \mathbf{M}_B + \mathbf{r}^{S^*B^*} \times \mathbf{F}_B + \sum_{i=1}^{\rho} \left( \mathbf{M}_i + \mathbf{r}^{S^*R_i^*} \times \mathbf{F}_i \right) \right] \\ &\quad + \sum_{i=1}^{\rho} {}^B\boldsymbol{\omega}_r^{R_i} \cdot \left( \mathbf{M}_i + \mathbf{M}^{B/R_i} \right) \\ &= {}^N\mathbf{v}_r^{S^*} \cdot \mathbf{F} + {}^N\boldsymbol{\omega}_r^B \cdot \mathbf{M} + \sum_{i=1}^{\rho} {}^B\boldsymbol{\omega}_r^{R_i} \cdot \left( \mathbf{M}_i + \mathbf{M}^{B/R_i} \right) \quad (r = 1, \dots, n) \end{aligned} \quad (2.12)$$

where  $\mathbf{F}$  is the resultant of the forces in  $\sigma$  acting on  $S$ ,

$$\mathbf{F} = \mathbf{F}_B + \sum_{i=1}^{\rho} \mathbf{F}_i \quad (2.13)$$

and  $\mathbf{M}$  is the moment of  $\sigma$  about  $S^*$ , given by

$$\mathbf{M} = \mathbf{M}_B + \mathbf{r}^{S^*B^*} \times \mathbf{F}_B + \sum_{i=1}^{\rho} \left( \mathbf{M}_i + \mathbf{r}^{S^*R_i^*} \times \mathbf{F}_i \right) \quad (2.14)$$

### 2.1.3 Generalized Inertia Forces

All bodies belonging to  $S$  contribute to the  $r$ th generalized inertia force  $F_r^*$  according to Eqs. (4.11.5)–(4.11.7) of Ref. [17]. As pointed out in part (c) of Problem 8.18, Ref. [17], the inertia torque in  $N$  of a rigid body  $B$  is simply the negative of the time derivative in  $N$  of the central angular momentum of  $B$  in  $N$ ,  ${}^N\mathbf{H}^{B/B^*}$ ; hence,

$$\begin{aligned} F_r^* &= (F_r^*)_B + \sum_{i=1}^{\rho} (F_r^*)_{R_i} \\ &= - \left( {}^N\mathbf{v}_r^{B^*} \cdot m_B {}^N\mathbf{a}^{B^*} + {}^N\boldsymbol{\omega}_r^B \cdot \frac{d}{dt} {}^N\mathbf{H}^{B/B^*} \right) \\ &\quad - \sum_{i=1}^{\rho} \left( {}^N\mathbf{v}_r^{R_i^*} \cdot m_i {}^N\mathbf{a}^{R_i^*} + {}^N\boldsymbol{\omega}_r^{R_i} \cdot \frac{d}{dt} {}^N\mathbf{H}^{R_i/R_i^*} \right) \quad (r = 1, \dots, n) \end{aligned} \quad (2.15)$$

where  $m_B$  is the mass of  $B$ ,  ${}^N \mathbf{a}^{B^*}$  is the acceleration of  $B^*$  in  $N$ , and so forth. Substitution from Eqs. (2.11), (2.9), and (2.8) into (2.15) yields, after some manipulation,

$$F_r^* = -{}^N \mathbf{v}_r^{S^*} \cdot \left( m_B {}^N \mathbf{a}^{B^*} + \sum_{i=1}^{\rho} m_i {}^N \mathbf{a}^{R_i^*} \right) - \sum_{i=1}^{\rho} {}^B \boldsymbol{\omega}_r^{R_i} \cdot \frac{{}^N d}{{}^N dt} {}^N \mathbf{H}^{R_i/R_i^*} \\ - {}^N \boldsymbol{\omega}_r^B \cdot \left[ \frac{{}^N d}{{}^N dt} {}^N \mathbf{H}^{B/B^*} + \mathbf{r}^{S^*B^*} \times m_B {}^N \mathbf{a}^{B^*} + \sum_{i=1}^{\rho} \left( \frac{{}^N d}{{}^N dt} {}^N \mathbf{H}^{R_i/R_i^*} + \mathbf{r}^{S^*R_i^*} \times m_i {}^N \mathbf{a}^{R_i^*} \right) \right] \\ (r = 1, \dots, n) \quad (2.16)$$

After noting once more that  $S^*$ ,  $B^*$ , and  $R_1^*, \dots, R_\rho^*$  are all fixed in  $B$ , the accelerations of  $B^*$  and  $R_i^*$  in  $N$  can be written in terms of the acceleration of  $S^*$  in  $N$ ,

$${}^N \mathbf{a}^{B^*} = {}^N \mathbf{a}^{S^*} + {}^N \boldsymbol{\alpha}^B \times \mathbf{r}^{S^*B^*} + {}^N \boldsymbol{\omega}^B \times {}^N \boldsymbol{\omega}^B \times \mathbf{r}^{S^*B^*} \quad (2.17)$$

$${}^N \mathbf{a}^{R_i^*} = {}^N \mathbf{a}^{S^*} + {}^N \boldsymbol{\alpha}^B \times \mathbf{r}^{S^*R_i^*} + {}^N \boldsymbol{\omega}^B \times {}^N \boldsymbol{\omega}^B \times \mathbf{r}^{S^*R_i^*} \quad (i = 1, \dots, \rho) \quad (2.18)$$

where  ${}^N \boldsymbol{\alpha}^B$  is the angular acceleration of  $B$  in  $N$ . Thus,

$$\mathbf{r}^{S^*B^*} \times m_B {}^N \mathbf{a}^{B^*} + \sum_{i=1}^{\rho} \mathbf{r}^{S^*R_i^*} \times m_i {}^N \mathbf{a}^{R_i^*} \\ = \mathbf{r}^{S^*B^*} \times m_B ({}^N \mathbf{a}^{S^*} + {}^N \boldsymbol{\alpha}^B \times \mathbf{r}^{S^*B^*} + {}^N \boldsymbol{\omega}^B \times {}^N \boldsymbol{\omega}^B \times \mathbf{r}^{S^*B^*}) \\ + \sum_{i=1}^{\rho} \mathbf{r}^{S^*R_i^*} \times m_i ({}^N \mathbf{a}^{S^*} + {}^N \boldsymbol{\alpha}^B \times \mathbf{r}^{S^*R_i^*} + {}^N \boldsymbol{\omega}^B \times {}^N \boldsymbol{\omega}^B \times \mathbf{r}^{S^*R_i^*}) \\ = \left( m_B \mathbf{r}^{S^*B^*} + \sum_{i=1}^{\rho} m_i \mathbf{r}^{S^*R_i^*} \right) \times {}^N \mathbf{a}^{S^*} \\ + \left\{ m_B \left[ (\mathbf{r}^{S^*B^*})^2 \underline{\mathbf{U}} - \mathbf{r}^{S^*B^*} \mathbf{r}^{S^*B^*} \right] + \sum_{i=1}^{\rho} m_i \left[ (\mathbf{r}^{S^*R_i^*})^2 \underline{\mathbf{U}} - \mathbf{r}^{S^*R_i^*} \mathbf{r}^{S^*R_i^*} \right] \right\} \cdot {}^N \boldsymbol{\alpha}^B \\ + {}^N \boldsymbol{\omega}^B \times \left\{ m_B \left[ (\mathbf{r}^{S^*B^*})^2 \underline{\mathbf{U}} - \mathbf{r}^{S^*B^*} \mathbf{r}^{S^*B^*} \right] + \sum_{i=1}^{\rho} m_i \left[ (\mathbf{r}^{S^*R_i^*})^2 \underline{\mathbf{U}} - \mathbf{r}^{S^*R_i^*} \mathbf{r}^{S^*R_i^*} \right] \right\} \cdot {}^N \boldsymbol{\omega}^B \\ = \mathbf{0} \times {}^N \mathbf{a}^{S^*} \\ + \left( \underline{\mathbf{I}}^{B^*/S^*} + \sum_{i=1}^{\rho} \underline{\mathbf{I}}^{R_i^*/S^*} \right) \cdot {}^N \boldsymbol{\alpha}^B + {}^N \boldsymbol{\omega}^B \times \left( \underline{\mathbf{I}}^{B^*/S^*} + \sum_{i=1}^{\rho} \underline{\mathbf{I}}^{R_i^*/S^*} \right) \cdot {}^N \boldsymbol{\omega}^B \quad (2.19)$$

where the vector that premultiplies  ${}^N \mathbf{a}^{S^*}$  vanishes because of the definition of the system mass center, and where  $\underline{\mathbf{U}}$  represents the unit dyadic. As described in Sec. 3.6 of Ref. [17],  $\underline{\mathbf{I}}^{B^*/S^*}$  denotes the inertia dyadic relative to  $S^*$  of a fictitious particle situated at  $B^*$  and having a mass equal to  $m_B$ . A similar description applies to the dyadic  $\underline{\mathbf{I}}^{R_i^*/S^*}$ .

The central angular momentum of  $B$  in  $N$  is simply

$${}^N \mathbf{H}^{B/B^*} = \underline{\mathbf{I}}^{B/B^*} \cdot {}^N \boldsymbol{\omega}^B \quad (2.20)$$

where  $\underline{\mathbf{I}}^{B/B^*}$  is the inertia dyadic of  $B$  relative to  $B^*$ . Hence the time derivative of  ${}^N \mathbf{H}^{B/B^*}$  in  $N$  is given by

$$\frac{{}^N d}{{}^N dt} {}^N \mathbf{H}^{B/B^*} = \underline{\mathbf{I}}^{B/B^*} \cdot {}^N \boldsymbol{\alpha}^B + {}^N \boldsymbol{\omega}^B \times \underline{\mathbf{I}}^{B/B^*} \cdot {}^N \boldsymbol{\omega}^B \quad (2.21)$$

The central angular momentum of any rotor in  $N$  can be written as

$$\begin{aligned} {}^N \mathbf{H}^{R_i/R_i^*} &= \underline{\mathbf{I}}^{R_i/R_i^*} \cdot ({}^N \boldsymbol{\omega}^B + {}^B \boldsymbol{\omega}^{R_i}) \\ &= \underline{\mathbf{I}}^{R_i/R_i^*} \cdot {}^N \boldsymbol{\omega}^B + {}^B \mathbf{H}^{R_i/R_i^*} \quad (i = 1, \dots, \rho) \end{aligned} \quad (2.22)$$

where  $\underline{\mathbf{I}}^{R_i/R_i^*}$  is the inertia dyadic of  $R_i$  relative to  $R_i^*$ , and  ${}^B \mathbf{H}^{R_i/R_i^*}$  is called the central angular momentum of  $R_i$  in  $B$ . The time derivative of  ${}^N \mathbf{H}^{R_i/R_i^*}$  in the case of a flywheel rotor is different from that of a CMG because the mass distribution of the rotor does not change relative to  $B$  in the former case, whereas it does change in the latter. For flywheel rotors,

$$\begin{aligned} \frac{d}{dt} {}^N \mathbf{H}^{R_i/R_i^*} &= \frac{d}{dt} {}^B \mathbf{H}^{R_i/R_i^*} + {}^N \boldsymbol{\omega}^B \times {}^N \mathbf{H}^{R_i/R_i^*} \\ &= \frac{d}{dt} \left( \underline{\mathbf{I}}^{R_i/R_i^*} \cdot {}^N \boldsymbol{\omega}^B + {}^B \mathbf{H}^{R_i/R_i^*} \right) + {}^N \boldsymbol{\omega}^B \times \left( \underline{\mathbf{I}}^{R_i/R_i^*} \cdot {}^N \boldsymbol{\omega}^B + {}^B \mathbf{H}^{R_i/R_i^*} \right) \\ &= \underline{\mathbf{0}} \cdot {}^N \boldsymbol{\omega}^B + \underline{\mathbf{I}}^{R_i/R_i^*} \cdot {}^N \boldsymbol{\alpha}^B + {}^N \boldsymbol{\omega}^B \times \underline{\mathbf{I}}^{R_i/R_i^*} \cdot {}^N \boldsymbol{\omega}^B + \frac{d}{dt} {}^B \mathbf{H}^{R_i/R_i^*} + {}^N \boldsymbol{\omega}^B \times {}^B \mathbf{H}^{R_i/R_i^*} \end{aligned} \quad (i = 1, \dots, \mathcal{F}) \quad (2.23)$$

where the zero dyadic  $\underline{\mathbf{0}}$  results because there is no change in the inertia dyadic  $\underline{\mathbf{I}}^{R_i/R_i^*}$  with respect to time in reference frame  $B$ . Unlike the flywheel rotor, the CMG rotor's inertia dyadic does change with respect to time in  $B$ , and in view of Problem 5.14, Ref. [17],

$$\begin{aligned} \frac{d}{dt} \underline{\mathbf{I}}^{R_i/R_i^*} &= \frac{d}{dt} \underline{\mathbf{I}}^{R_i/R_i^*} + {}^B \boldsymbol{\omega}^{R_i} \times \underline{\mathbf{I}}^{R_i/R_i^*} - \underline{\mathbf{I}}^{R_i/R_i^*} \times {}^B \boldsymbol{\omega}^{R_i} \\ &= \underline{\mathbf{0}} + {}^B \boldsymbol{\omega}^{R_i} \times \underline{\mathbf{I}}^{R_i/R_i^*} - \underline{\mathbf{I}}^{R_i/R_i^*} \times {}^B \boldsymbol{\omega}^{R_i} \quad (i = \mathcal{F} + 1, \dots, \rho) \end{aligned} \quad (2.24)$$

This result is then used in place of  $\underline{\mathbf{0}}$  in Eqs. (2.23) and yields

$$\begin{aligned} \frac{d}{dt} {}^N \mathbf{H}^{R_i/R_i^*} &= \underline{\mathbf{I}}^{R_i/R_i^*} \cdot {}^N \boldsymbol{\alpha}^B + {}^N \boldsymbol{\omega}^B \times \underline{\mathbf{I}}^{R_i/R_i^*} \cdot {}^N \boldsymbol{\omega}^B + \frac{d}{dt} {}^B \mathbf{H}^{R_i/R_i^*} + {}^N \boldsymbol{\omega}^B \times {}^B \mathbf{H}^{R_i/R_i^*} \\ &\quad + \left( {}^B \boldsymbol{\omega}^{R_i} \times \underline{\mathbf{I}}^{R_i/R_i^*} - \underline{\mathbf{I}}^{R_i/R_i^*} \times {}^B \boldsymbol{\omega}^{R_i} \right) \cdot {}^N \boldsymbol{\omega}^B \quad (i = \mathcal{F} + 1, \dots, \rho) \end{aligned} \quad (2.25)$$

After noting that  $m_B {}^N \mathbf{a}^{B^*} + \sum_{i=1}^{\rho} m_i {}^N \mathbf{a}^{R_i^*} = m_S {}^N \mathbf{a}^{S^*}$ , where  $m_S$  is the mass of system  $S$  and  ${}^N \mathbf{a}^{S^*}$  is the acceleration of  $S^*$  in  $N$ , and then substituting from Eqs. (2.25), (2.23), (2.21), and (2.19) into (2.16), one obtains

$$\begin{aligned} F_r^* &= -{}^N \mathbf{v}_r^{S^*} \cdot m_S {}^N \mathbf{a}^{S^*} - {}^N \boldsymbol{\omega}_r^B \cdot \left[ \underline{\mathbf{I}}^{S/S^*} \cdot {}^N \boldsymbol{\alpha}^B + {}^N \boldsymbol{\omega}^B \times \underline{\mathbf{I}}^{S/S^*} \cdot {}^N \boldsymbol{\omega}^B \right. \\ &\quad \left. + \sum_{i=1}^{\rho} \left( \frac{d}{dt} {}^B \mathbf{H}^{R_i/R_i^*} + {}^N \boldsymbol{\omega}^B \times {}^B \mathbf{H}^{R_i/R_i^*} \right) \right. \\ &\quad \left. + \sum_{i=\mathcal{F}+1}^{\rho} \left( {}^B \boldsymbol{\omega}^{R_i} \times \underline{\mathbf{I}}^{R_i/R_i^*} - \underline{\mathbf{I}}^{R_i/R_i^*} \times {}^B \boldsymbol{\omega}^{R_i} \right) \cdot {}^N \boldsymbol{\omega}^B \right] \\ &\quad - \sum_{i=1}^{\rho} {}^B \boldsymbol{\omega}_r^{R_i} \cdot \frac{d}{dt} {}^N \mathbf{H}^{R_i/R_i^*} \quad (r = 1, \dots, n) \end{aligned} \quad (2.26)$$

where  $\underline{\mathbf{I}}^{S/S^*}$ , the inertia dyadic of  $S$  for  $S^*$ , is given by

$$\underline{\mathbf{I}}^{S/S^*} = \underline{\mathbf{I}}^{B/B^*} + \underline{\mathbf{I}}^{B^*/S^*} + \sum_{i=1}^{\rho} \left( \underline{\mathbf{I}}^{R_i/R_i^*} + \underline{\mathbf{I}}^{R_i^*/S^*} \right) \quad (2.27)$$

#### 2.1.4 General Vector-Dyadic Equations

According to Eqs. (2.1) the generalized inertia forces from Eqs. (2.26) can now be added to the generalized active forces from Eqs. (2.12) to yield vector-dyadic equations of motion for a spacecraft containing flywheels and CMGs

$$\begin{aligned} & {}^N \mathbf{v}_r^{S^*} \cdot \left( \mathbf{F} - m_S {}^N \mathbf{a}^{S^*} \right) \\ & + {}^N \boldsymbol{\omega}_r^B \cdot \left\{ \mathbf{M} - \left[ \underline{\mathbf{I}}^{S/S^*} \cdot {}^N \boldsymbol{\alpha}^B + {}^N \boldsymbol{\omega}^B \times \underline{\mathbf{I}}^{S/S^*} \cdot {}^N \boldsymbol{\omega}^B \right. \right. \\ & + \sum_{i=1}^{\rho} \left( \frac{d}{dt} {}^B \mathbf{H}^{R_i/R_i^*} + {}^N \boldsymbol{\omega}^B \times {}^B \mathbf{H}^{R_i/R_i^*} \right) \\ & \left. \left. + \sum_{i=\mathcal{F}+1}^{\rho} \left( {}^B \boldsymbol{\omega}^{R_i} \times \underline{\mathbf{I}}^{R_i/R_i^*} - \underline{\mathbf{I}}^{R_i/R_i^*} \times {}^B \boldsymbol{\omega}^{R_i} \right) \cdot {}^N \boldsymbol{\omega}^B \right] \right\} \\ & + \sum_{i=1}^{\rho} {}^B \boldsymbol{\omega}_r^{R_i} \cdot \left( \mathbf{M}_i + \mathbf{M}^{B/R_i} - \frac{d}{dt} {}^N \mathbf{H}^{R_i/R_i^*} \right) = 0 \quad (r = 1, \dots, n) \end{aligned} \quad (2.28)$$

Eqs. (2.28) are completely general with regard to the number and orientation of flywheel rotors, and the number of CMG rotors and gimbals. In this form, they are applicable to variable-speed CMG rotors. These equations of motion, and the expression for generalized inertia forces, can be compared to previous work.

Reference [18] is concerned with gyrostats and relevant equations that can be dealt with easily by an analyst, and quickly by a computer. Expressions for generalized inertia forces are presented separately for a gyrostat containing a single cylindrical rotor, and for one containing a single spherical rotor; an underlying general relationship (C65) developed in Appendix C can be shown to give rise to Eqs. (2.26) presented here, when no CMGs are present ( $\rho = \mathcal{F}$ ).

The term in the second line of Eqs. (C65) accounts for but a single rotor, although additional rotors can be handled straightforwardly by adding a sum of similar terms. By appealing to Eqs. (24), (C61), and (C35) of Ref. [18], and replacing their labels  $G$ ,  $B$ , and  $A$  for the gyrostat, rotor, and carrier respectively with our  $S$ ,  $R_i$ , and  $B$ , we can write

$$\begin{aligned} -F_r^* &= {}^N \mathbf{v}_r^{S^*} \cdot {}^N \mathbf{F}^S + {}^N \boldsymbol{\omega}_r^B \cdot {}^N \mathbf{T}^S + \sum_{i=1}^{\rho} {}^B \boldsymbol{\omega}_r^{R_i} \cdot \left( \underline{\mathbf{I}}^{R_i/R_i^*} \cdot {}^N \boldsymbol{\alpha}^{R_i} + {}^N \boldsymbol{\omega}^{R_i} \times \underline{\mathbf{I}}^{R_i/R_i^*} \cdot {}^N \boldsymbol{\omega}^{R_i} \right) \\ &= {}^N \mathbf{v}_r^{S^*} \cdot m_S {}^N \mathbf{a}^{S^*} + {}^N \boldsymbol{\omega}_r^B \cdot \frac{d}{dt} {}^N \mathbf{H}^{S/S^*} + \sum_{i=1}^{\rho} {}^B \boldsymbol{\omega}_r^{R_i} \cdot \frac{d}{dt} {}^N \mathbf{H}^{R_i/R_i^*} \quad (r = 1, \dots, n) \end{aligned} \quad (2.29)$$

The central angular momentum in  $N$  of a gyrostat containing a single rotor, expressed by Eqs. (C24) and (3) of Ref. [18], is easily modified to include multiple rotors as in Eq. (14) in Sec. 6.1 of Ref. [19],

$${}^N \mathbf{H}^{S/S^*} = \underline{\mathbf{I}}^{S/S^*} \cdot {}^N \boldsymbol{\omega}^B + \sum_{i=1}^{\rho} \underline{\mathbf{I}}^{R_i/R_i^*} \cdot {}^B \boldsymbol{\omega}^{R_i} = \underline{\mathbf{I}}^{S/S^*} \cdot {}^N \boldsymbol{\omega}^B + \sum_{i=1}^{\rho} {}^B \mathbf{H}^{R_i/R_i^*} \quad (2.30)$$

and differentiation with respect to time in  $N$  yields, after reference to Eq. (C34) of Ref. [18],

$$\frac{d}{dt} {}^N \mathbf{H}^{S/S^*} = \underline{\mathbf{I}}^{S/S^*} \cdot {}^N \boldsymbol{\alpha}^B + {}^N \boldsymbol{\omega}^B \times \underline{\mathbf{I}}^{S/S^*} \cdot {}^N \boldsymbol{\omega}^B + \sum_{i=1}^{\rho} \left( \frac{d}{dt} {}^B \mathbf{H}^{R_i/R_i^*} + {}^N \boldsymbol{\omega}^B \times {}^B \mathbf{H}^{R_i/R_i^*} \right) \quad (2.31)$$

Substitution from Eq. (2.31) into (2.29) clearly reproduces Eqs. (2.26) when CMGs are absent.

The use of the system mass and inertia scalars, together with the moment of inertia for the axis of symmetry of each rotor, is shown in Ref. [18] to lead to greater efficiency than use of mass properties of individual bodies in a gyrostat; this advantage happens to accrue to Eqs. (2.26) and (2.28) developed here. Additionally, in the interest of efficient equations of motion, the authors of Ref. [18] advocate the use of the partial angular velocities  ${}^N \boldsymbol{\omega}_r^{R_i}$  of a gyrostat rotor in  $N$ , rather than partial angular velocities  ${}^B \boldsymbol{\omega}_r^{R_i}$  in  $B$ , when motion of the rotor relative to  $B$  is not prescribed (known a priori). The latter are chosen here because they bring into evidence  ${}^B \mathbf{H}^{R_i/R_i^*}$  and its time derivative in  $B$ , quantities which are needed for the forthcoming comparison in Sec. 2.3 to relationships used by others for dealing with CMGs.

Rheinfurth and Carroll present in Ref. [20] vector-dyadic equations of motion (27) for a spacecraft composed of a rigid carrier and a rigid appendage whose mass center is fixed in the carrier. Additional appendages are accounted for easily by forming a sum, as they do in Eq. (16), but the resulting vector-dyadic expression will give rise to only three scalar equations. It is pointed out near the bottom of p. 6 that a CMG can be regarded as an appendage; however, the motion of every appendage relative to the carrier must be prescribed if the three relationships are to serve as dynamical equations governing the motion of the carrier. Reference [20] does not contain counterparts to the  $n - 6$  of our Eqs. (2.28) that govern the motion of the rotors, or to the three equations governing the translational motion of the system. It is now shown that Rheinfurth and Carroll's Eqs. (27) give way to the first three of Eqs. (2.28) here when all rotors are permitted to be CMGs ( $\mathcal{F} = 0$ ). After forming the required sum, and replacing their symbols  $\underline{\mathbf{L}}$  with  $\mathbf{M}$ ,  $\underline{\mathbf{I}}$  with  $\underline{\mathbf{I}}^{S/S^*}$ ,  $\underline{\mathbf{I}}_p$  with  $\underline{\mathbf{I}}^{R_i/R_i^*}$ ,  $\underline{\boldsymbol{\Omega}}$  with  ${}^N \boldsymbol{\omega}^B$ ,  $\underline{\boldsymbol{\omega}}_p$  with  ${}^B \boldsymbol{\omega}^{R_i}$ ,  $(\underline{\boldsymbol{\Omega}})_v$  with  ${}^N \boldsymbol{\alpha}^B$ , and  $(\underline{\boldsymbol{\omega}}_p)_p$  with  ${}^B \boldsymbol{\alpha}^{R_i}$ , one obtains

$$\begin{aligned} \mathbf{M} = & \underline{\mathbf{I}}^{S/S^*} \cdot {}^N \boldsymbol{\alpha}^B + {}^N \boldsymbol{\omega}^B \times \underline{\mathbf{I}}^{S/S^*} \cdot {}^N \boldsymbol{\omega}^B + \sum_{i=1}^{\rho} \left[ \underline{\mathbf{I}}^{R_i/R_i^*} \cdot {}^B \boldsymbol{\alpha}^{R_i} + {}^B \boldsymbol{\omega}^{R_i} \times \underline{\mathbf{I}}^{R_i/R_i^*} \cdot {}^B \boldsymbol{\omega}^{R_i} \right. \\ & \left. + \left( {}^B \boldsymbol{\omega}^{R_i} \times \underline{\mathbf{I}}^{R_i/R_i^*} - \underline{\mathbf{I}}^{R_i/R_i^*} \times {}^B \boldsymbol{\omega}^{R_i} \right) \cdot {}^N \boldsymbol{\omega}^B + {}^N \boldsymbol{\omega}^B \times \underline{\mathbf{I}}^{R_i/R_i^*} \cdot {}^B \boldsymbol{\omega}^{R_i} \right] \end{aligned} \quad (2.32)$$

After noting that  $\underline{\mathbf{I}}^{R_i/R_i^*} \cdot {}^B \boldsymbol{\omega}^{R_i} = {}^B \mathbf{H}^{R_i/R_i^*}$ , and  $\underline{\mathbf{I}}^{R_i/R_i^*} \cdot {}^B \boldsymbol{\alpha}^{R_i} + {}^B \boldsymbol{\omega}^{R_i} \times \underline{\mathbf{I}}^{R_i/R_i^*} \cdot {}^B \boldsymbol{\omega}^{R_i} = {}^B d {}^B \mathbf{H}^{R_i/R_i^*} / dt$ , Eq. (2.32) can be rewritten as

$$\begin{aligned} \mathbf{M} = & \underline{\mathbf{I}}^{S/S^*} \cdot {}^N \boldsymbol{\alpha}^B + {}^N \boldsymbol{\omega}^B \times \underline{\mathbf{I}}^{S/S^*} \cdot {}^N \boldsymbol{\omega}^B \\ & + \sum_{i=1}^{\rho} \left[ \frac{d}{dt} {}^B \mathbf{H}^{R_i/R_i^*} + {}^N \boldsymbol{\omega}^B \times {}^B \mathbf{H}^{R_i/R_i^*} + \left( {}^B \boldsymbol{\omega}^{R_i} \times \underline{\mathbf{I}}^{R_i/R_i^*} - \underline{\mathbf{I}}^{R_i/R_i^*} \times {}^B \boldsymbol{\omega}^{R_i} \right) \cdot {}^N \boldsymbol{\omega}^B \right] \end{aligned} \quad (2.33)$$

It is evident that forming dot products with this expression and three vectors  ${}^N \boldsymbol{\omega}_r^B$  produces the first three scalar relationships given by Eqs. (2.28).

## 2.2 Dynamical Equations for A Complex Gyrostat

A spacecraft known as a simple gyrostat is described in Sec. 3.6 of Ref. [16]; the system  $S$  in the preceding discussion becomes a simple gyrostat when the number of flywheels  $\mathcal{F}$  is equal to 1, and

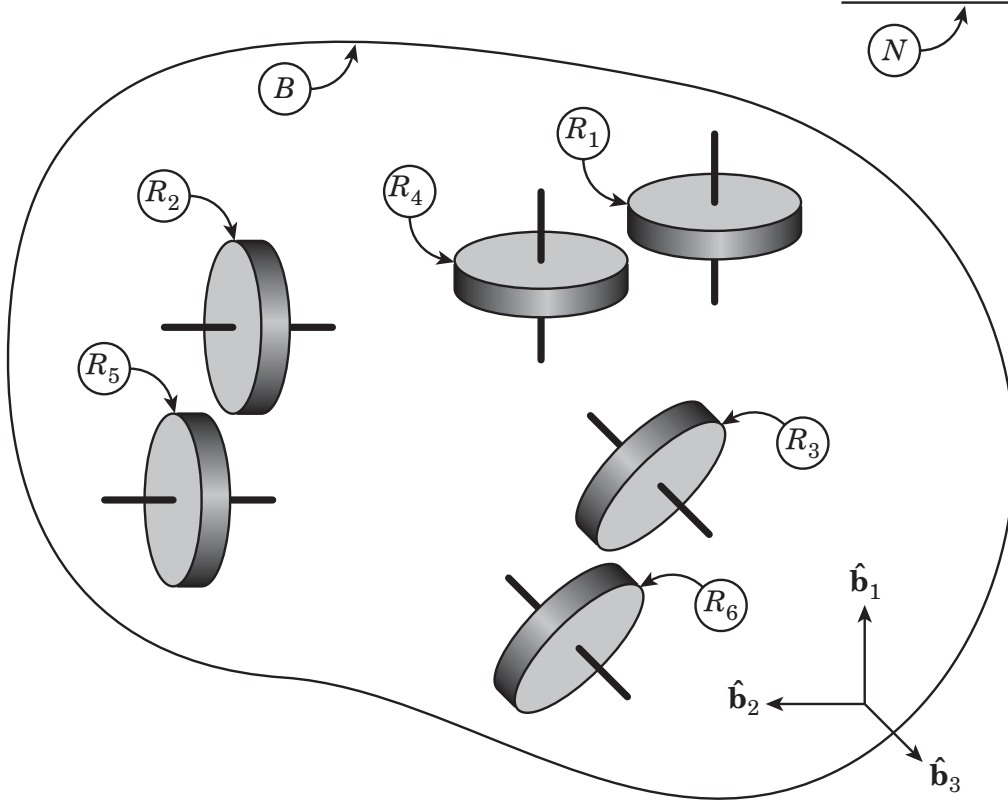


Figure 2.2: Spacecraft with Flywheels

when no CMGs are present ( $\mathcal{C} = 0$ , thus  $\rho = \mathcal{F}$ ). A spacecraft with more than one flywheel, such as the one shown in Fig. 2.2, will be referred to as a complex gyrostat; equations of motion with  $\mathcal{F} = 6$  are given in the following material, and are shown to correspond to those given in Sec. 3.7 of Ref. [16] when  $\mathcal{F} = 1$ .

Without a great loss of generality one can at this point work with six flywheel rotors  $R_1, \dots, R_6$  ( $\mathcal{F} = 6$ ) arranged in three counter-rotating pairs as shown in Fig. 2.2, with the spin axes of  $R_1$  and  $R_4$  parallel to  $\hat{\mathbf{b}}_1$ ,  $R_2$  and  $R_5$  parallel to  $\hat{\mathbf{b}}_2$ , and  $R_3$  and  $R_6$  parallel to  $\hat{\mathbf{b}}_3$ . The generalized speeds  $u_4, \dots, u_9$  associated with the flywheels are then used to form the angular velocities  ${}^B\boldsymbol{\omega}^{R_i}$  of  $R_i$  in  $B$ , ( $i = 1, \dots, 6$ )

$$\begin{aligned} {}^B\boldsymbol{\omega}^{R_1} &= u_4 \hat{\mathbf{b}}_1, & {}^B\boldsymbol{\omega}^{R_2} &= u_6 \hat{\mathbf{b}}_2, & {}^B\boldsymbol{\omega}^{R_3} &= u_8 \hat{\mathbf{b}}_3, \\ {}^B\boldsymbol{\omega}^{R_4} &= u_5 \hat{\mathbf{b}}_1, & {}^B\boldsymbol{\omega}^{R_5} &= u_7 \hat{\mathbf{b}}_2, & {}^B\boldsymbol{\omega}^{R_6} &= u_9 \hat{\mathbf{b}}_3 \end{aligned} \quad (2.34)$$

Since the axis of symmetry of each flywheel remains fixed in  $B$ , and is in the case of  $R_1$  parallel to  $\hat{\mathbf{b}}_1$ , the central inertia dyadic of  $R_1$  can be expressed as

$$\underline{\mathbf{I}}^{R_1/R_1^*} = J \hat{\mathbf{b}}_1 \hat{\mathbf{b}}_1 + K (\hat{\mathbf{b}}_2 \hat{\mathbf{b}}_2 + \hat{\mathbf{b}}_3 \hat{\mathbf{b}}_3) = J \hat{\mathbf{b}}_1 \hat{\mathbf{b}}_1 + K (\underline{\mathbf{U}} - \hat{\mathbf{b}}_1 \hat{\mathbf{b}}_1) \quad (2.35)$$

where  $J$  and  $K$  are the central principal moments of inertia of a flywheel rotor for, respectively, the axis of symmetry, and any line perpendicular to the axis of symmetry. In fact, the inertia dyadics for the 6 flywheel rotors are given by

$$\underline{\mathbf{I}}^{R_i/R_i^*} = \underline{\mathbf{I}}^{R_{i+3}/R_{i+3}^*} = J \hat{\mathbf{b}}_i \hat{\mathbf{b}}_i + K (\underline{\mathbf{U}} - \hat{\mathbf{b}}_i \hat{\mathbf{b}}_i) \quad (i = 1, 2, 3) \quad (2.36)$$

The angular velocities of the rotors in  $B$  are

$${}^B\boldsymbol{\omega}^{R_i} = \begin{cases} u_{2i+2}\hat{\mathbf{b}}_i & (i = 1, 2, 3) \\ u_{2i-3}\hat{\mathbf{b}}_{i-3} & (i = 4, 5, 6) \end{cases} \quad (2.37)$$

In order to evaluate Eqs. (2.28) one must develop expressions for angular momenta of  $R_i$  appearing there, and time derivatives and sums thereof. In view of Eqs. (2.34), (2.2), and (2.10),

$$\begin{aligned} {}^B\mathbf{H}^{R_i/R_i^*} &= \mathbf{I}^{R_i/R_i^*} \cdot {}^B\boldsymbol{\omega}^{R_i} = \begin{cases} \left[ J\hat{\mathbf{b}}_i\hat{\mathbf{b}}_i + K(\underline{\mathbf{U}} - \hat{\mathbf{b}}_i\hat{\mathbf{b}}_i) \right] \cdot u_{2i+2}\hat{\mathbf{b}}_i & (i = 1, 2, 3) \\ \left[ J\hat{\mathbf{b}}_{i-3}\hat{\mathbf{b}}_{i-3} + K(\underline{\mathbf{U}} - \hat{\mathbf{b}}_{i-3}\hat{\mathbf{b}}_{i-3}) \right] \cdot u_{2i-3}\hat{\mathbf{b}}_{i-3} & (i = 4, 5, 6) \end{cases} \\ &= \begin{cases} Ju_{2i+2}\hat{\mathbf{b}}_i & (i = 1, 2, 3) \\ Ju_{2i-3}\hat{\mathbf{b}}_{i-3} & (i = 4, 5, 6) \end{cases} \end{aligned} \quad (2.38)$$

$$\sum_{i=1}^6 {}^B\mathbf{H}^{R_i/R_i^*} = J[(u_4 + u_5)\hat{\mathbf{b}}_1 + (u_6 + u_7)\hat{\mathbf{b}}_2 + (u_8 + u_9)\hat{\mathbf{b}}_3] \quad (2.39)$$

$${}^N\boldsymbol{\omega}^B \times \sum_{i=1}^6 {}^B\mathbf{H}^{R_i/R_i^*} = \quad (2.40)$$

$$J\{[u_2(u_8 + u_9) - u_3(u_6 + u_7)]\hat{\mathbf{b}}_1 + [u_3(u_4 + u_5) - u_1(u_8 + u_9)]\hat{\mathbf{b}}_2 + [u_1(u_6 + u_7) - u_2(u_4 + u_5)]\hat{\mathbf{b}}_3\}$$

$$\frac{{}^B d}{{}^B dt} {}^B\mathbf{H}^{R_i/R_i^*} = \begin{cases} J\dot{u}_{2i+2}\hat{\mathbf{b}}_i & (i = 1, 2, 3) \\ J\dot{u}_{2i-3}\hat{\mathbf{b}}_{i-3} & (i = 4, 5, 6) \end{cases} \quad (2.41)$$

$$\sum_{i=1}^6 \frac{{}^B d}{{}^B dt} {}^B\mathbf{H}^{R_i/R_i^*} = J[(\dot{u}_4 + \dot{u}_5)\hat{\mathbf{b}}_1 + (\dot{u}_6 + \dot{u}_7)\hat{\mathbf{b}}_2 + (\dot{u}_8 + \dot{u}_9)\hat{\mathbf{b}}_3] \quad (2.42)$$

$$\begin{aligned} {}^N\mathbf{H}^{R_i/R_i^*} &= \mathbf{I}^{R_i/R_i^*} \cdot {}^N\boldsymbol{\omega}^{R_i} \\ &= \begin{cases} \left[ J\hat{\mathbf{b}}_i\hat{\mathbf{b}}_i + K(\underline{\mathbf{U}} - \hat{\mathbf{b}}_i\hat{\mathbf{b}}_i) \right] \cdot {}^N\boldsymbol{\omega}^{R_i} & (i = 1, 2, 3) \\ \left[ J\hat{\mathbf{b}}_{i-3}\hat{\mathbf{b}}_{i-3} + K(\underline{\mathbf{U}} - \hat{\mathbf{b}}_{i-3}\hat{\mathbf{b}}_{i-3}) \right] \cdot {}^N\boldsymbol{\omega}^{R_i} & (i = 4, 5, 6) \end{cases} \\ &= \begin{cases} (J - K)(u_i + u_{2i+2})\hat{\mathbf{b}}_i + K {}^N\boldsymbol{\omega}^{R_i} & (i = 1, 2, 3) \\ (J - K)(u_{i-3} + u_{2i-3})\hat{\mathbf{b}}_{i-3} + K {}^N\boldsymbol{\omega}^{R_i} & (i = 4, 5, 6) \end{cases} \end{aligned} \quad (2.43)$$

$$\begin{aligned} \frac{{}^N d}{{}^N dt} {}^N\mathbf{H}^{R_i/R_i^*} &= \frac{{}^{R_i} d}{{}^{R_i} dt} {}^N\mathbf{H}^{R_i/R_i^*} + {}^N\boldsymbol{\omega}^{R_i} \times {}^N\mathbf{H}^{R_i/R_i^*} \\ &= \frac{{}^{R_i} d}{{}^{R_i} dt} \left( \mathbf{I}^{R_i/R_i^*} \cdot {}^N\boldsymbol{\omega}^{R_i} \right) + {}^N\boldsymbol{\omega}^{R_i} \times \left( \mathbf{I}^{R_i/R_i^*} \cdot {}^N\boldsymbol{\omega}^{R_i} \right) \\ &= \underline{\mathbf{0}} \cdot {}^N\boldsymbol{\omega}^{R_i} + \mathbf{I}^{R_i/R_i^*} \cdot {}^N\boldsymbol{\alpha}^{R_i} + {}^N\boldsymbol{\omega}^{R_i} \times \mathbf{I}^{R_i/R_i^*} \cdot {}^N\boldsymbol{\omega}^{R_i} \end{aligned} \quad (2.44)$$

but

$$\begin{aligned}
{}^N\boldsymbol{\alpha}^{R_i} &= \frac{{}^N d}{dt} {}^N\boldsymbol{\omega}^{R_i} = \frac{{}^B d}{dt} {}^N\boldsymbol{\omega}^{R_i} + {}^N\boldsymbol{\omega}^B \times {}^N\boldsymbol{\omega}^{R_i} \\
&= \frac{{}^B d}{dt} ({}^N\boldsymbol{\omega}^B + {}^B\boldsymbol{\omega}^{R_i}) + {}^N\boldsymbol{\omega}^B \times ({}^N\boldsymbol{\omega}^B + {}^B\boldsymbol{\omega}^{R_i}) \\
&= {}^N\boldsymbol{\alpha}^B + \frac{{}^B d}{dt} {}^B\boldsymbol{\omega}^{R_i} + {}^N\boldsymbol{\omega}^B \times {}^B\boldsymbol{\omega}^{R_i} \\
&= \begin{cases} {}^N\boldsymbol{\alpha}^B + \dot{u}_{2i+2}\hat{\mathbf{b}}_i + {}^N\boldsymbol{\omega}^B \times u_{2i+2}\hat{\mathbf{b}}_i & (i = 1, 2, 3) \\ {}^N\boldsymbol{\alpha}^B + \dot{u}_{2i-3}\hat{\mathbf{b}}_{i-3} + {}^N\boldsymbol{\omega}^B \times u_{2i-3}\hat{\mathbf{b}}_{i-3} & (i = 4, 5, 6) \end{cases} \quad (2.45)
\end{aligned}$$

so

$$\begin{aligned}
\underline{\mathbf{I}}^{R_i/R_i^*} \cdot {}^N\boldsymbol{\alpha}^{R_i} &= \begin{cases} \left[ J\hat{\mathbf{b}}_i\hat{\mathbf{b}}_i + K(\underline{\mathbf{U}} - \hat{\mathbf{b}}_i\hat{\mathbf{b}}_i) \right] \cdot {}^N\boldsymbol{\alpha}^{R_i} & (i = 1, 2, 3) \\ \left[ J\hat{\mathbf{b}}_{i-3}\hat{\mathbf{b}}_{i-3} + K(\underline{\mathbf{U}} - \hat{\mathbf{b}}_{i-3}\hat{\mathbf{b}}_{i-3}) \right] \cdot {}^N\boldsymbol{\alpha}^{R_i} & (i = 4, 5, 6) \end{cases} \\
&= \begin{cases} J \left( {}^N\boldsymbol{\alpha}^B \cdot \hat{\mathbf{b}}_i + \dot{u}_{2i+2} + 0 \right) \hat{\mathbf{b}}_i + K(\underline{\mathbf{U}} - \hat{\mathbf{b}}_i\hat{\mathbf{b}}_i) \cdot {}^N\boldsymbol{\alpha}^{R_i} \\ J \left( {}^N\boldsymbol{\alpha}^B \cdot \hat{\mathbf{b}}_{i-3} + \dot{u}_{2i-3} + 0 \right) \hat{\mathbf{b}}_{i-3} + K(\underline{\mathbf{U}} - \hat{\mathbf{b}}_{i-3}\hat{\mathbf{b}}_{i-3}) \cdot {}^N\boldsymbol{\alpha}^{R_i} \end{cases} \\
&= \begin{cases} J(\dot{u}_i + \dot{u}_{2i+2})\hat{\mathbf{b}}_i + K(\underline{\mathbf{U}} - \hat{\mathbf{b}}_i\hat{\mathbf{b}}_i) \cdot {}^N\boldsymbol{\alpha}^{R_i} & (i = 1, 2, 3) \\ J(\dot{u}_{i-3} + \dot{u}_{2i-3})\hat{\mathbf{b}}_{i-3} + K(\underline{\mathbf{U}} - \hat{\mathbf{b}}_{i-3}\hat{\mathbf{b}}_{i-3}) \cdot {}^N\boldsymbol{\alpha}^{R_i} & (i = 4, 5, 6) \end{cases} \quad (2.46)
\end{aligned}$$

and

$$\begin{aligned}
{}^N\boldsymbol{\omega}^{R_i} \times \underline{\mathbf{I}}^{R_i/R_i^*} \cdot {}^N\boldsymbol{\omega}^{R_i} &= \begin{cases} {}^N\boldsymbol{\omega}^{R_i} \times \left[ (J - K)(u_i + u_{2i+2})\hat{\mathbf{b}}_i + K{}^N\boldsymbol{\omega}^{R_i} \right] & (i = 1, 2, 3) \\ {}^N\boldsymbol{\omega}^{R_i} \times \left[ (J - K)(u_{i-3} + u_{2i-3})\hat{\mathbf{b}}_{i-3} + K{}^N\boldsymbol{\omega}^{R_i} \right] & (i = 4, 5, 6) \end{cases} \\
&= \begin{cases} (J - K)(u_i + u_{2i+2}){}^N\boldsymbol{\omega}^{R_i} \times \hat{\mathbf{b}}_i & (i = 1, 2, 3) \\ (J - K)(u_{i-3} + u_{2i-3}){}^N\boldsymbol{\omega}^{R_i} \times \hat{\mathbf{b}}_{i-3} & (i = 4, 5, 6) \end{cases} \quad (2.47)
\end{aligned}$$

Therefore, substituting from Eqs. (2.47) and (2.46) into (2.44), one obtains

$$\begin{aligned}
\frac{{}^N d}{dt} {}^N\mathbf{H}^{R_i/R_i^*} &= \begin{cases} J(\dot{u}_i + \dot{u}_{2i+2})\hat{\mathbf{b}}_i + K(\underline{\mathbf{U}} - \hat{\mathbf{b}}_i\hat{\mathbf{b}}_i) \cdot {}^N\boldsymbol{\alpha}^{R_i} + (J - K)(u_i + u_{2i+2}){}^N\boldsymbol{\omega}^{R_i} \times \hat{\mathbf{b}}_i & (i = 1, 2, 3) \\ J(\dot{u}_{i-3} + \dot{u}_{2i-3})\hat{\mathbf{b}}_{i-3} + K(\underline{\mathbf{U}} - \hat{\mathbf{b}}_{i-3}\hat{\mathbf{b}}_{i-3}) \cdot {}^N\boldsymbol{\alpha}^{R_i} + (J - K)(u_{i-3} + u_{2i-3}){}^N\boldsymbol{\omega}^{R_i} \times \hat{\mathbf{b}}_{i-3} & (i = 4, 5, 6) \end{cases} \quad (2.48)
\end{aligned}$$

Now write  $\mathbf{M}$  as

$$\mathbf{M} = M_1\hat{\mathbf{b}}_1 + M_2\hat{\mathbf{b}}_2 + M_3\hat{\mathbf{b}}_3 \quad (2.49)$$

and let unit vectors  $\hat{\mathbf{b}}_1$ ,  $\hat{\mathbf{b}}_2$ , and  $\hat{\mathbf{b}}_3$  be parallel to central principal axes of inertia of  $S$ , so that

$$\underline{\mathbf{I}}^{S/S^*} = I_1\hat{\mathbf{b}}_1\hat{\mathbf{b}}_1 + I_2\hat{\mathbf{b}}_2\hat{\mathbf{b}}_2 + I_3\hat{\mathbf{b}}_3\hat{\mathbf{b}}_3 \quad (2.50)$$

where  $I_1$ ,  $I_2$ , and  $I_3$  are central principal moments of inertia of  $S$ .

By inspecting Eqs. (2.2), (2.34), and (2.4), one can construct a table of partial angular velocities and partial velocities necessary for forming scalar relationships from Eqs. (2.28). Upon referring to

Table 2.1: Partial Angular Velocities and Partial Velocities for Complex Gyrostat

$r$	1	2	3	4	5	6	7	8	9	10	11	12
${}^N\boldsymbol{\omega}_r^B$	$\hat{\mathbf{b}}_1$	$\hat{\mathbf{b}}_2$	$\hat{\mathbf{b}}_3$	$\mathbf{0}$								
${}^B\boldsymbol{\omega}_r^{R_1}$	$\mathbf{0}$	$\mathbf{0}$	$\mathbf{0}$	$\hat{\mathbf{b}}_1$	$\mathbf{0}$							
${}^B\boldsymbol{\omega}_r^{R_2}$	$\mathbf{0}$	$\mathbf{0}$	$\mathbf{0}$	$\mathbf{0}$	$\mathbf{0}$	$\hat{\mathbf{b}}_2$	$\mathbf{0}$	$\mathbf{0}$	$\mathbf{0}$	$\mathbf{0}$	$\mathbf{0}$	$\mathbf{0}$
${}^B\boldsymbol{\omega}_r^{R_3}$	$\mathbf{0}$	$\hat{\mathbf{b}}_3$	$\mathbf{0}$	$\mathbf{0}$	$\mathbf{0}$	$\mathbf{0}$						
${}^B\boldsymbol{\omega}_r^{R_4}$	$\mathbf{0}$	$\mathbf{0}$	$\mathbf{0}$	$\mathbf{0}$	$\hat{\mathbf{b}}_1$	$\mathbf{0}$						
${}^B\boldsymbol{\omega}_r^{R_5}$	$\mathbf{0}$	$\mathbf{0}$	$\mathbf{0}$	$\mathbf{0}$	$\mathbf{0}$	$\mathbf{0}$	$\hat{\mathbf{b}}_2$	$\mathbf{0}$	$\mathbf{0}$	$\mathbf{0}$	$\mathbf{0}$	$\mathbf{0}$
${}^B\boldsymbol{\omega}_r^{R_6}$	$\mathbf{0}$	$\hat{\mathbf{b}}_3$	$\mathbf{0}$	$\mathbf{0}$	$\mathbf{0}$							
${}^N\mathbf{v}_r^{S^*}$	$\mathbf{0}$	$\hat{\mathbf{n}}_1$	$\hat{\mathbf{n}}_2$	$\hat{\mathbf{n}}_3$								

Table 2.1, it is evident that the terms involving  ${}^N\mathbf{v}_r^{S^*}$  and  ${}^B\boldsymbol{\omega}_r^{R_i}$  ( $i = 1, \dots, 6$ ) contribute nothing to equations of motion (2.28) for  $r = 1, 2$ , and  $3$ . Substituting from Eqs. (2.50), (2.49), (2.42), and (2.40) into (2.28), one obtains

$$I_1\dot{u}_1 + J(\dot{u}_4 + \dot{u}_5) = (I_2 - I_3)u_2u_3 - J[u_2(u_8 + u_9) - u_3(u_6 + u_7)] + M_1 \quad (2.51)$$

$$I_2\dot{u}_2 + J(\dot{u}_6 + \dot{u}_7) = (I_3 - I_1)u_1u_3 - J[u_3(u_4 + u_5) - u_1(u_8 + u_9)] + M_2 \quad (2.52)$$

$$I_3\dot{u}_3 + J(\dot{u}_8 + \dot{u}_9) = (I_1 - I_2)u_1u_2 - J[u_1(u_6 + u_7) - u_2(u_4 + u_5)] + M_3 \quad (2.53)$$

It is also apparent from Table 2.1 that  ${}^N\mathbf{v}_r^{S^*}$  and  ${}^N\boldsymbol{\omega}_r^B$  contribute nothing to Eqs. (2.28) for  $r = 4, \dots, 9$ , and substitution from Eqs. (2.48) into (2.28) yields

$$J(\dot{u}_1 + \dot{u}_4) = \left(\mathbf{M}_1 + \mathbf{M}^{B/R_1}\right) \cdot \hat{\mathbf{b}}_1 \quad (2.54)$$

$$J(\dot{u}_1 + \dot{u}_5) = \left(\mathbf{M}_4 + \mathbf{M}^{B/R_4}\right) \cdot \hat{\mathbf{b}}_1 \quad (2.55)$$

$$J(\dot{u}_2 + \dot{u}_6) = \left(\mathbf{M}_2 + \mathbf{M}^{B/R_2}\right) \cdot \hat{\mathbf{b}}_2 \quad (2.56)$$

$$J(\dot{u}_2 + \dot{u}_7) = \left(\mathbf{M}_5 + \mathbf{M}^{B/R_5}\right) \cdot \hat{\mathbf{b}}_2 \quad (2.57)$$

$$J(\dot{u}_3 + \dot{u}_8) = \left(\mathbf{M}_3 + \mathbf{M}^{B/R_3}\right) \cdot \hat{\mathbf{b}}_3 \quad (2.58)$$

$$J(\dot{u}_3 + \dot{u}_9) = \left(\mathbf{M}_6 + \mathbf{M}^{B/R_6}\right) \cdot \hat{\mathbf{b}}_3 \quad (2.59)$$

Although translational equations of motion are not used in what follows, they are obtained easily from differentiation of Eqs. (2.4) with respect to time in  $N$ , and from Eqs. (2.28) with  $r = 10, 11$ , and  $12$ , and are simply

$$m_S\dot{u}_r = F_{r-9} \quad (r = 10, 11, 12) \quad (2.60)$$

where

$$\mathbf{F} = F_1\hat{\mathbf{n}}_1 + F_2\hat{\mathbf{n}}_2 + F_3\hat{\mathbf{n}}_3 \quad (2.61)$$

Eqs. (2.51)–(2.60) are thus a complete set of nonlinear dynamical equations of motion for a complex gyrostat composed of a body  $B$  and six axisymmetric rotors  $R_1, \dots, R_6$  whose mass centers and spin axes are fixed in  $B$ ; the rotors are arranged in pairs, with the spin axes in each pair parallel to each other and to a central principal axis of inertia of the gyrostat.

Eqs. (2.51)–(2.59) exhibit dynamic coupling; numerical solution of these differential equations can proceed more efficiently when the equations are decoupled, and this is accomplished easily by substituting from, for example, Eqs. (2.54) and (2.55) into (2.51). Consequently, Eqs. (2.51)–(2.53) give way to

$$(I_1 - 2J)\dot{u}_1 = (I_2 - I_3)u_2u_3 - J[u_2(u_8 + u_9) - u_3(u_6 + u_7)] + M_1 - \left(\mathbf{M}_1 + \mathbf{M}^{B/R_1} + \mathbf{M}_4 + \mathbf{M}^{B/R_4}\right) \cdot \hat{\mathbf{b}}_1 \quad (2.62)$$

$$(I_2 - 2J)\dot{u}_2 = (I_3 - I_1)u_1u_3 - J[u_3(u_4 + u_5) - u_1(u_8 + u_9)] + M_2 - \left(\mathbf{M}_2 + \mathbf{M}^{B/R_2} + \mathbf{M}_5 + \mathbf{M}^{B/R_5}\right) \cdot \hat{\mathbf{b}}_2 \quad (2.63)$$

$$(I_3 - 2J)\dot{u}_3 = (I_1 - I_2)u_1u_2 - J[u_1(u_6 + u_7) - u_2(u_4 + u_5)] + M_3 - \left(\mathbf{M}_3 + \mathbf{M}^{B/R_3} + \mathbf{M}_6 + \mathbf{M}^{B/R_6}\right) \cdot \hat{\mathbf{b}}_3 \quad (2.64)$$

which yield  $\dot{u}_1$ ,  $\dot{u}_2$ , and  $\dot{u}_3$  effortlessly and, with these in hand,  $\dot{u}_4, \dots, \dot{u}_9$  are obtained straightforwardly from Eqs. (2.54)–(2.59).

In Sec. 3.7 of Ref. [16], Kane, Likins, and Levinson give rotational equations of motion for a simple gyrostat, where their body  $A$  plays the part of  $B$  in the preceding discussion. Eqs. (3.7.28)–(3.7.31) are obtained by supposing the spin axis of the rotor to be parallel to the third central principal axis of inertia of the gyrostat, therefore Kane's unit vector  $\boldsymbol{\beta}$  plays the part of  $\hat{\mathbf{b}}_3$ , and  $B$  plays the part of rotor  $R_3$  (or  $R_6$ ). To show the correspondence between the aforementioned equations and Eqs. (2.51)–(2.59), note that  $\omega_1$ ,  $\omega_2$ , and  $\omega_3$  play the parts of  $u_1$ ,  $u_2$ , and  $u_3$  respectively, that  ${}^A\omega^B$  plays the part of  $u_8$ , and set generalized speeds  $u_4, \dots, u_7$  and  $u_9$  and their time derivatives to zero. Eqs. (2.51), (2.52), and (2.53) then give way to

$$I_1\dot{u}_1 = (I_2 - I_3)u_2u_3 - Ju_2u_8 + M_1 \quad (2.65)$$

$$I_2\dot{u}_2 = (I_3 - I_1)u_1u_3 + Ju_1u_8 + M_2 \quad (2.66)$$

$$I_3\dot{u}_3 = (I_1 - I_2)u_1u_2 - J\dot{u}_8 + M_3 \quad (2.67)$$

which are identical to Eqs. (3.7.29)–(3.7.31) of Ref. [16]. In the absence of rotors  $R_1$ ,  $R_2$ ,  $R_4$ ,  $R_5$ , and  $R_6$ , Eq. (2.58) is the only one of Eqs. (2.54)–(2.59) that remains applicable. Solving Eq. (2.67) for  $\dot{u}_3$  and then substituting from the result into (2.58), one obtains

$$\left(1 - \frac{J}{I_3}\right)\dot{u}_8 = \frac{\left(\mathbf{M}_3 + \mathbf{M}^{B/R_3}\right) \cdot \hat{\mathbf{b}}_3}{J} - \frac{(I_1 - I_2)u_1u_2 + M_3}{I_3} \quad (2.68)$$

which is the same as Eq. (3.7.28) in Ref. [16] provided the external torque  $\mathbf{M}_3$  acting on the rotor vanishes, or, to be more precise, the dot product  $\mathbf{M}_3 \cdot \hat{\mathbf{b}}_3$  vanishes. The disappearance of this dot product is perfectly reasonable if the rotor does not possess a magnetic dipole moment and is housed inside  $B$  where it is protected from the action of aerodynamic forces, in which case the principal contribution to  $\mathbf{M}_3$  is gravitational moment exerted by the celestial body about which the gyrostat orbits; an expression for an often used approximation of gravitational moment is given in Eq. (2.6.8) of Ref. [16], where it becomes clear that the dot product in question vanishes because  $\hat{\mathbf{b}}_3$  is parallel to an axis of symmetry of the rotor.

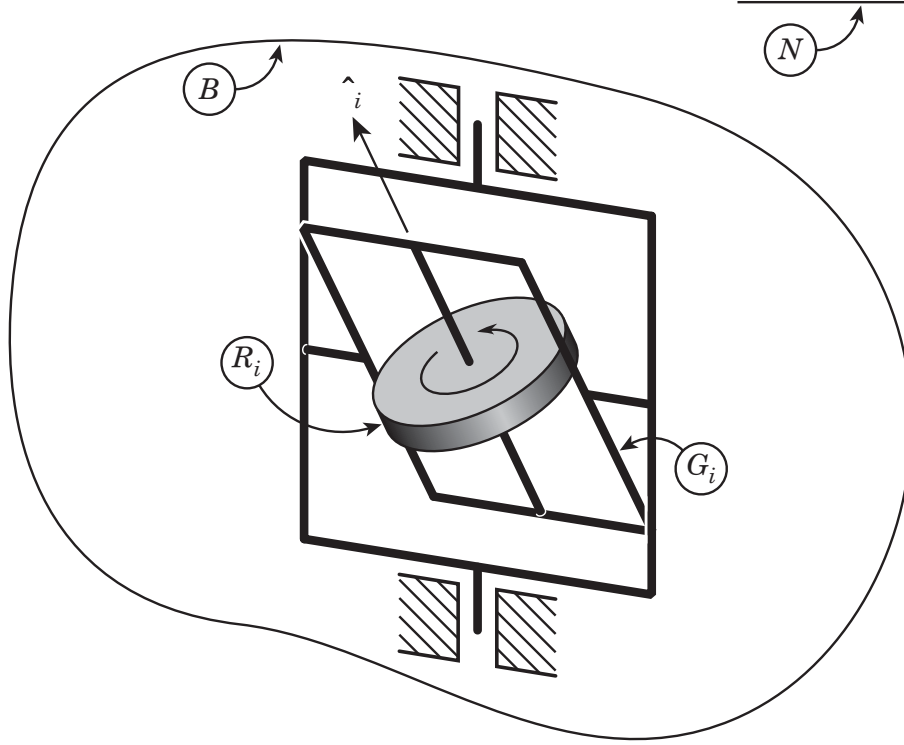


Figure 2.3: Spacecraft with CMG

## 2.3 Dynamical Equations for Spacecraft with CMGs

In Sec. 2.2, Eqs. (2.28) are tailored to describe the motion of a spacecraft carrying flywheels and no CMGs; in this section, the important case of a spacecraft with CMGs and no flywheels is examined ( $\mathcal{F} = 0$ ,  $\rho = \mathcal{C}$ ). In Ref. [6], Wie et al. develop a scheme for controlling a spacecraft's attitude and managing the angular momentum of a collection of CMGs, and the results are applied to a space station. Under certain conditions Eqs. (2.28) can be shown to give rise to the relationships employed in Ref. [6] as a basis for control law design.

One may recall that Eqs. (2.23) are developed differently from Eqs. (2.25) because the central inertia dyadic of a flywheel rotor does not change with respect to time in  $B$  whereas that of a CMG rotor does; consequently, the second sum in Eqs. (2.28) is made up entirely of contributions from CMGs but not from flywheels. Each CMG rotor  $R_i$  is attached to an inner gimbal  $G_i$  (treated as massless) as shown in Fig. 2.3; the axis of symmetry of  $R_i$  remains fixed in  $G_i$ , and the relative angular speed  $\Omega$  of  $R_i$  in  $G_i$  remains constant. The angular velocity of  $R_i$  in  $B$  can thus be expressed as

$${}^B\boldsymbol{\omega}^{R_i} = {}^B\boldsymbol{\omega}^{G_i} + {}^{G_i}\boldsymbol{\omega}^{R_i} = {}^B\boldsymbol{\omega}^{G_i} + \Omega\hat{\boldsymbol{\gamma}}_i \quad (i = \mathcal{F} + 1, \dots, \rho) \quad (2.69)$$

where  $\hat{\boldsymbol{\gamma}}_i$  is a unit vector parallel to the axis of symmetry of  $R_i$ , and the angular velocity  ${}^B\boldsymbol{\omega}^{G_i}$  of the inner gimbal in  $B$  accounts for the motion relative to  $G_i$  and to  $B$  of an outer gimbal (shown, but not labeled in Fig. 2.3) if one is present. The central inertia dyadics of the CMG rotors may be expressed as

$$\underline{\mathbf{I}}^{R_i/R_i^*} = \mathcal{J}\hat{\boldsymbol{\gamma}}_i\hat{\boldsymbol{\gamma}}_i + \mathcal{K}(\underline{\mathbf{U}} - \hat{\boldsymbol{\gamma}}_i\hat{\boldsymbol{\gamma}}_i) \quad (i = \mathcal{F} + 1, \dots, \rho) \quad (2.70)$$

where  $\mathcal{J}$  and  $\mathcal{K}$  are the central principal moments of inertia of a CMG rotor for, respectively, the axis of symmetry, and any line perpendicular to the axis of symmetry. With the aid of Eqs. (2.69) and (2.70), the second sum in Eqs. (2.28) can be written as

$$\begin{aligned}
& \sum_{i=\mathcal{F}+1}^{\rho} \left( {}^B\boldsymbol{\omega}^{R_i} \times \underline{\mathbf{I}}^{R_i/R_i^*} - \underline{\mathbf{I}}^{R_i/R_i^*} \times {}^B\boldsymbol{\omega}^{R_i} \right) \\
&= \sum_{i=\mathcal{F}+1}^{\rho} \left\{ {}^B\boldsymbol{\omega}^{R_i} \times [(\mathcal{J} - \mathcal{K})\hat{\boldsymbol{\gamma}}_i\hat{\boldsymbol{\gamma}}_i + \mathcal{K}\underline{\mathbf{U}}] - [(\mathcal{J} - \mathcal{K})\hat{\boldsymbol{\gamma}}_i\hat{\boldsymbol{\gamma}}_i + \mathcal{K}\underline{\mathbf{U}}] \times {}^B\boldsymbol{\omega}^{R_i} \right\} \\
&= \sum_{i=\mathcal{F}+1}^{\rho} \left[ (\mathcal{J} - \mathcal{K}) ({}^B\boldsymbol{\omega}^{R_i} \times \hat{\boldsymbol{\gamma}}_i\hat{\boldsymbol{\gamma}}_i - \hat{\boldsymbol{\gamma}}_i\hat{\boldsymbol{\gamma}}_i \times {}^B\boldsymbol{\omega}^{R_i}) + \mathcal{K} ({}^B\boldsymbol{\omega}^{R_i} \times \underline{\mathbf{U}} - \underline{\mathbf{U}} \times {}^B\boldsymbol{\omega}^{R_i}) \right] \\
&= \sum_{i=\mathcal{F}+1}^{\rho} \left\{ (\mathcal{J} - \mathcal{K}) [({}^B\boldsymbol{\omega}^{G_i} + \Omega\hat{\boldsymbol{\gamma}}_i) \times \hat{\boldsymbol{\gamma}}_i\hat{\boldsymbol{\gamma}}_i - \hat{\boldsymbol{\gamma}}_i\hat{\boldsymbol{\gamma}}_i \times ({}^B\boldsymbol{\omega}^{G_i} + \Omega\hat{\boldsymbol{\gamma}}_i)] + \mathcal{K}\underline{\mathbf{0}} \right\} \\
&= \sum_{i=\mathcal{F}+1}^{\rho} (\mathcal{J} - \mathcal{K}) ({}^B\boldsymbol{\omega}^{G_i} \times \hat{\boldsymbol{\gamma}}_i\hat{\boldsymbol{\gamma}}_i - \hat{\boldsymbol{\gamma}}_i\hat{\boldsymbol{\gamma}}_i \times {}^B\boldsymbol{\omega}^{G_i}) \tag{2.71}
\end{aligned}$$

where the zero dyadic  $\underline{\mathbf{0}}$  results because, for any vector  $\mathbf{v}$ , it can be shown that  $\mathbf{v} \times \underline{\mathbf{U}} = \underline{\mathbf{U}} \times \mathbf{v}$ .

Now, this second sum can be neglected in comparison to the first sum after considering typical numerical values involved in each. According to Ref. [21], p. 2.3-5, the International Space Station CMG rotor spin speed  $\Omega$  is constant, 6,600 rev/min or 691 rad/s. On p. 2.3-7, typical gimbal speeds are reported to be  $3.5 \times 10^{-3}$  rad/s (0.2 deg/s), with maximum gimbal speeds of  $5.4 \times 10^{-2}$  rad/s (3.1 deg/s), which gives an idea of the magnitude of  ${}^B\boldsymbol{\omega}^{G_i}$ . The central angular momentum of  $R_i$  in  $G_i$ ,  ${}^{G_i}\mathbf{H}^{R_i/R_i^*} = \underline{\mathbf{I}}^{R_i/R_i^*} \cdot {}^{G_i}\boldsymbol{\omega}^{R_i}$ , has a magnitude of  $\mathcal{J}\Omega = 4,745$  N-m-s (3,500 ft-lb<sub>f</sub>-s, often referred to as “the” momentum of a CMG) which is approximately the magnitude of  ${}^B\mathbf{H}^{R_i/R_i^*}$  since the gimbal speeds are so much less than the spin speed. From the values of momentum and spin speed, one may deduce that  $\mathcal{J} = 6.87$  kg-m<sup>2</sup>. When one compares the magnitude of  ${}^B\mathbf{H}^{R_i/R_i^*}$  that appears in the first sum to the product of  $\mathcal{J}$  and an approximate magnitude of  ${}^B\boldsymbol{\omega}^{G_i}$  that appears in the second sum, one finds that the former, 4,745 N-m-s, is some 4 orders of magnitude larger than the latter,  $(6.87 \text{ kg-m}^2)(5.4 \times 10^{-2} \text{ rad/s}) \approx 0.4$  N-m-s, and neglecting the second sum is easily justified.

The first sum in Eqs. (2.28) can be denoted by the vector  $\boldsymbol{\tau}$ ,

$$\begin{aligned}
\boldsymbol{\tau} &\triangleq \sum_{i=\mathcal{F}+1}^{\rho} \left( \frac{{}^B d}{dt} {}^B\mathbf{H}^{R_i/R_i^*} + {}^N\boldsymbol{\omega}^B \times {}^B\mathbf{H}^{R_i/R_i^*} \right) \\
&= \frac{{}^B d}{dt} \left( \sum_{i=\mathcal{F}+1}^{\rho} {}^B\mathbf{H}^{R_i/R_i^*} \right) + {}^N\boldsymbol{\omega}^B \times \left( \sum_{i=\mathcal{F}+1}^{\rho} {}^B\mathbf{H}^{R_i/R_i^*} \right) \tag{2.72}
\end{aligned}$$

where the term in parentheses, the resultant of the central angular momenta in  $B$  of all CMGs, can be defined as the vector  $\mathbf{h}$

$$\mathbf{h} \triangleq \sum_{i=\mathcal{F}+1}^{\rho} {}^B\mathbf{H}^{R_i/R_i^*} \tag{2.73}$$

and the time derivative of  $\mathbf{h}$  in  $B$  is thus

$$\dot{\mathbf{h}} \triangleq \frac{{}^B d}{dt} \mathbf{h} \tag{2.74}$$

Substitution from Eqs. (2.74) and (2.73) into (2.72) yields

$$\boldsymbol{\tau} = \dot{\mathbf{h}} + {}^N\boldsymbol{\omega}^B \times \mathbf{h} \quad (2.75)$$

which can be recognized as a vector form of Eqs. (3) in Ref. [6], three scalar equations that result from forming dot products between Eq. (2.75) and unit vectors  $\hat{\mathbf{b}}_1$ ,  $\hat{\mathbf{b}}_2$ , and  $\hat{\mathbf{b}}_3$ , fixed in  $B$  but not necessarily parallel to central principal axes of inertia of  $S$ . The measure numbers appearing in Eqs. (3) of Ref. [6] are related to the vectors in Eq. (2.75) as follows,  $\dot{h}_r \triangleq \dot{\mathbf{h}} \cdot \hat{\mathbf{b}}_r$ ,  $h_r \triangleq \mathbf{h} \cdot \hat{\mathbf{b}}_r$ ,  $\omega_r \triangleq {}^N\boldsymbol{\omega}^B \cdot \hat{\mathbf{b}}_r$ , and  $u_r \triangleq \boldsymbol{\tau} \cdot \hat{\mathbf{b}}_r$  [not to be confused with  $u_r$  defined in Eq. (2.2) here], ( $r = 1, 2, 3$ ).

Although  $\boldsymbol{\tau}$  represents in some sense the effect of CMGs on  $B$ , one must remember that it fails to account for those effects in the neglected second sum; furthermore  $\boldsymbol{\tau}$  is not the resultant moment of forces exerted by the CMGs on  $B$ , for this resultant is given by  $-\sum_{i=\mathcal{F}+1}^{\rho} \mathbf{M}^{B/R_i}$  by virtue of the law of action and reaction.

In addition to Eqs. (3), the control law design in Ref. [6] is based upon the three scalar Eqs. (1) appearing therein, and one may obtain these from Eqs. (2.28) by reasoning in the following manner. First, the term involving  ${}^N\mathbf{v}_r^{S^*}$  contributes nothing for  $r = 1, 2, 3$ , nor does the term containing  ${}^B\boldsymbol{\omega}_r^{R_i}$ . Although generalized speeds corresponding to angular gimbal speeds have not been introduced, the partial angular velocities  ${}^B\boldsymbol{\omega}_r^{R_i}$  of the CMG rotors in  $B$  vanish for  $r = 1, 2, 3$ , just as they do in the case of flywheel rotors (see Table 2.1). Next, the second sum is neglected as before and substitution is made from Eq. (2.72) into (2.28). Since  ${}^N\boldsymbol{\omega}_r^B = \hat{\mathbf{b}}_r$ , the first three of Eqs. (2.28) become

$$\left( \mathbf{I}^{S/S^*} \cdot {}^N\boldsymbol{\alpha}^B + {}^N\boldsymbol{\omega}^B \times \mathbf{I}^{S/S^*} \cdot {}^N\boldsymbol{\omega}^B + \boldsymbol{\tau} \right) \cdot \hat{\mathbf{b}}_r = \mathbf{M} \cdot \hat{\mathbf{b}}_r \quad (r = 1, 2, 3) \quad (2.76)$$

The purpose of control laws such as the one designed in Ref. [6] is to determine what  $\boldsymbol{\tau}$  should be in order to control the attitude of  $B$ , and minimize the magnitude of  $\mathbf{h}$ . One may regard  $\mathbf{M}$  as the sum of two terms, the gravitational moment exerted on  $S$ , and all other contributions to  $\mathbf{M}$ . Using an approximate expression for gravitational moment such as that given by Eq. (2.6.3) in Ref. [16], and the vector  $\mathbf{w}$  to represent the remaining contributions, Eqs. (2.76) can be rewritten as

$$\left( \mathbf{I}^{S/S^*} \cdot {}^N\boldsymbol{\alpha}^B \right) \cdot \hat{\mathbf{b}}_r = \left( -{}^N\boldsymbol{\omega}^B \times \mathbf{I}^{S/S^*} \cdot {}^N\boldsymbol{\omega}^B + 3n^2\hat{\mathbf{r}} \times \mathbf{I}^{S/S^*} \cdot \hat{\mathbf{r}} - \boldsymbol{\tau} + \mathbf{w} \right) \cdot \hat{\mathbf{b}}_r \quad (r = 1, 2, 3) \quad (2.77)$$

which are seen to be identical to Eqs. (1) of Ref. [6] once the measure numbers appearing therein are defined as  $\dot{\omega}_i \triangleq {}^N\boldsymbol{\alpha}^B \cdot \hat{\mathbf{b}}_r$ ,  $\omega_r \triangleq {}^N\boldsymbol{\omega}^B \cdot \hat{\mathbf{b}}_r$ ,  $c_r \triangleq \hat{\mathbf{r}} \cdot \hat{\mathbf{b}}_r$ ,  $u_r \triangleq \boldsymbol{\tau} \cdot \hat{\mathbf{b}}_r$ , and  $w_r \triangleq \mathbf{w} \cdot \hat{\mathbf{b}}_r$  ( $r = 1, 2, 3$ ). Here the symbol  $n$  represents angular speed of a circular orbit, rather than the number of degrees of freedom of a system; this will be the meaning of  $n$  henceforth when used in an equation, unless it is used as the limit of an index such as  $r$ , or in the index of a generalized speed  $u$  or its time derivative. The moments and products of inertia appearing in Eqs. (1) are defined as  $I_{rs} \triangleq \hat{\mathbf{b}}_r \cdot \mathbf{I}^{S/S^*} \cdot \hat{\mathbf{b}}_s$  ( $r, s = 1, 2, 3$ ); their absolute values range from  $0.15 \times 10^6$  to  $80 \times 10^6$  kg-m<sup>2</sup> in Ref. [6], and are currently expected to be in the range of  $1 \times 10^6$  to  $200 \times 10^6$  kg-m<sup>2</sup> for the Assembly Complete configuration of the International Space Station. Reorientation of a few CMG rotors with central inertia scalars on the order of  $\mathcal{J} = 6.87$  kg-m<sup>2</sup> changes the mass distribution of  $S$  by a negligible amount; therefore,  $I_{rs}$  may be regarded as constants although this is in fact an approximation.

A note is now in order regarding the number of differential equations (2.28) on the one hand, and, on the other hand, the number of differential equations employed in the approach of Ref. [6]. The number of dynamical equations of motion (2.28) is equal to the number  $n$  of degrees of freedom

of  $S$  in  $N$ , exactly the number required to specify the motion of  $S$  completely. Three of these equations describe the translation of  $S^*$ , and the remaining  $n - 3$  govern rotational motions of  $B$  and the CMG rotors. In contrast, rotational motion is represented in Ref. [6] by just 6 differential equations —3 of Eqs. (2.77) and 3 of Eqs. (2.75)— no matter what is the actual value of  $n$ .

## 2.4 Approximate Equations for a Spacecraft with Flywheels and CMGs

In Sec. 2.2, Eqs. (2.28) are applied to a spacecraft carrying only flywheels, whereas they are applied in Sec. 2.3 to a spacecraft containing only CMGs. The results from both Sections are combined here in order to produce equations of motion applicable to a spacecraft with both kinds of attitude control devices; the equations thus formed must be considered approximate as they include the considerations set forth in Sec. 2.3.

Even though the second sum in Eqs. (2.28) receives no contribution from the flywheel rotors, one can deal with their contribution to the first sum by forming counterparts to Eqs. (2.72)–(2.75),

$$\bar{\boldsymbol{\tau}} \triangleq \frac{B}{dt} \left( \sum_{i=1}^{\mathcal{F}} B \mathbf{H}^{R_i/R_i^*} \right) + {}^N \boldsymbol{\omega}^B \times \left( \sum_{i=1}^{\mathcal{F}} B \mathbf{H}^{R_i/R_i^*} \right) \quad (2.78)$$

$$\mathbf{H} \triangleq \sum_{i=1}^{\mathcal{F}} B \mathbf{H}^{R_i/R_i^*} \quad (2.79)$$

$$\dot{\mathbf{H}} \triangleq \frac{B}{dt} \mathbf{H} \quad (2.80)$$

and

$$\bar{\boldsymbol{\tau}} = \dot{\mathbf{H}} + {}^N \boldsymbol{\omega}^B \times \mathbf{H} \quad (2.81)$$

In view of Eqs. (2.39), (2.42), and (2.40), the following definitions can be made:

$$H_1 \triangleq \mathbf{H} \cdot \hat{\mathbf{b}}_1 = J(u_4 + u_5), \quad H_2 \triangleq \mathbf{H} \cdot \hat{\mathbf{b}}_2 = J(u_6 + u_7), \quad H_3 \triangleq \mathbf{H} \cdot \hat{\mathbf{b}}_3 = J(u_8 + u_9) \quad (2.82)$$

$$\dot{H}_1 \triangleq \dot{\mathbf{H}} \cdot \hat{\mathbf{b}}_1 = J(\dot{u}_4 + \dot{u}_5), \quad \dot{H}_2 \triangleq \dot{\mathbf{H}} \cdot \hat{\mathbf{b}}_2 = J(\dot{u}_6 + \dot{u}_7), \quad \dot{H}_3 \triangleq \dot{\mathbf{H}} \cdot \hat{\mathbf{b}}_3 = J(\dot{u}_8 + \dot{u}_9) \quad (2.83)$$

$$\bar{\tau}_1 \triangleq \bar{\boldsymbol{\tau}} \cdot \hat{\mathbf{b}}_1 = \dot{H}_1 + u_2 H_3 - u_3 H_2 \quad (2.84)$$

$$\bar{\tau}_2 \triangleq \bar{\boldsymbol{\tau}} \cdot \hat{\mathbf{b}}_2 = \dot{H}_2 + u_3 H_1 - u_1 H_3 \quad (2.85)$$

$$\bar{\tau}_3 \triangleq \bar{\boldsymbol{\tau}} \cdot \hat{\mathbf{b}}_3 = \dot{H}_3 + u_1 H_2 - u_2 H_1 \quad (2.86)$$

Using the same reasoning that preceded Eqs. (2.77), and substituting from Eq. (2.78) as well as (2.72), the first three of Eqs. (2.28) become

$$\begin{aligned} & \left( \underline{\mathbf{I}}^{S/S^*} \cdot {}^N \boldsymbol{\alpha}^B \right) \cdot \hat{\mathbf{b}}_r \\ & = \left( - {}^N \boldsymbol{\omega}^B \times \underline{\mathbf{I}}^{S/S^*} \cdot {}^N \boldsymbol{\omega}^B + 3n^2 \hat{\mathbf{r}} \times \underline{\mathbf{I}}^{S/S^*} \cdot \hat{\mathbf{r}} - \boldsymbol{\tau} - \bar{\boldsymbol{\tau}} + \mathbf{w} \right) \cdot \hat{\mathbf{b}}_r \quad (r = 1, 2, 3) \end{aligned} \quad (2.87)$$

In the term representing the gravitational moment, the coefficient  $n^2$  results from an assumption that  $S^*$  travels in a circular orbit about the mass center  $P^*$  of a primary celestial body. Unit vector  $\hat{\mathbf{r}}$  has the direction of the position vector from  $P^*$  to  $S^*$ , and is fixed in a local-horizontal-local-vertical reference frame  $L$  whose angular velocity  ${}^N\boldsymbol{\omega}^L$  in  $N$  has a magnitude of  $n$ .

In addition to the dynamical equations of motion dealt with thus far, kinematical differential equations for variables describing the orientation of  $B$  in some reference frame are required; it is convenient to choose  $L$  as this frame and to employ angles belonging to a body-three, 2-3-1 rotation sequence as set forth on p. 423 of Ref. [16]. The sequence is also known as pitch-yaw-roll, with the angles denoted by  $\theta_1$ ,  $\theta_2$ , and  $\theta_3$  respectively. An associated direction cosine matrix is given by

$$[{}^L C^B] = \begin{array}{cccc} & \hat{\mathbf{b}}_1 & \hat{\mathbf{b}}_2 & \hat{\mathbf{b}}_3 \\ \hat{\mathbf{i}}_1 & C_1 C_2 & S_3 S_1 - C_1 S_2 C_3 & C_1 S_2 S_3 + C_3 S_1 \\ \hat{\mathbf{i}}_2 & S_2 & C_2 C_3 & -C_2 S_3 \\ \hat{\mathbf{i}}_3 & -S_1 C_2 & S_1 S_2 C_3 + S_3 C_1 & C_3 C_1 - S_1 S_2 S_3 \end{array} \quad (2.88)$$

where  $S_1 \triangleq \sin \theta_1$ ,  $C_2 \triangleq \cos \theta_2$ , and so forth, and where  $\hat{\mathbf{i}}_1$ ,  $\hat{\mathbf{i}}_2$ , and  $\hat{\mathbf{i}}_3$  are a right-handed, mutually perpendicular set of unit vectors fixed in  $L$ , with  $\hat{\mathbf{i}}_3 \triangleq -\hat{\mathbf{r}}$ .  ${}^N\boldsymbol{\omega}^L$  is parallel to  $\hat{\mathbf{i}}_2$ ,

$${}^N\boldsymbol{\omega}^L = -n\hat{\mathbf{i}}_2 \quad (2.89)$$

According to p. 428 of Ref. [16], the angular velocity  ${}^L\boldsymbol{\omega}^B$  of  $B$  in  $L$  can be expressed as

$${}^L\boldsymbol{\omega}^B = (\dot{\theta}_1 S_2 + \dot{\theta}_3)\hat{\mathbf{b}}_1 + (\dot{\theta}_1 C_2 C_3 + \dot{\theta}_2 S_3)\hat{\mathbf{b}}_2 + (\dot{\theta}_2 C_3 - \dot{\theta}_1 C_2 S_3)\hat{\mathbf{b}}_3 \quad (2.90)$$

Consequently,

$$\begin{aligned} {}^N\boldsymbol{\omega}^B &= u_1 \hat{\mathbf{b}}_1 + u_2 \hat{\mathbf{b}}_2 + u_3 \hat{\mathbf{b}}_3 \\ &= {}^N\boldsymbol{\omega}^L + {}^L\boldsymbol{\omega}^B \\ &= (\dot{\theta}_1 S_2 + \dot{\theta}_3 - n S_2)\hat{\mathbf{b}}_1 + (\dot{\theta}_1 C_2 C_3 + \dot{\theta}_2 S_3 - n C_2 C_3)\hat{\mathbf{b}}_2 + (\dot{\theta}_2 C_3 - \dot{\theta}_1 C_2 S_3 + n C_2 S_3)\hat{\mathbf{b}}_3 \end{aligned} \quad (2.91)$$

from which three kinematical equations can be obtained,

$$\dot{\theta}_1 = \frac{(C_3 u_2 - S_3 u_3)}{C_2} + n, \quad \dot{\theta}_2 = S_3 u_2 + C_3 u_3, \quad \dot{\theta}_3 = u_1 + \frac{S_2(-C_3 u_2 + S_3 u_3)}{C_2} \quad (2.92)$$

If  $\hat{\mathbf{b}}_r$  are taken to be parallel to central principal axes of inertia of  $S$ , as they are in the latter part of Sec. 2.2, then Eqs. (2.87) give rise to three dynamical equations,

$$I_1 \dot{u}_1 = (I_3 - I_2)(3n^2 r_2 r_3 - u_2 u_3) - \tau_1 - \bar{\tau}_1 + w_1 \quad (2.93)$$

$$I_2 \dot{u}_2 = (I_1 - I_3)(3n^2 r_1 r_3 - u_1 u_3) - \tau_2 - \bar{\tau}_2 + w_2 \quad (2.94)$$

$$I_3 \dot{u}_3 = (I_2 - I_1)(3n^2 r_1 r_2 - u_1 u_2) - \tau_3 - \bar{\tau}_3 + w_3 \quad (2.95)$$

where  $\tau_i \triangleq \boldsymbol{\tau} \cdot \hat{\mathbf{b}}_i$ ,  $r_i \triangleq \hat{\mathbf{r}} \cdot \hat{\mathbf{b}}_i$  ( $i = 1, 2, 3$ ), and in view of Eqs. (2.88),

$$r_1 = S_1 C_2, \quad r_2 = -(S_1 S_2 C_3 + S_3 C_1), \quad r_3 = S_1 S_2 S_3 - C_3 C_1 \quad (2.96)$$

The purpose of developing a control law will be to determine values of  $\tau_i$  and  $\bar{\tau}_i$  ( $i = 1, 2, 3$ ) that best control the orientation of  $B$  in  $L$ , and minimize the magnitudes of  $\mathbf{h}$  and  $\mathbf{H}$ . In addition

to Eqs. (2.92) and (2.93)–(2.95), six more equations will be used, three of which are simply a rearrangement of Eqs. (2.84)–(2.86),

$$\dot{H}_1 = u_3 H_2 - u_2 H_3 + \bar{\tau}_1 \quad (2.97)$$

$$\dot{H}_2 = u_1 H_3 - u_3 H_1 + \bar{\tau}_2 \quad (2.98)$$

$$\dot{H}_3 = u_2 H_1 - u_1 H_2 + \bar{\tau}_3 \quad (2.99)$$

and three of which are analogous and obtained from Eq. (2.75),

$$\dot{h}_1 = u_3 h_2 - u_2 h_3 + \tau_1 \quad (2.100)$$

$$\dot{h}_2 = u_1 h_3 - u_3 h_1 + \tau_2 \quad (2.101)$$

$$\dot{h}_3 = u_2 h_1 - u_1 h_2 + \tau_3 \quad (2.102)$$

## 2.5 Linearized Equations for Control Law Design

A law for controlling the attitude of  $B$  with flywheels and CMGs can be developed from linearized forms of Eqs. (2.92)–(2.95) and (2.97)–(2.102). In the absence of  $\mathbf{w}$ ,  $\boldsymbol{\tau}$ , and  $\bar{\boldsymbol{\tau}}$  (meaning, for the last two vectors, that the resultant of momenta  $\mathbf{h}$  and  $\mathbf{H}$  vanish, rotor spin speeds do not change, and CMG gimbals do not move) it is possible for  $B$  to remain fixed in  $L$  with  $\hat{\mathbf{l}}_r$  having the same directions as  $\hat{\mathbf{b}}_r$ , parallel to central principal axes of inertia of  $S$ ; one may linearize “about” this condition by letting the orientation angles  $\theta_r$  ( $r = 1, 2, 3$ ) have nominal values of zero, and introducing perturbations  $\tilde{\theta}_1$ ,  $\tilde{\theta}_2$ , and  $\tilde{\theta}_3$  such that

$$\theta_1 = 0 + \tilde{\theta}_1, \quad \theta_2 = 0 + \tilde{\theta}_2, \quad \theta_3 = 0 + \tilde{\theta}_3 \quad (2.103)$$

In addition,  $\tilde{u}_1$ ,  $\tilde{u}_2$ , and  $\tilde{u}_3$  are introduced as perturbations of the angular speeds of  $B$  in  $N$ ,

$$u_1 = 0 + \tilde{u}_1, \quad u_2 = -n + \tilde{u}_2, \quad u_3 = 0 + \tilde{u}_3 \quad (2.104)$$

Similarly, we linearize “about”  $\mathbf{H} = \mathbf{h} = \mathbf{0}$  by introducing the following perturbations to  $H_r$  and  $h_r$  ( $r = 1, 2, 3$ ),

$$H_1 = 0 + \tilde{H}_1, \quad H_2 = 0 + \tilde{H}_2, \quad H_3 = 0 + \tilde{H}_3 \quad (2.105)$$

and

$$h_1 = 0 + \tilde{h}_1, \quad h_2 = 0 + \tilde{h}_2, \quad h_3 = 0 + \tilde{h}_3 \quad (2.106)$$

Differentiating Eqs. (2.103)–(2.106) with respect to time gives

$$\dot{\theta}_r = \dot{\tilde{\theta}}_r, \quad \dot{u}_r = \dot{\tilde{u}}_r, \quad \dot{H}_r = \dot{\tilde{H}}_r, \quad \dot{h}_r = \dot{\tilde{h}}_r, \quad (r = 1, 2, 3) \quad (2.107)$$

Kinematical differential Eqs. (2.92) are linearized by substituting from Eqs. (2.103) and (2.104), and discarding terms of second or higher degree in the perturbations. When the trigonometric functions of the attitude angles are expanded in power series, the linearization means

$$\sin \theta_r = \sin \tilde{\theta}_r \approx \tilde{\theta}_r, \quad \cos \theta_r = \cos \tilde{\theta}_r \approx 1, \quad (r = 1, 2, 3) \quad (2.108)$$

Therefore, Eqs. (2.92) become

$$\begin{aligned}\dot{\tilde{\theta}}_1 &= \frac{[1(\tilde{u}_2 - n) - \tilde{\theta}_3\tilde{u}_3]}{1} + n \\ &\approx \tilde{u}_2\end{aligned}\tag{2.109}$$

$$\begin{aligned}\dot{\tilde{\theta}}_2 &= \tilde{\theta}_3(\tilde{u}_2 - n) + 1\tilde{u}_3 \\ &\approx \tilde{u}_3 - n\tilde{\theta}_3\end{aligned}\tag{2.110}$$

$$\begin{aligned}\dot{\tilde{\theta}}_3 &= \tilde{u}_1 + \frac{\tilde{\theta}_2[-1(\tilde{u}_2 - n) + \tilde{\theta}_3\tilde{u}_3]}{1} \\ &\approx \tilde{u}_1 + n\tilde{\theta}_2\end{aligned}\tag{2.111}$$

Similarly, linearization of Eqs. (2.93)–(2.95) performed with the aid of Eqs. (2.108), (2.104), and (2.96) yields

$$\begin{aligned}I_1\dot{\tilde{u}}_1 &= (I_3 - I_2)\{3n^2[\tilde{\theta}_1\tilde{\theta}_2(1) + \tilde{\theta}_3(1)][(1)(1) - \tilde{\theta}_1\tilde{\theta}_2\tilde{\theta}_3] - (\tilde{u}_2 - n)(\tilde{u}_3)\} - \tau_1 - \bar{\tau}_1 + w_1 \\ &\approx (I_3 - I_2)(3n^2\tilde{\theta}_3 + n\tilde{u}_3) - \tau_1 - \bar{\tau}_1 + w_1\end{aligned}\tag{2.112}$$

$$\begin{aligned}I_2\dot{\tilde{u}}_2 &= (I_1 - I_3)\{3n^2\tilde{\theta}_1(1)[\tilde{\theta}_1\tilde{\theta}_2\tilde{\theta}_3 - (1)(1)] - \tilde{u}_1\tilde{u}_3\} - \tau_2 - \bar{\tau}_2 + w_2 \\ &\approx (I_3 - I_1)(3n^2\tilde{\theta}_1) - \tau_2 - \bar{\tau}_2 + w_2\end{aligned}\tag{2.113}$$

$$\begin{aligned}I_3\dot{\tilde{u}}_3 &= (I_2 - I_1)\{-3n^2\tilde{\theta}_1(1)[\tilde{\theta}_1\tilde{\theta}_2(1) + \tilde{\theta}_3(1)] - \tilde{u}_1(\tilde{u}_2 - n)\} - \tau_3 - \bar{\tau}_3 + w_3 \\ &\approx (I_2 - I_1)n\tilde{u}_1 - \tau_3 - \bar{\tau}_3 + w_3\end{aligned}\tag{2.114}$$

Upon appealing to Eqs. (2.104)–(2.107), the linearized forms of Eqs. (2.97)–(2.102) are

$$\begin{aligned}\dot{\tilde{H}}_1 &= \tilde{u}_3\tilde{H}_2 - (\tilde{u}_2 - n)\tilde{H}_3 + \bar{\tau}_1 \\ &\approx n\tilde{H}_3 + \bar{\tau}_1\end{aligned}\tag{2.115}$$

$$\begin{aligned}\dot{\tilde{H}}_2 &= \tilde{u}_1\tilde{H}_3 - \tilde{u}_3\tilde{H}_1 + \bar{\tau}_2 \\ &\approx \bar{\tau}_2\end{aligned}\tag{2.116}$$

$$\begin{aligned}\dot{\tilde{H}}_3 &= (\tilde{u}_2 - n)\tilde{H}_1 - \tilde{u}_1\tilde{H}_2 + \bar{\tau}_3 \\ &\approx -n\tilde{H}_1 + \bar{\tau}_3\end{aligned}\tag{2.117}$$

and

$$\begin{aligned}\dot{\tilde{h}}_1 &= \tilde{u}_3\tilde{h}_2 - (\tilde{u}_2 - n)\tilde{h}_3 + \tau_1 \\ &\approx n\tilde{h}_3 + \tau_1\end{aligned}\tag{2.118}$$

$$\begin{aligned}\dot{\tilde{h}}_2 &= \tilde{u}_1\tilde{h}_3 - \tilde{u}_3\tilde{h}_1 + \tau_2 \\ &\approx \tau_2\end{aligned}\tag{2.119}$$

$$\begin{aligned}\dot{\tilde{h}}_3 &= (\tilde{u}_2 - n)\tilde{h}_1 - \tilde{u}_1\tilde{h}_2 + \tau_3 \\ &\approx -n\tilde{h}_1 + \tau_3\end{aligned}\tag{2.120}$$

## 2.6 Nondimensional Equations for Control Law Design

The linearized relationships (2.109)–(2.120) in Sec. 2.5 become better suited for control law design after they have been made nondimensional by use of the following definitions,

$$\theta_i^* \triangleq \tilde{\theta}_i, \quad u_i^* \triangleq \frac{\tilde{u}_i}{n}, \quad h_i^* \triangleq \frac{\tilde{h}_i}{I_i n}, \quad H_i^* \triangleq \frac{\tilde{H}_i}{I_i n} \quad (i = 1, 2, 3)\tag{2.121}$$

$$\tau_i^* \triangleq \frac{\tau_i}{I_i n^2}, \quad \bar{\tau}_i^* \triangleq \frac{\bar{\tau}_i}{I_i n^2}, \quad w_i^* \triangleq \frac{w_i}{I_i n^2} \quad (i = 1, 2, 3) \quad (2.122)$$

$$t^* \triangleq nt \quad (2.123)$$

from which one obtains

$$\dot{\theta}_i^* \triangleq \frac{d\theta_i^*}{dt^*} = \frac{d\tilde{\theta}_i}{dt} \frac{dt}{dt^*} = \frac{\dot{\tilde{\theta}}_i}{n} \quad (i = 1, 2, 3) \quad (2.124)$$

$$\dot{u}_i^* \triangleq \frac{du_i^*}{dt^*} = \frac{d}{dt} \left( \frac{\tilde{u}_i}{n} \right) \frac{dt}{dt^*} = \frac{\dot{\tilde{u}}_i}{n^2} \quad (i = 1, 2, 3) \quad (2.125)$$

$$\dot{h}_i^* \triangleq \frac{dh_i^*}{dt^*} = \frac{d}{dt} \left( \frac{\tilde{h}_i}{I_i n} \right) \frac{dt}{dt^*} = \frac{\dot{\tilde{h}}_i}{I_i n^2} \quad (i = 1, 2, 3) \quad (2.126)$$

$$\dot{H}_i^* \triangleq \frac{dH_i^*}{dt^*} = \frac{d}{dt} \left( \frac{\tilde{H}_i}{I_i n} \right) \frac{dt}{dt^*} = \frac{\dot{\tilde{H}}_i}{I_i n^2} \quad (i = 1, 2, 3) \quad (2.127)$$

Substitution from Eqs. (2.121), (2.122), and (2.124)–(2.127) into (2.109)–(2.120) yields

$$\dot{\theta}_1^* = u_2^*, \quad \dot{\theta}_2^* = u_3^* - \theta_3^*, \quad \dot{\theta}_3^* = u_1^* + \theta_2^* \quad (2.128)$$

$$\dot{u}_1^* = 3k_1\theta_3^* + k_1u_3^* - \tau_1^* - \bar{\tau}_1^* + w_1^* \quad (2.129)$$

$$\dot{u}_2^* = 3k_2\theta_1^* - \tau_2^* - \bar{\tau}_2^* + w_2^* \quad (2.130)$$

$$\dot{u}_3^* = k_3u_1^* - \tau_3^* - \bar{\tau}_3^* + w_3^* \quad (2.131)$$

$$\dot{h}_1^* = h_3^* + \tau_1^*, \quad \dot{h}_2^* = \tau_2^*, \quad \dot{h}_3^* = -h_1^* + \tau_3^* \quad (2.132)$$

and

$$\dot{H}_1^* = H_3^* + \bar{\tau}_1^*, \quad \dot{H}_2^* = \bar{\tau}_2^*, \quad \dot{H}_3^* = -H_1^* + \bar{\tau}_3^* \quad (2.133)$$

where  $k_i$  in Eqs. (2.129)–(2.131) are defined as

$$k_1 \triangleq \frac{I_3 - I_2}{I_1}, \quad k_2 \triangleq \frac{I_3 - I_1}{I_2}, \quad k_3 \triangleq \frac{I_2 - I_1}{I_3} \quad (2.134)$$

Additional differential equations governing  $\int h_i dt$  and  $\int H_i dt$ , such as those introduced in Ref. [6], are sometimes needed to eliminate biases in the time histories of  $h_i$  and  $H_i$  ( $i = 1, 2, 3$ ). If one makes the following definitions

$$x_{i+12} \triangleq \int h_i^* dt^*, \quad x_{i+15} \triangleq \int H_i^* dt^* \quad (i = 1, 2, 3) \quad (2.135)$$

then the associated differential equations are given by

$$\dot{x}_{i+12} \triangleq dx_{i+12}/dt^* = h_i^*, \quad \dot{x}_{i+15} \triangleq dx_{i+15}/dt^* = H_i^* \quad (i = 1, 2, 3) \quad (2.136)$$

If the control law is to maintain a specified orientation of  $B$  in  $L$ , feedback of integrals of attitude errors is required, therefore we define the quantities

$$x_{i+18} \triangleq \int \theta_i^* dt^* \quad (i = 1, 2, 3) \quad (2.137)$$

which are governed by the differential equations

$$\dot{x}_{i+18} \triangleq dx_{i+18}/dt^* = \theta_i^* \quad (i = 1, 2, 3) \quad (2.138)$$

The foregoing nondimensional, linear differential equations have the form required for design of linear control laws

$$\{\dot{x}\} = [A] \{x\} + [B] \{\tau\} + \{W\} \quad (2.139)$$

where  $\{x\}$  is a  $21 \times 1$  column matrix whose first 12 elements are defined as

$$x_i \triangleq \theta_i^*, \quad x_{i+3} \triangleq u_i^*, \quad x_{i+6} \triangleq h_i^*, \quad x_{i+9} \triangleq H_i^*, \quad (i = 1, 2, 3) \quad (2.140)$$

and whose final 9 elements are defined in Eqs. (2.135) and (2.137), respectively. The elements of the  $21 \times 1$  column matrix  $\{\dot{x}\}$  are defined as

$$\dot{x}_i \triangleq dx_i/dt^* \quad (i = 1, \dots, 21) \quad (2.141)$$

and the column matrix  $\{\tau\}$  is dimensioned  $6 \times 1$  with the elements

$$\{\tau\} \triangleq [ \tau_1^* \quad \tau_2^* \quad \tau_3^* \quad \bar{\tau}_1^* \quad \bar{\tau}_2^* \quad \bar{\tau}_3^* ]^T \quad (2.142)$$

where the superscript T indicates the transpose of a matrix. The  $21 \times 1$  column matrix  $\{W\}$  is defined as

$$\{W\} \triangleq [ 0 \quad 0 \quad 0 \quad w_1^* \quad w_2^* \quad w_3^* \quad 0 ]^T \quad (2.143)$$

The  $21 \times 21$  square matrix  $[A]$  is

$$[A] \triangleq \begin{bmatrix} 0 & 0 & 0 & 0 & 1 & 0 & 0 & 0 & 0 & 0 & 0 & 0 & 0 & 0 & 0 & 0 & 0 & 0 & 0 & 0 \\ 0 & 0 & -1 & 0 & 0 & 1 & 0 & 0 & 0 & 0 & 0 & 0 & 0 & 0 & 0 & 0 & 0 & 0 & 0 & 0 \\ 0 & 1 & 0 & 1 & 0 & 0 & 0 & 0 & 0 & 0 & 0 & 0 & 0 & 0 & 0 & 0 & 0 & 0 & 0 & 0 \\ 0 & 0 & 3k_1 & 0 & 0 & k_1 & 0 & 0 & 0 & 0 & 0 & 0 & 0 & 0 & 0 & 0 & 0 & 0 & 0 & 0 \\ 3k_2 & 0 & 0 & 0 & 0 & 0 & 0 & 0 & 0 & 0 & 0 & 0 & 0 & 0 & 0 & 0 & 0 & 0 & 0 & 0 \\ 0 & 0 & 0 & k_3 & 0 & 0 & 0 & 0 & 0 & 0 & 0 & 0 & 0 & 0 & 0 & 0 & 0 & 0 & 0 & 0 \\ 0 & 0 & 0 & 0 & 0 & 0 & 0 & 0 & 1 & 0 & 0 & 0 & 0 & 0 & 0 & 0 & 0 & 0 & 0 & 0 \\ 0 & 0 & 0 & 0 & 0 & 0 & 0 & 0 & 0 & 0 & 0 & 0 & 0 & 0 & 0 & 0 & 0 & 0 & 0 & 0 \\ 0 & 0 & 0 & 0 & 0 & 0 & -1 & 0 & 0 & 0 & 0 & 0 & 0 & 0 & 0 & 0 & 0 & 0 & 0 & 0 \\ 0 & 0 & 0 & 0 & 0 & 0 & 0 & 0 & 0 & 0 & 0 & 1 & 0 & 0 & 0 & 0 & 0 & 0 & 0 & 0 \\ 0 & 0 & 0 & 0 & 0 & 0 & 0 & 0 & 0 & 0 & 0 & 0 & 0 & 0 & 0 & 0 & 0 & 0 & 0 & 0 \\ 0 & 0 & 0 & 0 & 0 & 0 & 0 & 0 & 0 & -1 & 0 & 0 & 0 & 0 & 0 & 0 & 0 & 0 & 0 & 0 \\ 0 & 0 & 0 & 0 & 0 & 0 & 1 & 0 & 0 & 0 & 0 & 0 & 0 & 0 & 0 & 0 & 0 & 0 & 0 & 0 \\ 0 & 0 & 0 & 0 & 0 & 0 & 0 & 1 & 0 & 0 & 0 & 0 & 0 & 0 & 0 & 0 & 0 & 0 & 0 & 0 \\ 0 & 0 & 0 & 0 & 0 & 0 & 0 & 0 & 1 & 0 & 0 & 0 & 0 & 0 & 0 & 0 & 0 & 0 & 0 & 0 \\ 0 & 0 & 0 & 0 & 0 & 0 & 0 & 0 & 0 & 1 & 0 & 0 & 0 & 0 & 0 & 0 & 0 & 0 & 0 & 0 \\ 0 & 0 & 0 & 0 & 0 & 0 & 0 & 0 & 0 & 0 & 1 & 0 & 0 & 0 & 0 & 0 & 0 & 0 & 0 & 0 \\ 0 & 0 & 0 & 0 & 0 & 0 & 0 & 0 & 0 & 0 & 0 & 1 & 0 & 0 & 0 & 0 & 0 & 0 & 0 & 0 \\ 1 & 0 & 0 & 0 & 0 & 0 & 0 & 0 & 0 & 0 & 0 & 0 & 0 & 0 & 0 & 0 & 0 & 0 & 0 & 0 \\ 0 & 1 & 0 & 0 & 0 & 0 & 0 & 0 & 0 & 0 & 0 & 0 & 0 & 0 & 0 & 0 & 0 & 0 & 0 & 0 \\ 0 & 0 & 1 & 0 & 0 & 0 & 0 & 0 & 0 & 0 & 0 & 0 & 0 & 0 & 0 & 0 & 0 & 0 & 0 & 0 \end{bmatrix} \quad (2.144)$$

and the matrix  $[B]$  is dimensioned  $21 \times 6$ ,

$$[B] \triangleq \begin{bmatrix} 0 & 0 & 0 & 0 & 0 & 0 \\ 0 & 0 & 0 & 0 & 0 & 0 \\ 0 & 0 & 0 & 0 & 0 & 0 \\ -1 & 0 & 0 & -1 & 0 & 0 \\ 0 & -1 & 0 & 0 & -1 & 0 \\ 0 & 0 & -1 & 0 & 0 & -1 \\ 1 & 0 & 0 & 0 & 0 & 0 \\ 0 & 1 & 0 & 0 & 0 & 0 \\ 0 & 0 & 1 & 0 & 0 & 0 \\ 0 & 0 & 0 & 1 & 0 & 0 \\ 0 & 0 & 0 & 0 & 1 & 0 \\ 0 & 0 & 0 & 0 & 0 & 1 \\ 0 & 0 & 0 & 0 & 0 & 0 \\ 0 & 0 & 0 & 0 & 0 & 0 \\ 0 & 0 & 0 & 0 & 0 & 0 \\ 0 & 0 & 0 & 0 & 0 & 0 \\ 0 & 0 & 0 & 0 & 0 & 0 \\ 0 & 0 & 0 & 0 & 0 & 0 \\ 0 & 0 & 0 & 0 & 0 & 0 \\ 0 & 0 & 0 & 0 & 0 & 0 \\ 0 & 0 & 0 & 0 & 0 & 0 \\ 0 & 0 & 0 & 0 & 0 & 0 \\ 0 & 0 & 0 & 0 & 0 & 0 \end{bmatrix} \quad (2.145)$$

## 2.7 Nonlinear Equations used in Simulations

In the physical system, relative motion between a flywheel rotor and the spacecraft will undoubtedly meet with some form of resistance that will necessitate consumption of power to overcome and, if not countered, will cause the actual amount of stored energy to diverge from the required amount. Section 4.3 deals with a control law designed to compensate for any such error in flywheel rotational kinetic energy, and consequently we now introduce terms to represent damping in the equations used for simulations of nonlinear motion, the results of which are presented in Chapters 4 and 5.

Up to this point the moment about  $R_i^*$  of forces exerted by  $B$  on  $R_i$  has been represented by  $\mathbf{M}^{B/R_i}$ ; henceforth we regard the dot product  $\mathbf{M}^{B/R_i} \cdot \hat{\boldsymbol{\beta}}_i$  ( $i = 1, \dots, \mathcal{F}$ ) as the sum of two contributions. The first is from a motor-generator, and will be denoted by  $\mathbf{M}^{B/R_i} \cdot \hat{\boldsymbol{\beta}}_i$  for convenience. The second is due to damping, related by a constant of proportionality  $C_d$  to the angular speed of  $R_i$  relative to  $B$ . For example, in connection with rotor  $R_4$ ,  $\mathbf{M}^{B/R_4} \cdot \hat{\mathbf{b}}_1$  is replaced by  $\mathbf{M}^{B/R_4} \cdot \hat{\mathbf{b}}_1 - C_d u_5$  in Eq. (2.55). As a result Eqs. (2.87) give way, after decoupling, to

$$(I_1 - 2J)\dot{u}_1 = (I_3 - I_2)(3n^2 r_2 r_3 - u_2 u_3) - J[u_2(u_8 + u_9) - u_3(u_6 + u_7)] \\ + w_1 - \tau_1 - \left( \mathbf{M}^{B/R_1} + \mathbf{M}^{B/R_4} \right) \cdot \hat{\mathbf{b}}_1 + C_d(u_4 + u_5) \quad (2.146)$$

$$(I_2 - 2J)\dot{u}_2 = (I_1 - I_3)(3n^2 r_1 r_3 - u_1 u_3) - J[u_3(u_4 + u_5) - u_1(u_8 + u_9)] \\ + w_2 - \tau_2 - \left( \mathbf{M}^{B/R_2} + \mathbf{M}^{B/R_5} \right) \cdot \hat{\mathbf{b}}_2 + C_d(u_6 + u_7) \quad (2.147)$$

$$(I_3 - 2J)\dot{u}_3 = (I_2 - I_1)(3n^2 r_1 r_2 - u_1 u_2) - J[u_1(u_6 + u_7) - u_2(u_4 + u_5)] \\ + w_3 - \tau_3 - \left( \mathbf{M}^{B/R_3} + \mathbf{M}^{B/R_6} \right) \cdot \hat{\mathbf{b}}_3 + C_d(u_8 + u_9) \quad (2.148)$$

and Eqs. (2.54)–(2.59) governing flywheel speeds are restated as

$$J(\dot{u}_1 + \dot{u}_4) = \mathbf{M}^{B/R_1} \cdot \hat{\mathbf{b}}_1 - C_d u_4 \quad (2.149)$$

$$J(\dot{u}_1 + \dot{u}_5) = \mathbf{M}^{B/R_4} \cdot \hat{\mathbf{b}}_1 - C_d u_5 \quad (2.150)$$

$$J(\dot{u}_2 + \dot{u}_6) = \mathbf{M}^{B/R_2} \cdot \hat{\mathbf{b}}_2 - C_d u_6 \quad (2.151)$$

$$J(\dot{u}_2 + \dot{u}_7) = \mathbf{M}^{B/R_5} \cdot \hat{\mathbf{b}}_2 - C_d u_7 \quad (2.152)$$

$$J(\dot{u}_3 + \dot{u}_8) = \mathbf{M}^{B/R_3} \cdot \hat{\mathbf{b}}_3 - C_d u_8 \quad (2.153)$$

$$J(\dot{u}_3 + \dot{u}_9) = \mathbf{M}^{B/R_6} \cdot \hat{\mathbf{b}}_3 - C_d u_9 \quad (2.154)$$

where the dot products  $\mathbf{M}_i \cdot \hat{\mathbf{b}}_i$  and  $\mathbf{M}_{i+3} \cdot \hat{\mathbf{b}}_i$  ( $i = 1, 2, 3$ ) are neglected for the reasons discussed at the conclusion of Sec. 2.2. The simulation results presented in Chapters 4 and 5 are obtained from numerical solutions of nonlinear differential equations (2.146)–(2.154), together with the differential equations (2.100)–(2.102) for CMG momentum, kinematical differential equations for quaternion elements [see Eqs. (5.7) and (5.8)] in place of Eqs. (2.92), and dimensionalized counterparts to Eqs. (2.136) and (2.138) for integrals of momentum and attitude.

## Chapter 3

# Flywheel Steering Laws

The great benefit of utilizing flywheels is that they can serve simultaneously as attitude control actuators and as energy storage devices; this dual role requires that  $\bar{\boldsymbol{\tau}}$ , obtained on the basis of attitude control considerations, be applied in a way that allows energy to be stored or discharged as needed. A flywheel rotor  $R_i$  is suspended in a vacuum housing in  $B$  with magnetic bearings, and relative motion between  $R_i$  and  $B$  is brought about by a motor-generator that enables  $B$  to exert on  $R_i$  a torque with magnitude  $\mathbf{M}^{B/R_i} \cdot \hat{\boldsymbol{\beta}}_i$ , the purpose of which is to produce and change rotor momentum in order to furnish attitude control, and to alter the rotor's rotational kinetic energy. An important measure of energy storage is power, or the rate at which rotational kinetic energy is changed. In this chapter relationships for  $\mathbf{M}^{B/R_i} \cdot \hat{\boldsymbol{\beta}}_i$  as functions of power,  $\bar{\boldsymbol{\tau}}$ , and rotor speeds are developed; they are referred to collectively as a *flywheel steering law* because they are similar in nature to a CMG steering law that determines gimbal speeds (and thus, indirectly, gimbal motor torques) needed to produce  $\boldsymbol{\tau}$  as requested by a control law. Two such steering laws are presented; the first is the result of simply prescribing the total power of the flywheel system, whereas specification of the power required for each of three flywheel pairs gives rise to the second law. Bearing friction and damping are neglected in the design of the steering laws.

The flywheel rotors are arranged in counter-rotating pairs; each pair, denoted by  $F_i$ , consists of rotors  $R_i$  and  $R_{i+3}$  ( $i = 1, 2, 3$ ). Referring to Eq. (5) of Ref. [22], the power  ${}^B P^{F_i}$  of  $F_i$  in  $B$  can be expressed as

$${}^B P^{F_i} = \left( \mathbf{I}^{R_i/R_i^*} \cdot {}^B \boldsymbol{\alpha}^{R_i} \right) \cdot {}^B \boldsymbol{\omega}^{R_i} + \left( \mathbf{I}^{R_{i+3}/R_{i+3}^*} \cdot {}^B \boldsymbol{\alpha}^{R_{i+3}} \right) \cdot {}^B \boldsymbol{\omega}^{R_{i+3}} \quad (i = 1, 2, 3) \quad (3.1)$$

or, in view of Eqs. (2.36) and (2.37),

$${}^B P^{F_i} = J (\dot{u}_{2i+2} u_{2i+2} + \dot{u}_{2i+3} u_{2i+3}) \quad (i = 1, 2, 3) \quad (3.2)$$

and therefore the total power may be expressed as

$${}^B P^F \triangleq \sum_{i=1}^3 {}^B P^{F_i} = J \sum_{i=1}^3 (\dot{u}_{2i+2} u_{2i+2} + \dot{u}_{2i+3} u_{2i+3}) \quad (3.3)$$

Now, if  $\dot{u}_1$ ,  $\dot{u}_2$ , and  $\dot{u}_3$  are assumed to be small in comparison to  $\dot{u}_4, \dots, \dot{u}_9$ , and if  $\mathbf{M}_i \cdot \hat{\mathbf{b}}_i$  and  $\mathbf{M}_{i+3} \cdot \hat{\mathbf{b}}_i$  ( $i = 1, 2, 3$ ) vanish for the reasons put forth at the conclusion of Sec. 2.2, then Eqs. (2.54)–(2.59) may be approximated as

$$J \dot{u}_{2i+2} \approx \mathbf{M}^{B/R_i} \cdot \hat{\mathbf{b}}_i, \quad J \dot{u}_{2i+3} \approx \mathbf{M}^{B/R_{i+3}} \cdot \hat{\mathbf{b}}_i \quad (i = 1, 2, 3) \quad (3.4)$$

which, together with Eqs. (2.81) and (2.83), lead to

$$\begin{aligned} (\bar{\boldsymbol{\tau}} - {}^N\boldsymbol{\omega}^B \times \mathbf{H}) \cdot \hat{\mathbf{b}}_i &= \dot{H}_i = J(\dot{u}_{2i+2} + \dot{u}_{2i+3}) \\ &\approx \left( \mathbf{M}^{B/R_i} + \mathbf{M}^{B/R_{i+3}} \right) \cdot \hat{\mathbf{b}}_i \quad (i = 1, 2, 3) \end{aligned} \quad (3.5)$$

or

$$\mathbf{M}^{B/R_{i+3}} \cdot \hat{\mathbf{b}}_i \approx \left( \bar{\boldsymbol{\tau}} - {}^N\boldsymbol{\omega}^B \times \mathbf{H} - \mathbf{M}^{B/R_i} \right) \cdot \hat{\mathbf{b}}_i \quad (i = 1, 2, 3) \quad (3.6)$$

Substitution from Eqs. (3.4) into Eq. (3.3) produces

$${}^B P^F \approx \sum_{i=1}^3 \left( u_{2i+2} \mathbf{M}^{B/R_i} + u_{2i+3} \mathbf{M}^{B/R_{i+3}} \right) \cdot \hat{\mathbf{b}}_i \quad (3.7)$$

Eqs. (3.6) and (3.7) constitute a system of four equations, linear in the six unknowns  $\mathbf{M}^{B/R_i} \cdot \hat{\mathbf{b}}_i$  and  $\mathbf{M}^{B/R_{i+3}} \cdot \hat{\mathbf{b}}_i$ , ( $i = 1, 2, 3$ ). This underdetermined system can be written in matrix form as

$$[A_s] \{y\} = \{z\} \quad (3.8)$$

where

$$[A_s] \triangleq \begin{bmatrix} 1 & 1 & 0 & 0 & 0 & 0 \\ 0 & 0 & 1 & 1 & 0 & 0 \\ 0 & 0 & 0 & 0 & 1 & 1 \\ u_4 & u_5 & u_6 & u_7 & u_8 & u_9 \end{bmatrix} \quad (3.9)$$

$$\{y\} \triangleq \begin{Bmatrix} \mathbf{M}^{B/R_1} \cdot \hat{\mathbf{b}}_1 \\ \mathbf{M}^{B/R_4} \cdot \hat{\mathbf{b}}_1 \\ \mathbf{M}^{B/R_2} \cdot \hat{\mathbf{b}}_2 \\ \mathbf{M}^{B/R_5} \cdot \hat{\mathbf{b}}_2 \\ \mathbf{M}^{B/R_3} \cdot \hat{\mathbf{b}}_3 \\ \mathbf{M}^{B/R_6} \cdot \hat{\mathbf{b}}_3 \end{Bmatrix} \quad (3.10)$$

$$\{z\} \triangleq \begin{Bmatrix} (\bar{\boldsymbol{\tau}} - {}^N\boldsymbol{\omega}^B \times \mathbf{H}) \cdot \hat{\mathbf{b}}_1 \\ (\bar{\boldsymbol{\tau}} - {}^N\boldsymbol{\omega}^B \times \mathbf{H}) \cdot \hat{\mathbf{b}}_2 \\ (\bar{\boldsymbol{\tau}} - {}^N\boldsymbol{\omega}^B \times \mathbf{H}) \cdot \hat{\mathbf{b}}_3 \\ {}^B P^F \end{Bmatrix} \quad (3.11)$$

One may solve Eqs. (3.8) by forming a matrix pseudo-inverse such as the one presented in Ref. [23] and developed by Moore and Penrose for underdetermined systems,

$$[A_s]^+ \triangleq [A_s]^T \left( [A_s][A_s]^T \right)^{-1} \quad (3.12)$$

which yields the solution

$$\{y\} = [A_s]^+ \{z\} \quad (3.13)$$

that minimizes the sum of the squares of the unknowns,  $\{y\}^T \{y\}$ . (There exist several other performance measures that could be considered in solving an underdetermined system of equations.)

Use of a pseudo-inverse is in essence the suggestion made by Hall in Sec. 4 of Ref. [9], yielding a steering law wherein the power and attitude control requirements are met simultaneously, and a function of the instantaneous motor torques, the sum  $\sum_{i=1}^3 [(\mathbf{M}^{B/R_i} \cdot \hat{\mathbf{b}}_i)^2 + (\mathbf{M}^{B/R_{i+3}} \cdot \hat{\mathbf{b}}_i)^2]$ , is minimized.

Upon making the definitions

$$d_1 \triangleq u_5 - u_4, \quad d_2 \triangleq u_7 - u_6, \quad d_3 \triangleq u_9 - u_8 \quad (3.14)$$

$$s_1 \triangleq u_5 + u_4, \quad s_2 \triangleq u_7 + u_6, \quad s_3 \triangleq u_9 + u_8 \quad (3.15)$$

the pseudo-inverse can be written explicitly as

$$[A_s]^+ = \frac{1}{2(d_1^2 + d_2^2 + d_3^2)} \begin{bmatrix} 2u_5d_1 + d_2^2 + d_3^2 & s_2d_1 & s_3d_1 & -2d_1 \\ -2u_4d_1 + d_2^2 + d_3^2 & -s_2d_1 & -s_3d_1 & 2d_1 \\ s_1d_2 & 2u_7d_2 + d_1^2 + d_3^2 & s_3d_2 & -2d_2 \\ -s_1d_2 & -2u_6d_2 + d_1^2 + d_3^2 & -s_3d_2 & 2d_2 \\ s_1d_3 & s_2d_3 & 2u_9d_3 + d_1^2 + d_2^2 & -2d_3 \\ -s_1d_3 & -s_2d_3 & -2u_8d_3 + d_1^2 + d_2^2 & 2d_3 \end{bmatrix} \quad (3.16)$$

It is worth noting that if the rotor speed differences  $d_1$ ,  $d_2$ , and  $d_3$  vanish for all three flywheel pairs, the pseudo-inverse becomes infinite and the steering law does not furnish a result. Since the rotor speeds of the flywheels in each pair will normally have opposite signs, this condition should be unlikely. In addition, examination of Eqs. (3.10), (3.11), (3.13), and (3.16) reveals that when the flywheels are not required to provide attitude control ( $\bar{\boldsymbol{\tau}} = \mathbf{0}$ ), and the condition of counter-rotation is present ( $u_{2i+3} = -u_{2i+2}$ , thus  $\mathbf{H} = \mathbf{0}$ ), this steering law dictates that  $\mathbf{M}^{B/R_{i+3}} \cdot \hat{\mathbf{b}}_i = -\mathbf{M}^{B/R_i} \cdot \hat{\mathbf{b}}_i$ , and counter-rotation is preserved.

As an alternative to dealing with the four Eqs. (3.6) and (3.7), one could replace the single Eq. (3.7) with three others by choosing to divide the power requirement evenly among the three flywheel pairs,  ${}^B P^{F_1} = {}^B P^{F_2} = {}^B P^{F_3} = \frac{1}{3} {}^B P^F$ , yielding six equations in six unknowns. Substitution from Eqs. (3.4) into Eqs. (3.2) gives the three new equations

$${}^B P^{F_i} \approx \left( u_{2i+2} \mathbf{M}^{B/R_i} + u_{2i+3} \mathbf{M}^{B/R_{i+3}} \right) \cdot \hat{\mathbf{b}}_i \quad (i = 1, 2, 3) \quad (3.17)$$

Now, substitution from Eqs. (3.6) gives

$$\begin{aligned} {}^B P^{F_i} &\approx u_{2i+2} \left( \mathbf{M}^{B/R_i} \cdot \hat{\mathbf{b}}_i \right) + u_{2i+3} \left( \bar{\boldsymbol{\tau}} - {}^N \boldsymbol{\omega}^B \times \mathbf{H} - \mathbf{M}^{B/R_i} \right) \cdot \hat{\mathbf{b}}_i \\ &= (u_{2i+2} - u_{2i+3}) \left( \mathbf{M}^{B/R_i} \cdot \hat{\mathbf{b}}_i \right) + u_{2i+3} \left( \bar{\boldsymbol{\tau}} - {}^N \boldsymbol{\omega}^B \times \mathbf{H} \right) \cdot \hat{\mathbf{b}}_i \quad (i = 1, 2, 3) \end{aligned} \quad (3.18)$$

which can be rearranged to yield

$$\mathbf{M}^{B/R_i} \cdot \hat{\mathbf{b}}_i = \frac{{}^B P^{F_i} - u_{2i+3} \left( \bar{\boldsymbol{\tau}} - {}^N \boldsymbol{\omega}^B \times \mathbf{H} \right) \cdot \hat{\mathbf{b}}_i}{u_{2i+2} - u_{2i+3}} \quad (i = 1, 2, 3) \quad (3.19)$$

and, when one substitutes from this expression into Eq. (3.6), the result is

$$\mathbf{M}^{B/R_{i+3}} \cdot \hat{\mathbf{b}}_i = \frac{u_{2i+2} \left( \bar{\boldsymbol{\tau}} - {}^N \boldsymbol{\omega}^B \times \mathbf{H} \right) \cdot \hat{\mathbf{b}}_i - {}^B P^{F_i}}{u_{2i+2} - u_{2i+3}} \quad (i = 1, 2, 3) \quad (3.20)$$

Eqs. (3.19) and (3.20) constitute another flywheel steering law, indicating the moment that must be applied by a motor-generator to each of two rotors belonging to a counter-rotating pair in order to apply  $\bar{\boldsymbol{\tau}}$  as called for by an attitude control law, and at the same time satisfy power requirements specified by  ${}^B P^{F_i}$ . Each flywheel pair is expected to operate with the sign of the rotor speed  $u_{2i+3}$  opposite the sign of  $u_{2i+2}$ ; hence, the denominators  $u_{2i+2} - u_{2i+3}$  should remain well away from zero. In the event that the flywheels are not required to participate in attitude control, and the condition of counter-rotation is present, the steering law yields  $\mathbf{M}^{B/R_{i+3}} \cdot \hat{\mathbf{b}}_i = -\mathbf{M}^{B/R_i} \cdot \hat{\mathbf{b}}_i$  and thus maintains the condition of counter-rotation.

## Chapter 4

# Linear Controllers

The linearized, nondimensional equations presented in Sec. 2.6 are used together with the Linear Quadratic Regulator (LQR) technique to obtain linear laws for controlling motion associated with two important orientations of an Earth-pointing spacecraft: torque equilibrium attitude (TEA), and attitude that is fixed (or held) with respect to a local-vertical-local-horizontal reference frame. Sections 4.1 and 4.2 contain the numerical values for LQR weighting and other simulation parameters, respectively. The design of a method for feeding back error in the rotational kinetic energy of the flywheel rotors in order to eliminate problems caused by rotor damping is discussed in Sec. 4.3. The comprehensive control system formed by the combination of a LQR for attitude control and momentum management, a flywheel steering law, and feedback of kinetic energy error is depicted in Sec. 4.4 with a block diagram. Section 4.5 begins with a brief discussion of the design of a control law that seeks TEA with CMGs and flywheels, and continues with a presentation of simulation results that illustrate the performance and features of the control and steering laws. First, TEA seeking behavior in the absence of flywheel rotor damping is examined, then the consequences of failing to counteract damping, and the advantages of kinetic energy error feedback are demonstrated in turn, and finally the performances of the pseudo-inverse and divided power steering laws are compared in some detail. The subject of Sec. 4.6 is the design and application of several control laws for holding attitude: without management of angular momentum of flywheels or CMGs, with inclusion of flywheel momentum management, and by means of thrusters. In conclusion, a comparison is undertaken of the amount of propellant required if each of these operational techniques is used in connection with the rendezvous and docking of ISS with another spacecraft.

### 4.1 Weighting

Laws for controlling the orientation of  $B$  in  $L$ , and the momentum of flywheels and CMGs, have been designed using the infinite-horizon Linear Quadratic Regulator technique, in which a scalar quadratic performance index given by

$$\mathcal{P} = \int_0^{\infty} \left( \{x\}^T [Q] \{x\} + \{\tau\}^T [R] \{\tau\} \right) dt \quad (4.1)$$

is minimized subject to the linear Eqs. (2.139) with  $\{W\} = \{0\}$ . The technique yields a state feedback gain matrix  $[K]$  which in turn is used to obtain  $\{\tau\}$ ,

$$\{\tau\} = -[K] \{x\} \quad (4.2)$$

Table 4.1: State Weightings

Parameter	Max Value	Nondimensional Value		
$i =$	1, 2, 3	1	2	3
$\tilde{\theta}_i$	1 deg	3282.8	3282.8	3282.8
$\tilde{u}_i$	0.2 deg/s	0.1050	0.1050	0.1050
$\tilde{h}_i$	6,779 N-m-s	237.9	11.0	322.9
$\tilde{H}_i$	6,779 N-m-s	237.9	11.0	322.9
$\int \tilde{h}_i dt$	$2.7 \times 10^6$ N-m-s <sup>2</sup>	1161.7	53.6	1576.9
$\int \tilde{H}_i dt$	$2.7 \times 10^6$ N-m-s <sup>2</sup>	1161.7	53.6	1576.9
$\int \tilde{\theta}_i dt$	1000 deg-s	2564.7	2564.7	2564.7

As suggested by Bryson and Ho in Ref. [24], the weighting matrix  $[Q]$  can be chosen as diagonal, and unity should be approximately equal to the product of  $Q_{jj}$  and the square of the maximum acceptable value of the associated element  $x_j$  of  $\{x\}$ , ( $j = 1, \dots, 21$ ). Likewise, a diagonal form of  $[R]$  is convenient, with unity approximately equal to the product of  $R_{kk}$  and the square of the maximum acceptable value of the associated element of  $\{\tau\}$  ( $k = 1, \dots, 6$ ).

Maximum acceptable values of several parameters used in constructing  $[Q]$  are listed in Table 4.1. A maximum maneuver rate of 0.1 deg/s specified on p. 7-6 of Ref. [25] provides a limit on the magnitude of  ${}^L\omega^B$ ; since the orbital angular speed  $n$  will not be greater than about 0.065 deg/s, a limit of 0.2 deg/s imposed on each of  $\tilde{u}_i$  appears reasonable. Each CMG possesses 4,745 N-m-s (3,500 ft-lb<sub>f</sub>-s) of momentum, therefore the magnitude of the resultant momentum of 4 CMGs is limited to 18,981 N-m-s (14,000 ft-lb<sub>f</sub>-s). Even if each of three components of momentum reach an absolute value of 6,779 N-m-s, the magnitude is well within the limit. For the sake of simplicity, the same limits are applied to flywheel momentum; it should be kept in mind that the spin speeds of the International Space Station flywheels are limited in absolute value to 60,000 rpm, the axial central principal moment of inertia  $J$  is expected to be approximately 0.3010 kg-m<sup>2</sup>, and there will be no more than 96 flywheel rotors (arranged in 48 pairs). Limits of  $2.7 \times 10^6$  N-m-s<sup>2</sup> on the integrals of momentum correspond to keeping momentum in each axis below 544 N-m-s for 5,000 s (almost one orbit). Similarly, the limit of 1000 deg-s on the integrals of attitude error arises from requiring the attitude error to be less than 0.2 deg for 5,000 s. Before constructing  $[Q]$ , the values in the second column of Table 4.1 are made nondimensional to be in correspondence with the elements of  $\{x\}$ , as indicated in the last three columns.

The maximum expected value of each element of  $\{\tau\}$  is taken to be 2.7 N-m; nondimensionalization yields  $R_{11} = R_{44} = 1903.2$ ,  $R_{22} = R_{55} = 87.8$ , and  $R_{33} = R_{66} = 2583.6$ .

It is important to point out that the preliminary control law designs presented herein do not address performance and stability robustness in the presence of model uncertainty. Such detailed designs are beyond the scope of the present work, although they would be required for an actual spacecraft.

## 4.2 Simulation Parameters

Other values required for a numerical simulation are as follows.

Moments and products of inertia of  $S$  with respect to  $S^*$  are taken to be

$$\left[ I^{S/S^*} \right] = 1.36 \times \begin{bmatrix} 50.28 & -0.39 & -0.24 \\ -0.39 & 10.80 & 0.16 \\ -0.24 & 0.16 & 58.57 \end{bmatrix} \times 10^6 \text{ kg-m}^2 \quad (4.3)$$

which are the same values (in metric units) as those associated with Phase 1 in Table 1 of Ref. [6], with the exception of  $I_{13}$  which is suspected to be a typographical error, the correct value being  $-0.24 \times 10^6 \text{ slug-ft}^2$ .

The value of  $\mathbf{w}$  used in Ref. [6] represents the moment about  $S^*$  of aerodynamic forces exerted on the Phase 1 configuration of  $S$  when the attitude is near TEA; it is given by

$$\mathbf{w} = 1.36 \left[ (1 + \sin nt + \frac{1}{2} \sin 2nt) \hat{\mathbf{b}}_1 + (4 + 2 \sin nt + \frac{1}{2} \sin 2nt) \hat{\mathbf{b}}_2 + (1 + \sin nt + \frac{1}{2} \sin 2nt) \hat{\mathbf{b}}_3 \right] \text{ N-m} \quad (4.4)$$

where  $n$ , the magnitude of  ${}^N\boldsymbol{\omega}^L$ , is taken to be 0.001131 rad/s.

Each flywheel pair in the physical system is required to discharge 4,400 W of power during the portion of the orbit that lies within the Earth's shadow, known as the period of eclipse. The remaining portion of the orbit, during which sunlight reaches the spacecraft, is taken to be twice as long as the eclipse. Therefore, for each orbit, the total power that must be supplied by the 48 pairs of flywheels in the physical system is given by

$${}^B\bar{P}^F = \begin{cases} 48 \times 2,200 \text{ W} = 105.6 \text{ kW} & 0 \leq t \leq \frac{2}{3} \frac{2\pi}{n} \quad (\text{charge}) \\ 48 \times -4,400 \text{ W} = -211.2 \text{ kW} & \frac{2}{3} \frac{2\pi}{n} \leq t \leq \frac{2\pi}{n} \quad (\text{discharge}) \end{cases} \quad (4.5)$$

where the bar over  $P$  indicates a known function of  $t$  to be used in connection with the pseudo-inverse steering law developed in Ch. 3. The alternative steering law is referred to as a divided power law because the power requirement is divided into three equal parts, therefore  ${}^B\bar{P}^{F_1} = {}^B\bar{P}^{F_2} = {}^B\bar{P}^{F_3} = \frac{1}{3} {}^B\bar{P}^F$ , or

$${}^B\bar{P}^{F_i} = \begin{cases} 35.2 \text{ kW} & 0 \leq t \leq \frac{2}{3} \frac{2\pi}{n} \quad (\text{charge}) \\ -70.4 \text{ kW} & \frac{2}{3} \frac{2\pi}{n} \leq t \leq \frac{2\pi}{n} \quad (\text{discharge}) \end{cases} \quad (i = 1, 2, 3) \quad (4.6)$$

As mentioned earlier, the physical system is made up of 96 flywheels; since the present model involves only 6 rotors, a scaling factor of  $96/6 = 16$  is used; thus  $J = 16 \times 0.3010 \text{ kg-m}^2 = 4.82 \text{ kg-m}^2$ .

## 4.3 Energy Feedback

The power possessed by the flywheels, given in Eq. (3.3), can differ from the value required by Eq. (4.5) if, for example, a rotor  $R_i$  and  $B$  exert on each other a couple whose torque is proportional to the rotor speed. If left unchecked, such unwanted resistance or damping will lead to a difference between  ${}^B P^F$  and  ${}^B \bar{P}^F$  that increases with time, to rotor speeds that exceed their maximum and minimum limits, and to singularities in the steering laws. These deleterious effects of damping can be eliminated by the control system through feedback of rotational kinetic energy error.

The total rotational kinetic energy  ${}^B K^F$  of the flywheel rotors relative to  $B$  can be expressed as

$${}^B K^F = \frac{J}{2} \sum_{i=4}^9 u_i^2 \quad (4.7)$$

and the power of  $F$  in  $B$  is given by the derivative of  ${}^B K^F$  with respect to  $t$ ,

$${}^B P^F = \frac{d}{dt} {}^B K^F \quad (4.8)$$

One can regard the required power  ${}^B \bar{P}^F$  as the time derivative of a required kinetic energy of  $F$  in  $B$

$${}^B \bar{P}^F = \frac{d}{dt} {}^B \bar{K}^F \quad (4.9)$$

and define a kinetic energy error  $e_k$  as the quantity

$$e_k \triangleq {}^B K^F - {}^B \bar{K}^F \quad (4.10)$$

that is governed by the differential equation

$$\dot{e}_k = \frac{d}{dt} ({}^B K^F - {}^B \bar{K}^F) = {}^B P^F - {}^B \bar{P}^F \triangleq e_p \quad (4.11)$$

where  $e_p$  is defined to be the error in power, or the difference between the actual and required values. The LQR technique can be used to control the kinetic energy error by minimizing the cost function

$$\mathcal{P}_E = \int_0^\infty (\lambda e_k^2 + e_p^2) dt \quad (4.12)$$

where  $\lambda$  is a weighting parameter on the kinetic energy error of the flywheel system. This leads to a feedback controller in which the required power is adjusted by the amount  $-\sqrt{\lambda} e_k$ . Thus, the *commanded* power is defined to be

$${}^B P_c^F \triangleq {}^B \bar{P}^F - \sqrt{\lambda} e_k \quad (4.13)$$

and is used in place of  ${}^B P^F$  in Eq. (3.11) for the pseudo-inverse steering law. Similarly, a commanded power  ${}^B P_c^{F_i}$  ( $i = 1, 2, 3$ ) is obtained for each of the three flywheel pairs and used together with Eqs. (3.19) and (3.20) for the divided power steering law. The merits of this kinetic energy error feedback are illustrated presently.

## 4.4 Control System Block Diagram

The block diagram in Fig. 4.1 shows the LQR (controller), flywheel steering law, and kinetic energy error feedback arranged to form a complete control system in MATLAB/Simulink®. The differential equations governing the behavior of the plant model (see Sec. 2.7) are placed in a Simulink S-Function to be numerically integrated and provide the value of the state  $\{x\}$  at the current simulation time. The current value of the state is fed to the controller S-Function, where it is made nondimensional and then multiplied by the LQR-derived state feedback gain matrix to

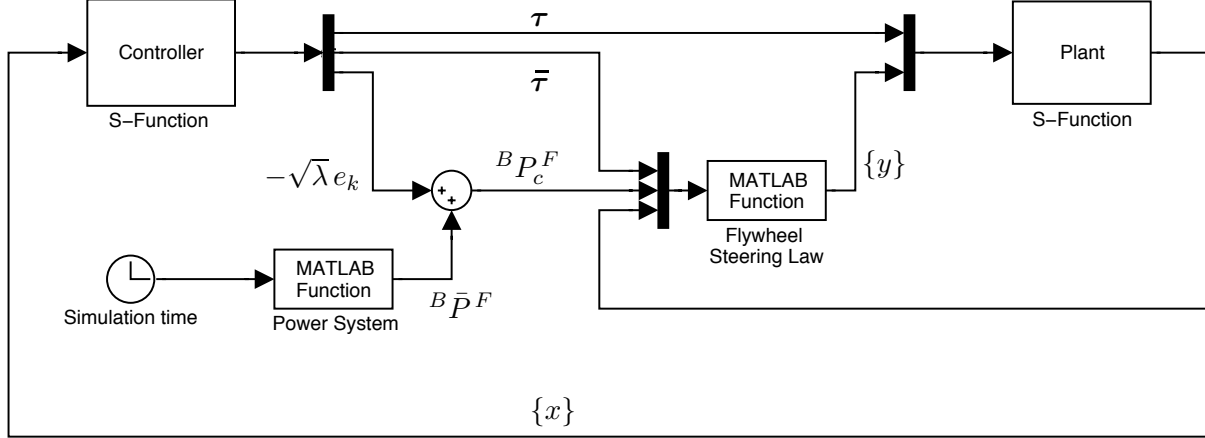


Figure 4.1: Control System Block Diagram

generate the control torques  $\tau$  and  $\bar{\tau}$ . The controller also determines the kinetic energy error of the flywheel system,  $e_k$ , needed to calculate the commanded power,  ${}^B P_c^F$ , that is used together with the flywheel control torque  $\bar{\tau}$  in the flywheel steering law to obtain the flywheel motor torque measure numbers in  $\{y\}$  [see Eq. (3.10)]. These are supplied to the plant model, and the control loop cycle is repeated. (The subject of CMG steering is well understood; therefore, our simulations do not include a model of individual CMG gimbal motions.)

## 4.5 TEA Seeking

The Torque Equilibrium Attitude (TEA) of a spacecraft is defined as the orientation for which the angular acceleration of  $B$  in  $N$  vanishes. The present ISS attitude and CMG momentum control algorithm can keep the orientation in the neighborhood of a time-varying TEA almost indefinitely, without requiring any expenditure of propellant from the Reaction Control System. In what follows, the design of a control law that seeks TEA with CMGs and flywheels is described briefly, and then simulation results are presented that illustrate the performance and features of our control and steering laws. We examine TEA seeking behavior in the absence of flywheel rotor damping in Sec. 4.5.1, illustrate the consequences of failing to counteract damping in Sec. 4.5.2, and then demonstrate the advantages of kinetic energy error feedback in Sec. 4.5.3. The performance of the pseudo-inverse steering law is compared to that of the divided power scheme in Sec. 4.5.4.

Seeking a TEA requires regulating the states contained in the  $18 \times 1$  column matrix

$$\{x\} = [\theta_1^*, \theta_2^*, \theta_3^*, u_1^*, \dots, h_1^*, \dots, H_1^*, \dots, \int h_1^* dt^*, \dots, \int H_1^* dt^*, \dots]^T \quad (4.14)$$

Average TEA angles are in general nonzero; therefore, the state does not include  $\int \tilde{\theta}_i dt$  as elements. Weighting matrices  $[Q]$  and  $[R]$  are constructed with the associated values presented in Sec. 4.1. The matrices  $[A]$ ,  $[Q]$ , and  $[B]$  are dimensioned  $18 \times 18$ ,  $18 \times 18$ , and  $18 \times 6$ , respectively, in accordance with the number of regulated state variables for this control scheme.

Figure 4.2 shows the eigenvalues of the matrix  $[A] - [B][K]$ , or the closed-loop poles of the system. The diagonal lines mark the points for which the magnitude of the eigenvalue's real number is equal to the magnitude of the eigenvalue's imaginary number; in other words, the points at which a damping ratio of  $1/\sqrt{2}$  is obtained. Regional pole-placement methods presented in

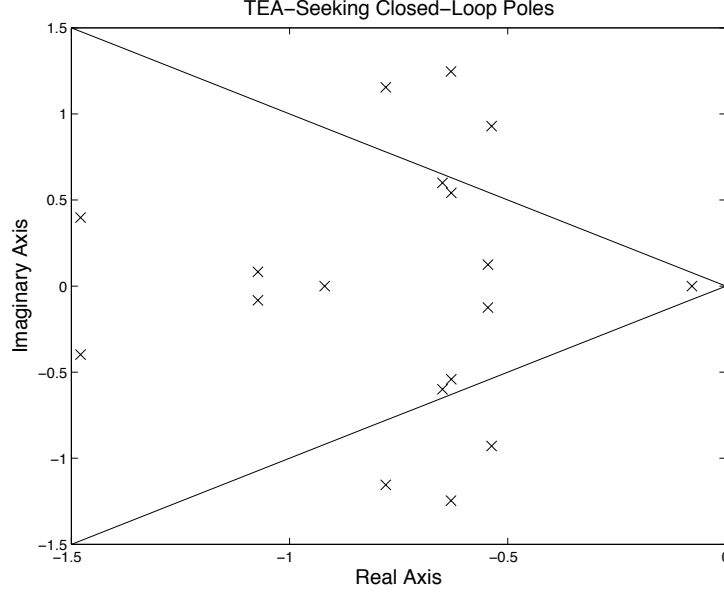


Figure 4.2: TEA-Seeking Closed-Loop Poles

Ref. [26] may also be used to generate pole locations resulting in damping ratios greater than or equal to  $1/\sqrt{2}$ ; however, such methods are beyond the scope of the current research. The transpose of the  $6 \times 18$  gain matrix  $[K]$  associated with these poles is given in Eq. (4.15).

$$[K]^T = \begin{bmatrix} -0.0000 & -4.8044 & -0.0000 & -0.0000 & -4.8044 & -0.0000 \\ -1.8758 & -0.0000 & -0.9269 & -1.8758 & -0.0000 & -0.9269 \\ -3.3422 & -0.0000 & -1.0359 & -3.3422 & -0.0000 & -1.0359 \\ -2.5593 & -0.0000 & -0.8914 & -2.5593 & -0.0000 & -0.8914 \\ -0.0000 & -3.3143 & -0.0000 & -0.0000 & -3.3143 & -0.0000 \\ -0.7727 & -0.0000 & -0.9304 & -0.7727 & -0.0000 & -0.9304 \\ -0.0417 & -0.0000 & -0.6230 & -1.4527 & 0.0000 & -0.4643 \\ -0.0000 & -0.5565 & -0.0000 & -0.0000 & -1.8555 & -0.0000 \\ -0.1041 & 0.0000 & 0.6150 & 0.2912 & -0.0000 & -0.3245 \\ -1.4527 & -0.0000 & -0.4643 & -0.0417 & -0.0000 & -0.6230 \\ -0.0000 & -1.8555 & -0.0000 & -0.0000 & -0.5565 & -0.0000 \\ 0.2912 & 0.0000 & -0.3245 & -0.1041 & -0.0000 & 0.6150 \\ 0.6686 & 0.0000 & 0.1248 & 0.0997 & 0.0000 & -0.2145 \\ -0.0000 & -0.0000 & -0.0000 & -0.0000 & -0.7813 & -0.0000 \\ -0.3108 & 0.0000 & 0.6686 & 0.5341 & -0.0000 & 0.0997 \\ 0.0997 & 0.0000 & -0.2145 & 0.6686 & -0.0000 & 0.1248 \\ -0.0000 & -0.7813 & -0.0000 & -0.0000 & -0.0000 & -0.0000 \\ 0.5341 & 0.0000 & 0.0997 & -0.3108 & -0.0000 & 0.6686 \end{bmatrix} \quad (4.15)$$

Simulation results for this control law, discussed in the remainder of this section, are obtained with the following initial values of the state variables. Angles describing the orientation of  $B$  in  $L$  at  $t = t_0$  are  $\theta_1(t_0) = 5^\circ$  (pitch),  $\theta_2(t_0) = 5^\circ$  (yaw), and  $\theta_3(t_0) = 5^\circ$  (roll). Angular speeds associated with  ${}^N\boldsymbol{\omega}^B$  (with  ${}^L\boldsymbol{\omega}^B = \mathbf{0}$ ) are  $u_1(t_0) = -9.86 \times 10^{-5}$  rad/s,  $u_2(t_0) = -1.12 \times 10^{-3}$  rad/s, and  $u_3(t_0) = 9.82 \times 10^{-5}$  rad/s. Rotor spin speeds are  $u_4(t_0) = u_6(t_0) = u_8(t_0) = -20,000$  rpm, and

$u_5(t_0) = u_7(t_0) = u_9(t_0) = 20,000$  rpm. Initial values of CMG momentum measure numbers are  $h_1(t_0) = h_2(t_0) = h_3(t_0) = 0$ .

#### 4.5.1 Undamped Flywheel Rotors

Figures 4.3–4.8 show performance of the TEA-seeking control law with undamped flywheel rotors, obtained by setting  $C_d = 0$  in Eqs. (2.146)–(2.154).

A time history of the orientation of  $B$  in  $L$ , described with a body-three, 2-3-1 sequence, is shown in the upper plot of Fig. 4.3; the solid curve is used for  $\theta_1$  (pitch), the dashed curve for  $\theta_2$  (yaw), and the dash-dot curve for  $\theta_3$  (roll). The average values of these orientation angles in the steady state are referred to as average torque equilibrium attitude angles, and are approximately the same as those shown in Ref. [6],  $-7.5^\circ$  in pitch,  $-1.2^\circ$  in yaw, and  $-0.2^\circ$  in roll. The amplitudes of the steady state oscillations can be reduced significantly with cyclic disturbance rejection filters, as shown in Ref. [6]. The initial values of the angles, being rather different from the torque equilibrium attitude, lead to the transient behavior evident in the first few orbits in Figs. 4.3–4.8.

The lower plot of Fig. 4.3 illustrates the behavior of  $u_1$ ,  $u_2$ , and  $u_3$ , shown with solid, dashed, and dash-dot curves respectively; their respective average values are 0,  $-n$ , and 0, the condition about which linearization was performed [see Eqs. (2.104)].

Figure 4.4 illustrates the progression of the magnitudes of CMG momentum  $\mathbf{h}$  in the upper curve, and flywheel momentum  $\mathbf{H}$  in the lower curve. The former is obtained from numerical integration of Eqs. (2.100)–(2.102), whereas the latter is calculated according to Eq. (2.39). In the latter portion of the simulation, CMG momentum magnitude remains well below 4,745 N-m-s, the capacity of a single CMG. The similarity of the two curves in Fig. 4.4 is to be expected in view of the equal weights on their errors used to obtain the gains.

Time histories of measure numbers of so-called CMG and flywheel control torques,  $\boldsymbol{\tau}$  and  $\bar{\boldsymbol{\tau}}$ , are presented in Fig. 4.5;  $\tau_1$ ,  $\tau_2$ , and  $\tau_3$  are shown with solid, dashed, and dash-dot curves respectively in the upper plot, whereas  $\bar{\tau}_1$ ,  $\bar{\tau}_2$ , and  $\bar{\tau}_3$  appear in the lower plot. In the steady state, all of these quantities have reasonable amplitudes of 3 or 4 N-m; since the CMG and flywheel momenta are weighted equally, it is not surprising that the curves in the upper plot appear to be the same as the corresponding curves in the lower plot.

Figure 4.6 displays the motor torques that must be applied to the flywheel rotors in order to meet the attitude control and power management requirements. Motor torques of the pair whose spin axes are parallel to  $\hat{\mathbf{b}}_1$  are contained in the upper plots, with  $\mathbf{M}^{B/R_1} \cdot \hat{\mathbf{b}}_1$  represented by the solid curve, and  $\mathbf{M}^{B/R_4} \cdot \hat{\mathbf{b}}_1$  indicated by the dashed curve. Motor torques of the pairs whose spin axes are parallel to  $\hat{\mathbf{b}}_2$  and  $\hat{\mathbf{b}}_3$  are shown in the middle and lower plots, respectively. The first column of Fig. 4.6 shows the flywheel motor torques as a function of time using the pseudo-inverse steering law, the first of two methods presented in Ch. 3, and the second column shows the response using the second method, referred to as the divided power steering law. The time histories resulting from the two steering laws are comparable, and both ultimately lead to the same control torque  $\bar{\boldsymbol{\tau}}$  and required power  ${}^B\bar{P}^F$  because this is the objective of both steering laws. The discontinuities in both instances occur as a result of alternating between charging and discharging in the required power profiles given by Eqs. (4.5) and (4.6).

Figure 4.7 displays the angular speeds of the 6 flywheel rotors relative to  $B$ . Speeds of the pair whose spin axes are parallel to  $\hat{\mathbf{b}}_1$  are contained in the upper plots, with  $u_4$  represented by the solid curve, and  $u_5$  indicated by the dashed curve. Speeds of the pairs whose spin axes are parallel to  $\hat{\mathbf{b}}_2$  and  $\hat{\mathbf{b}}_3$  are shown in the middle and lower plots, respectively. The first column of Fig. 4.7 shows the flywheel angular speeds obtained with the pseudo-inverse steering method, and second column of Fig. 4.7 shows the response using the divided power steering law. The angular speeds

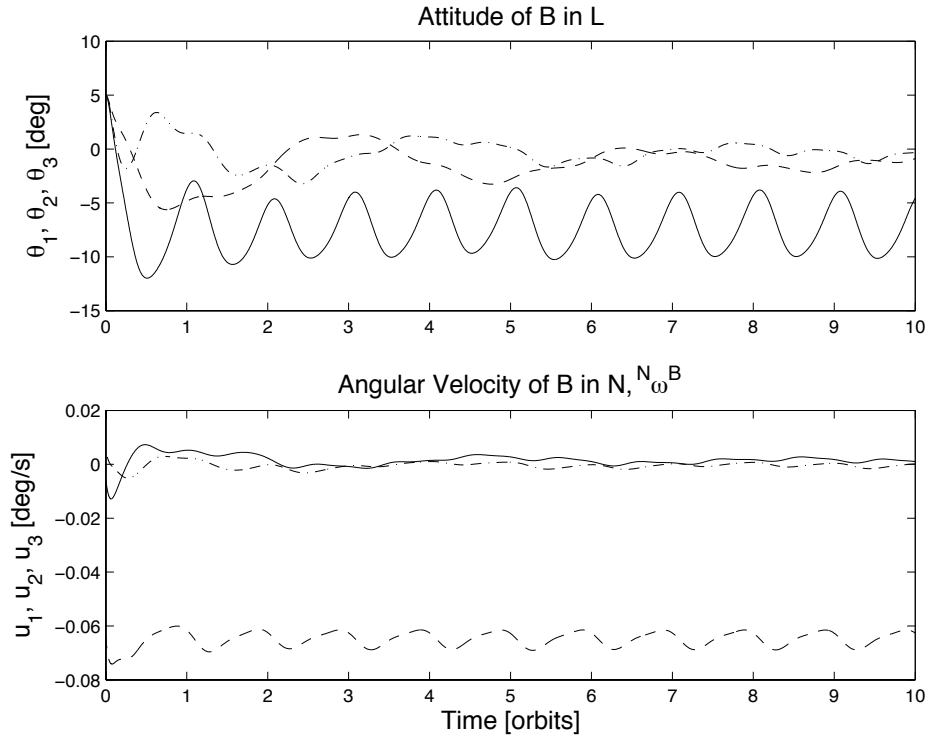


Figure 4.3: Attitude, Angular Velocity

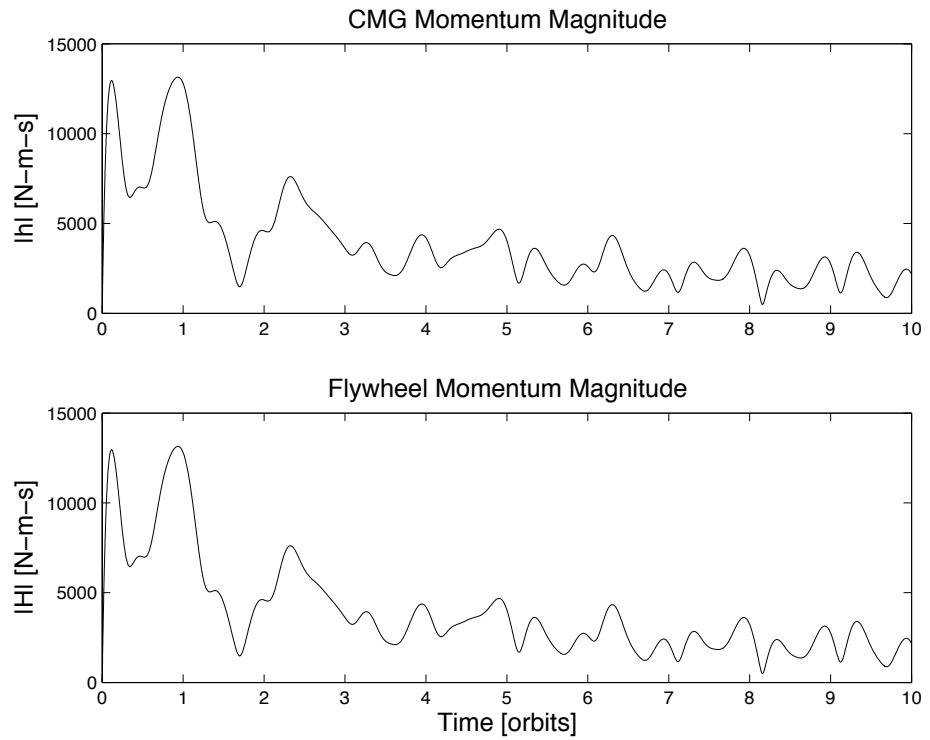


Figure 4.4: Resultant Momentum Magnitude

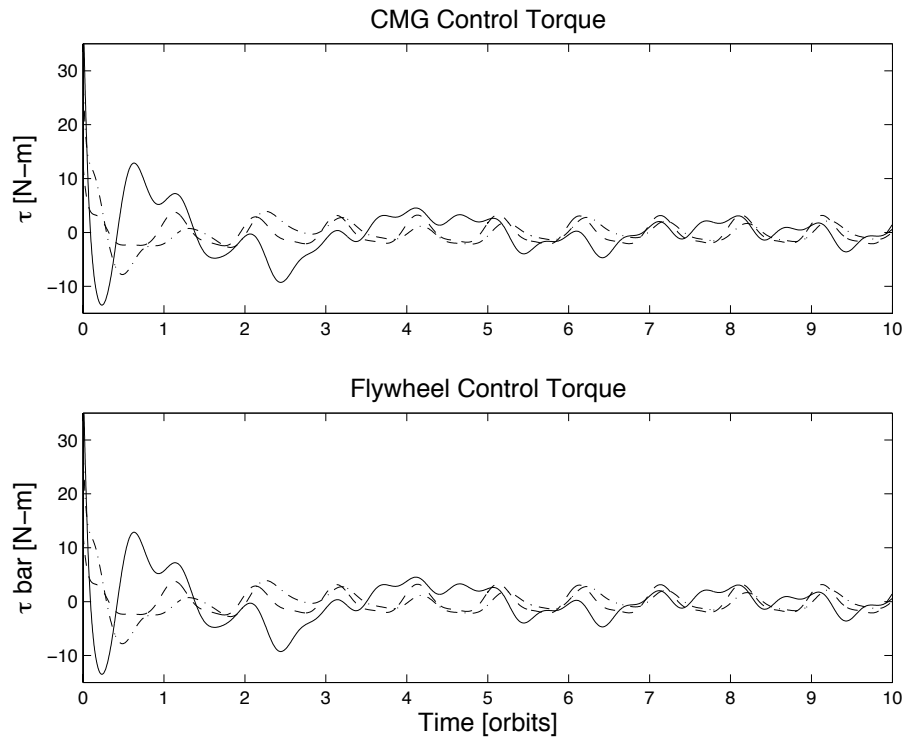


Figure 4.5: Control Torques

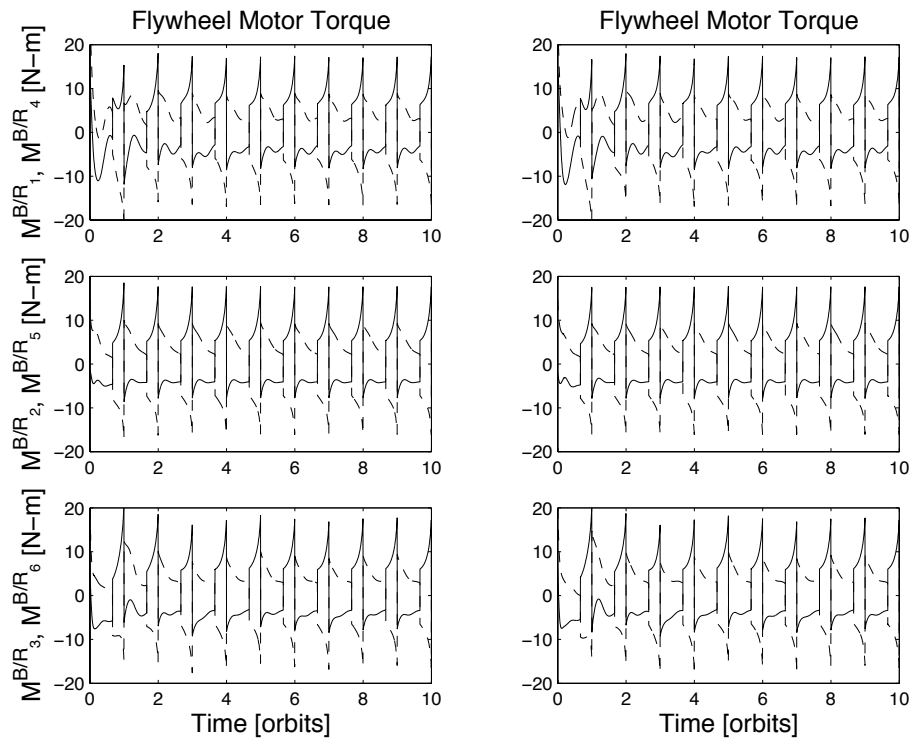


Figure 4.6: Flywheel Motor Torques (Pseudo-Inverse left, Divided Power right)

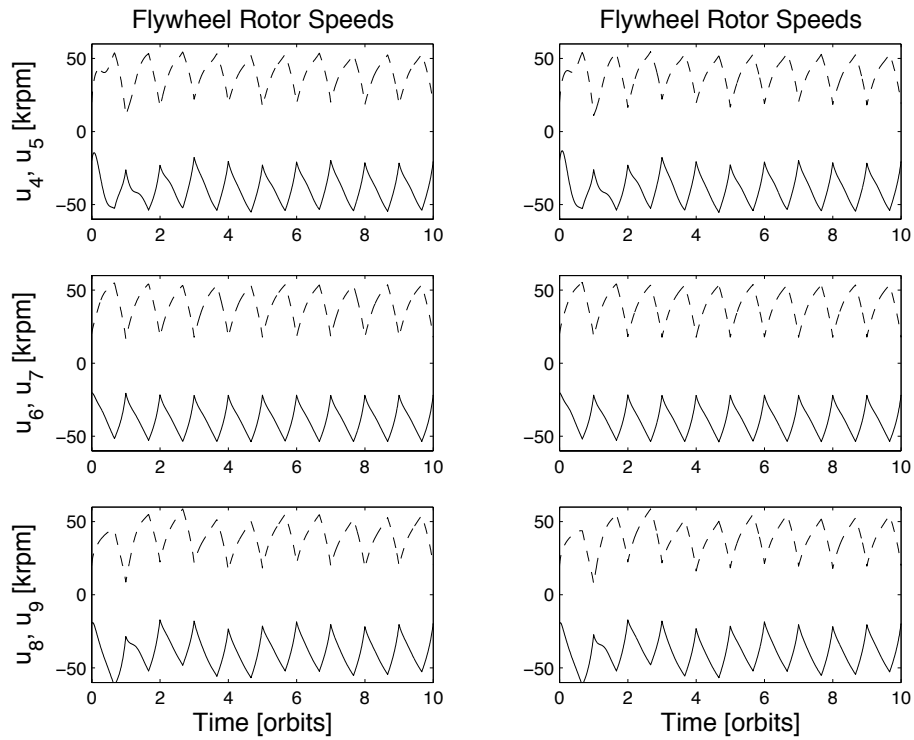


Figure 4.7: Flywheel Angular Speeds (Pseudo-Inverse left, Divided Power right)

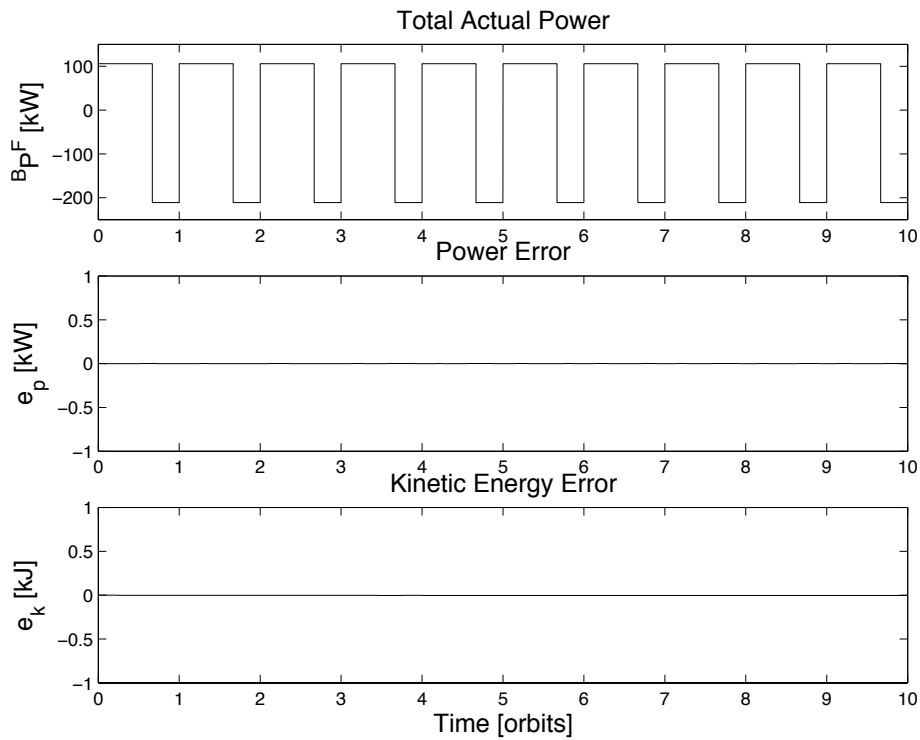


Figure 4.8: Power, Power Error, and Kinetic Energy Error

are similar, but not identical, because the flywheel motor torques are not unique, even though both steering laws produce flywheel motor torques that will meet the attitude control torque and power management requirements. With the exception of  $u_8$  during a brief period in the first orbit, the absolute values of the rotor speeds remain less than 60,000 rpm, as they must. In keeping with typical flywheel designs, all of the rotor speeds have a ratio of maximum to minimum absolute value of approximately 3 to 1 as they charge and discharge.

The total power of the flywheels  ${}^B P^F$  is calculated from the motor-generator torques and wheel speeds by means of Eqs. (3.7), and is seen in the upper plot of Fig. 4.8 to have very nearly the profile specified in Eqs. (4.5), 105.6 kW when the flywheels charge, and -211.2 kW when they discharge. In fact, the second and third plots of  $e_p$  and  $e_k$  [see Eqs. (4.10) and (4.11)] reveal no errors in power or kinetic energy; this is to be expected since  $C_d = 0$ . It is clear that the power tracking objectives are achieved at the same time that the flywheels are used to assist the CMGs in attitude control.

### 4.5.2 Damped Flywheel Rotors

The detrimental effects of damping are brought to light by repeating the simulation described in Sec. 4.5.1, with an illustrative value of  $10^{-5}$  N-m-s for the damping coefficient  $C_d$ . One might be tempted to neglect such a seemingly small effect, especially over the short term, but it is shown here to be troublesome if not dealt with over long periods. The performance of the TEA-seeking control law without feedback of kinetic energy error is recorded in Figs. 4.9–4.12.

Figure 4.9 shows the time history of the attitude angles and the inertial angular velocity. As in the previous example, the solid curve is used for  $\theta_1$  (pitch), the dashed curve for  $\theta_2$  (yaw), and the dash-dot curve is used for  $\theta_3$  (roll). The attitude response is virtually the same, and the average TEA found by the control system is the same as in the case with undamped rotors. The lower plot of Fig. 4.9 shows the inertial angular velocity response, with  $u_1$ ,  $u_2$ , and  $u_3$ , shown with solid, dashed, and dash-dot curves respectively.

The upper plot of Fig. 4.10 contains the actual power delivered to the spacecraft by the flywheel system as a function of time. The middle plot displays the error between the actual power and the required power due to the damping in the flywheel system, which leads to the large secular kinetic energy loss of more than 50,000 kJ after 10 orbits, shown in the lower plot.

The kinetic energy error of the flywheel system is reflected in the angular speeds of the flywheels relative to  $B$  shown in Fig. 4.11. As in Fig. 4.7, speeds of the flywheel pair whose spin axes are parallel to  $\hat{\mathbf{b}}_1$  are contained in the upper plots, with  $u_4$  represented by the solid curve, and  $u_5$  indicated by the dashed; speeds of the pairs whose spin axes are parallel to  $\hat{\mathbf{b}}_2$  and  $\hat{\mathbf{b}}_3$  are depicted in the middle and lower plots, respectively. The flywheel rotor speeds exhibit a secular decay which is not present in the undamped flywheel speeds seen in Fig. 4.7. No significant difference appears between the behavior resulting from the pseudo-inverse and divided power steering laws, presented in the left and right columns, respectively.

Time histories of flywheel motor torques, in the presence of damping, are displayed in Fig. 4.12 where the results in the left and right columns are associated with the pseudo-inverse and divided power steering laws, respectively. A comparison with Fig. 4.6 reveals the effects of damping to be negligible at first; however, after some time it is apparent that damping causes the motor torque magnitudes to increase, with either steering law. Inspection of Eq. (3.7) indicates that the secular decay in rotor speeds requires an increase in motor torques in order to produce the required power. The increase in motor torque magnitudes implies further power losses as more electrical power must be diverted to the motor-generators in order to meet the attitude control and power management requirements simultaneously.

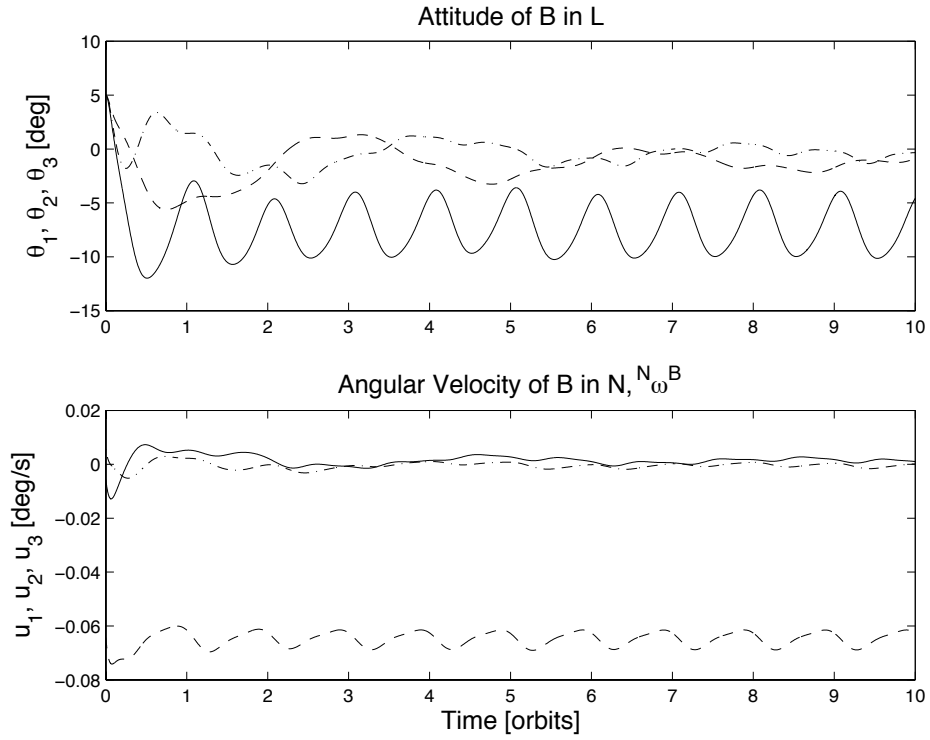


Figure 4.9: Attitude, Angular Velocity with Damped Flywheel Rotors

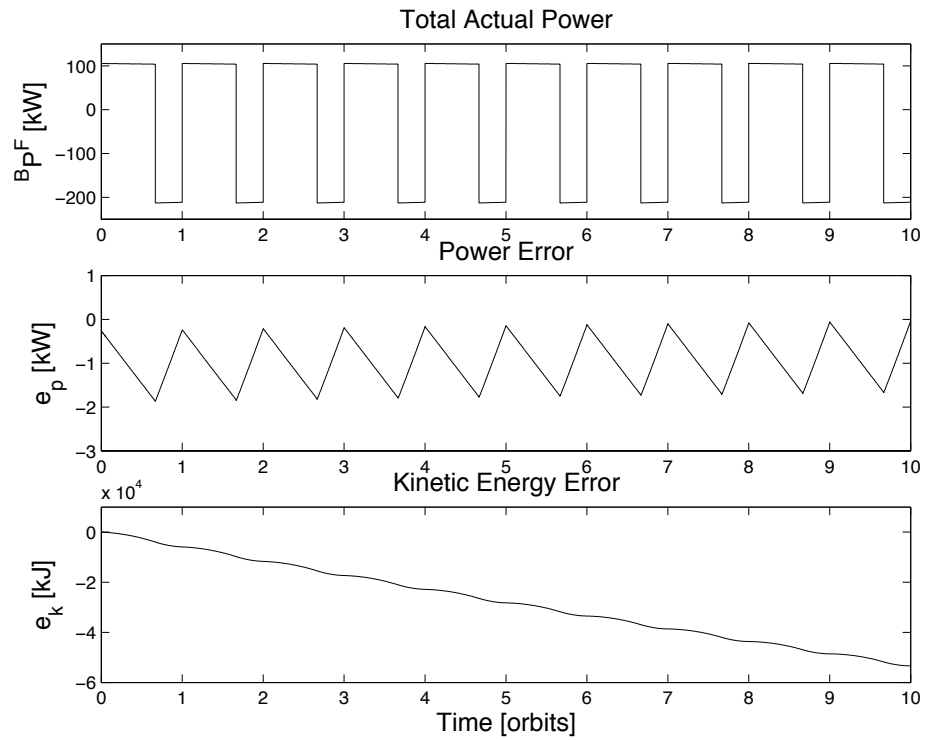


Figure 4.10: Power, Power Error, Kinetic Energy Error with Damped Flywheel Rotors

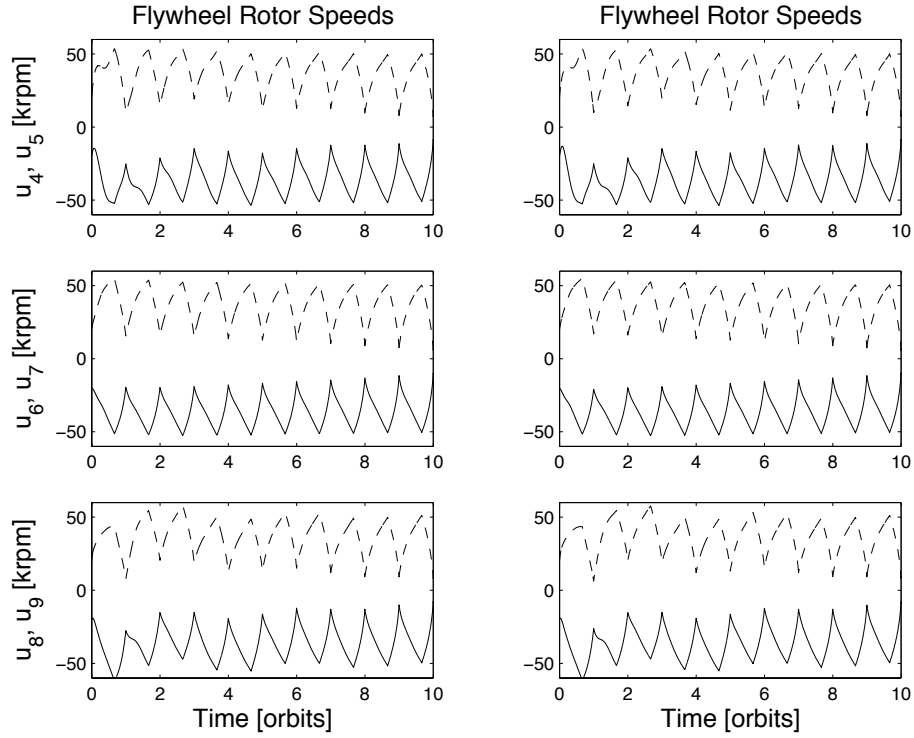


Figure 4.11: Flywheel Angular Speeds with Damped Flywheel Rotors (Pseudo-Inverse left, Divided Power right)

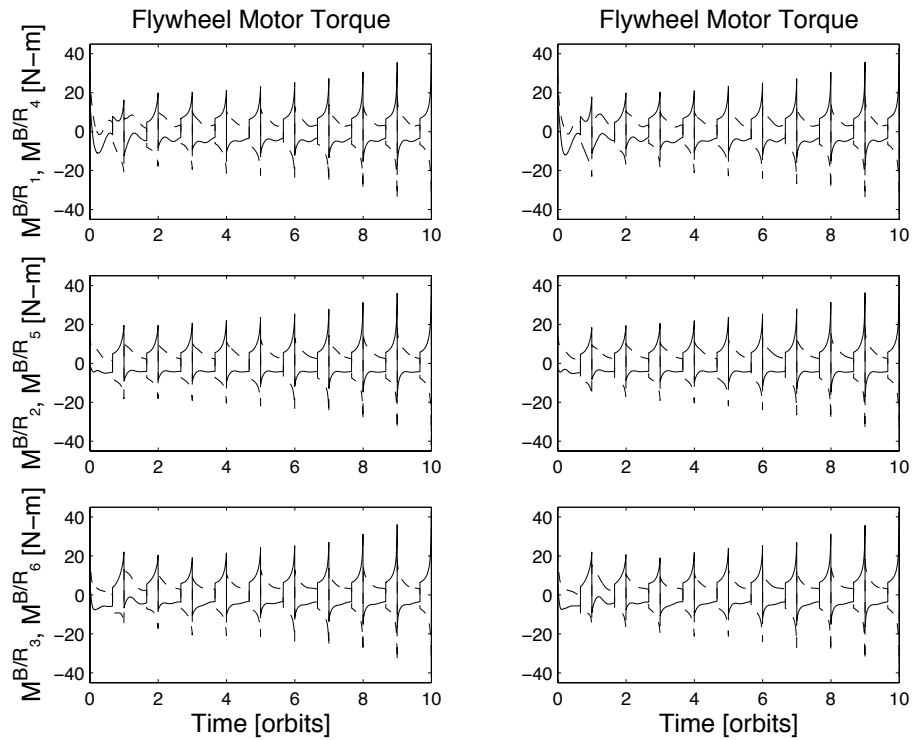


Figure 4.12: Flywheel Motor Torque with Damped Flywheel Rotors (Pseudo-Inverse left, Divided Power right)

### 4.5.3 Counteracting Damping with Kinetic Energy Error Feedback

To compensate for damping, the kinetic energy error feedback designed in Sec. 4.3 is employed with a weighting parameter  $\lambda$  of  $1 \text{ s}^{-2}$ . The parameters of the simulation discussed in Sec. 4.5.2 are used again, leading to the results reported in Figs. 4.13–4.15.

Figure 4.13 shows that kinetic energy feedback eliminates the secular decay of rotor speeds seen to result from flywheel rotor damping in Fig. 4.11.

The flywheel motor torques are shown in Fig. 4.14. It is immediately clear that the magnitudes do not increase with time as they do in Fig. 4.12.

The power error  $e_p$  shown in the middle plot of Fig. 4.15 is quite small and leads to the kinetic energy error  $e_k$  displayed in the lower plot, which is small and periodic, in contrast to the secular decay obtained without energy feedback ( $\lambda = 0 \text{ s}^{-2}$ ).

As evidenced by the results shown in this section, the kinetic energy error feedback method compensates for damping very effectively, and leads to power management results that are virtually the same as those for the undamped rotors.

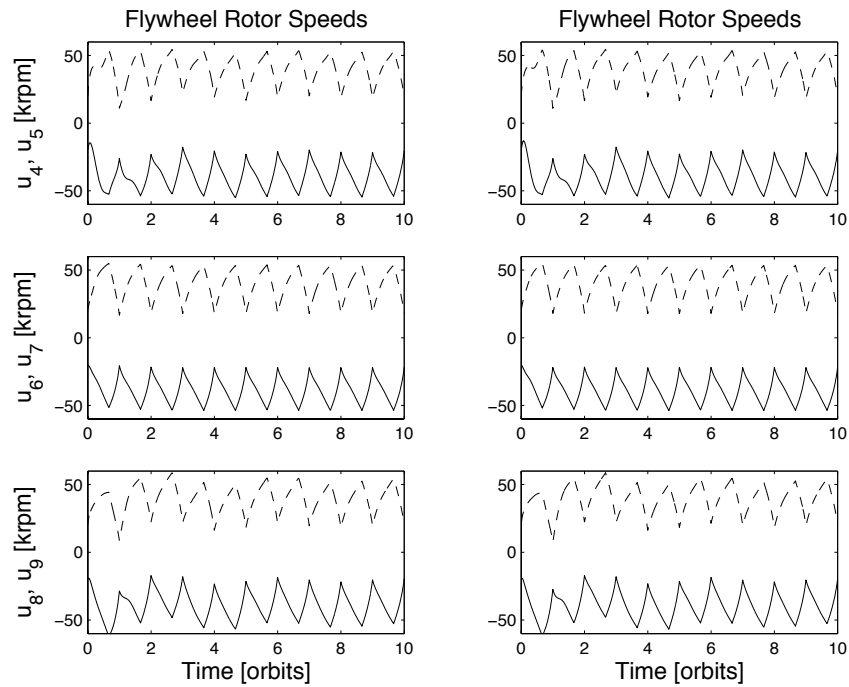


Figure 4.13: Flywheel Angular Speeds with Damped Flywheel Rotors and Kinetic Energy Error Feedback (Pseudo-Inverse left, Divided Power right)

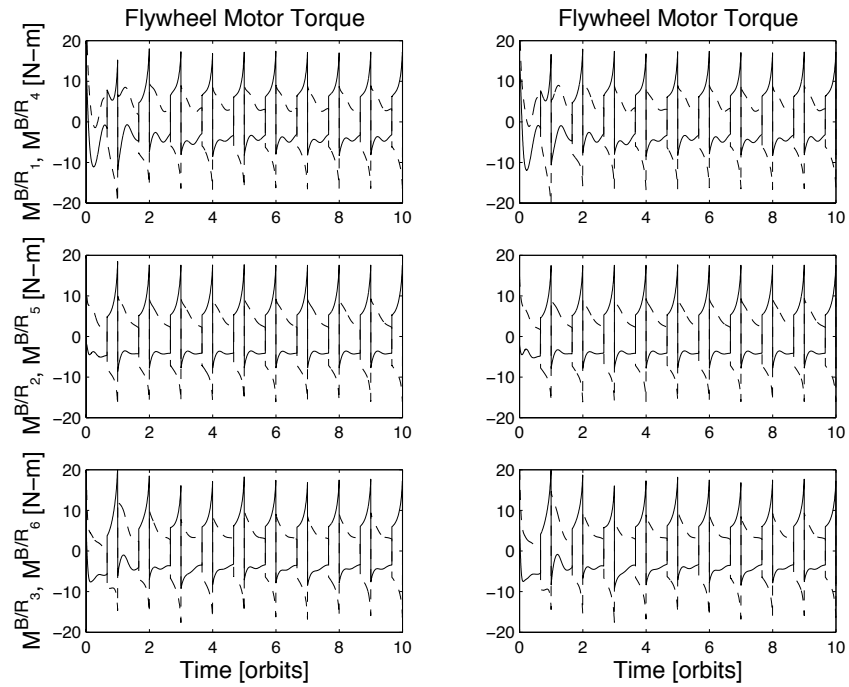


Figure 4.14: Flywheel Motor Torques with Damped Flywheel Rotors and Kinetic Energy Error Feedback (Pseudo-Inverse left, Divided Power right)

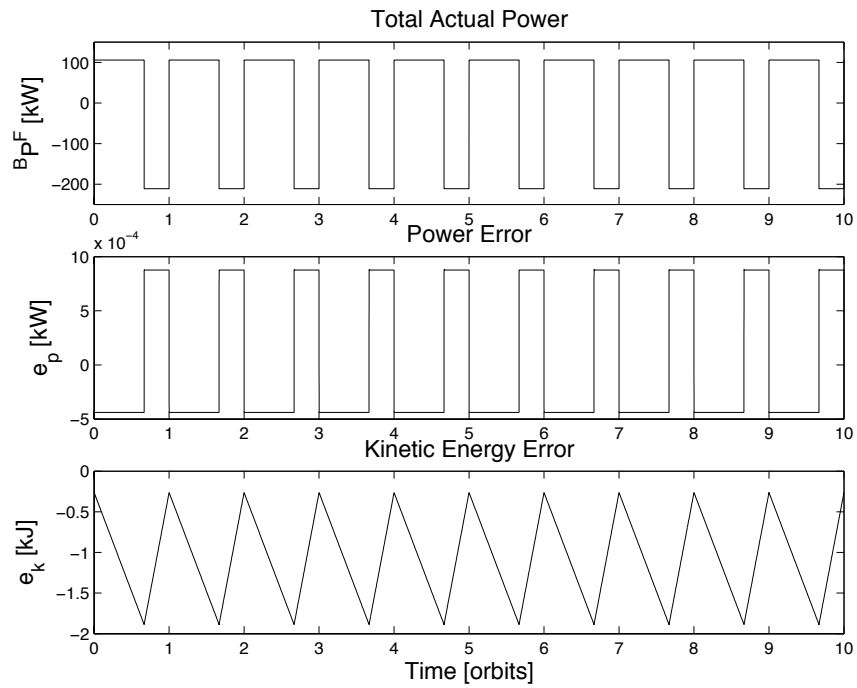


Figure 4.15: Power, Power Error, and Kinetic Energy Error with Damped Flywheel Rotors and Kinetic Energy Error Feedback

#### 4.5.4 Comparison of Steering Laws

In the results presented thus far, two steering laws have been used to determine the flywheel motor torques necessary to meet the attitude control and power management requirements simultaneously. The first of these involves formation of a pseudo-inverse to solve an underdetermined system of equations for flywheel motor torques, whereas the second divides the power requirements evenly among the three pairs of rotors, resulting in a uniquely determined solution. The objective of both approaches is to produce the same control torque  $\bar{\tau}$  and required power  ${}^B\bar{P}^F$ ; therefore, it is not surprising that large differences are not discernible in the left and right columns of the figures presented in Secs. 4.5.1–4.5.3. A more detailed comparison of the differences is now undertaken with the aid of Figs. 4.16–4.18, where results obtained with the pseudo-inverse and divided power methods are displayed with solid and dashed lines respectively.

Figure 4.16 shows time histories of the square root of the sum of the squares of the motor torques,  $\{\sum_{i=1}^3[(\mathbf{M}^{B/R_i} \cdot \hat{\mathbf{b}}_i)^2 + (\mathbf{M}^{B/R_{i+3}} \cdot \hat{\mathbf{b}}_i)^2]\}^{\frac{1}{2}}$ , a quantity that is minimized by the pseudo-inverse approach. Curves associated with undamped flywheel rotors are contained in the first row, damped rotors in the second row, and damped rotors with kinetic energy error feedback in the third row. The solutions of the pseudo-inverse and divided power methods are indistinguishable from one another when viewed over an interval of 10 orbits in the left column; consequently, detailed plots are shown in the right column for the first half of an orbit. As expected, it can be seen that the minimum-norm solution of the pseudo-inverse method is always less than or equal to the result given by the divided-power method. These plots also seem to indicate that the pseudo-inverse solution approaches the divided-power solution in the steady state. The benefit of the kinetic energy error feedback is apparent once more, by comparing the growth in the second row of the first column with the absence of growth in the third row.

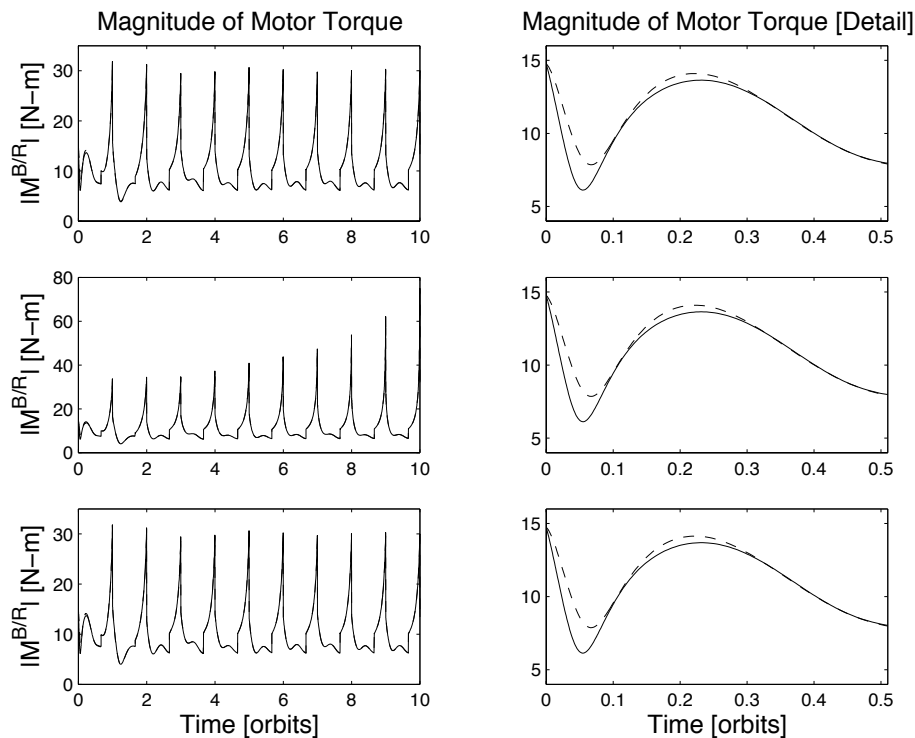


Figure 4.16: Magnitude of Flywheel Motor Torque

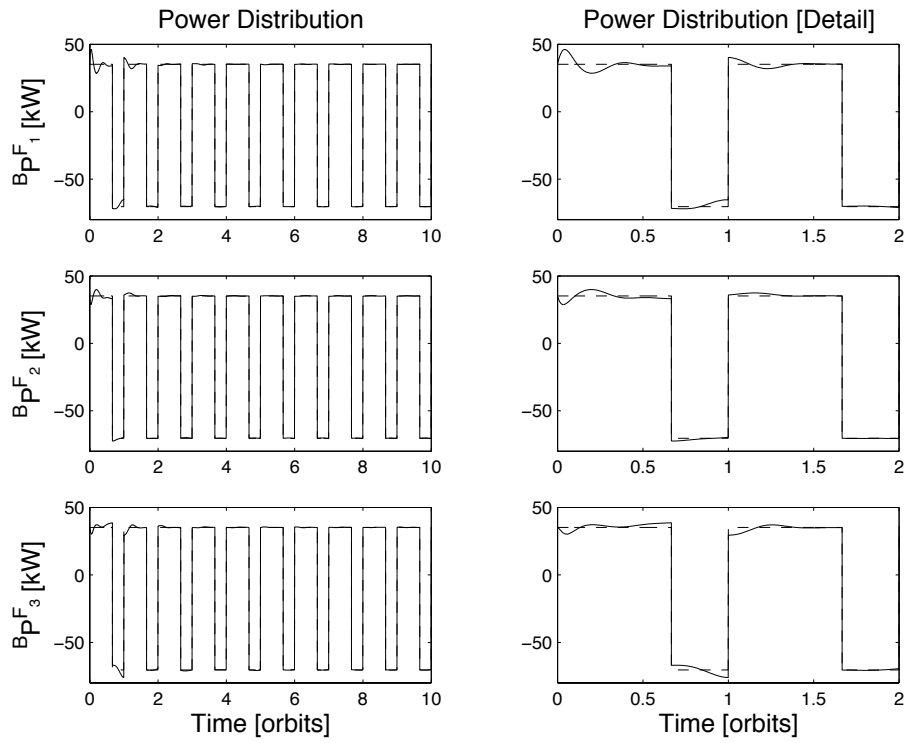


Figure 4.17: Power Distribution

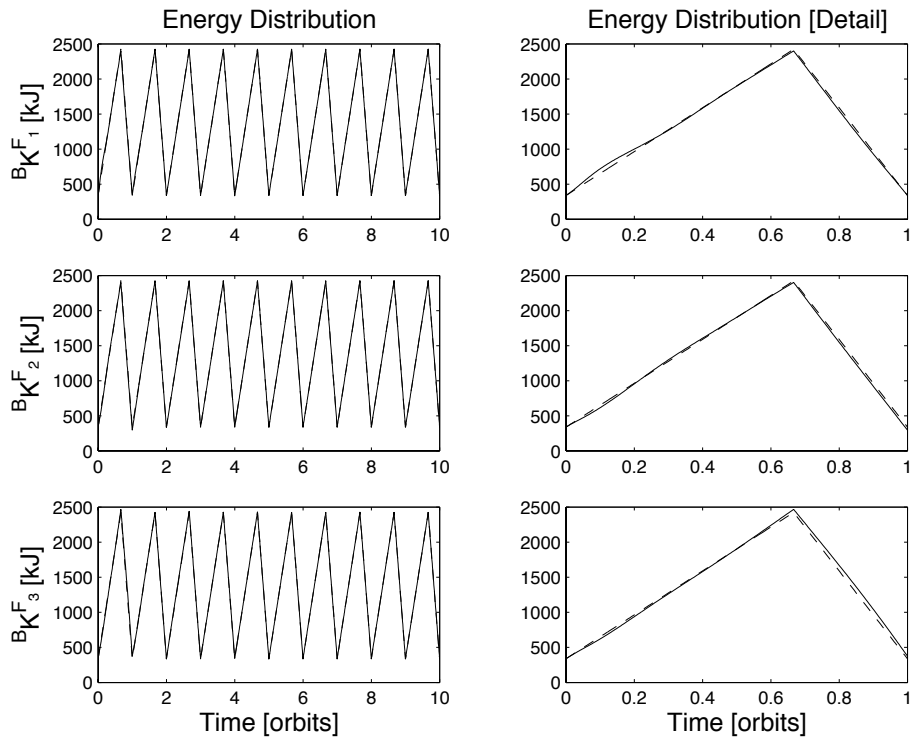


Figure 4.18: Energy Distribution

Figure 4.17 shows the distribution of power among the flywheel pairs, in the absence of damping. The first row contains the power  ${}^B P^{F_1}$  [see Eqs. (3.17)] of the rotor pair whose spin axes are aligned with  $\hat{\mathbf{b}}_1$ , and the second and third rows show  ${}^B P^{F_2}$  and  ${}^B P^{F_3}$ . A detail of the plots for the first 2 orbits is shown in the right column of Fig. 4.17.

Similarly, Fig. 4.18 displays the rotational kinetic energy possessed by each flywheel pair, in the absence of damping. The first, second, and third rows contain, respectively,  ${}^B K^{F_i} \triangleq J[(u_{2i+2})^2 + (u_{2i+3})^2]/2$ , ( $i = 1, 2, 3$ ). The kinetic energies resulting from the two steering laws are indistinguishable when viewed over 10 orbits in the left column; therefore, detailed plots are shown in the right column for a single orbit.

Naturally, the divided-power steering law distributes the power and energy equally between the three flywheel pairs. The pseudo-inverse steering law apportions the power profile among the three pairs in such a way that the total power requirement is met, but the minimum-norm solution for motor torques yields an unequal distribution of power and energy. As noted in connection with Fig. 4.16, the power and energy distributions resulting from the pseudo-inverse steering law appear to approach those of the divided power law in the steady state. Similar comparisons involving damping with and without kinetic energy feedback support these conclusions. Failure to meet power requirements exactly is remedied by the feedback of kinetic energy error, as previously discussed.

## 4.6 Attitude Hold

The operation involving rendezvous and docking of ISS with another spacecraft requires the attitude of the ISS to be held fixed in a local-vertical-local-horizontal reference frame, an objective that differs from maintenance of a continuously varying TEA, and management of angular momentum. Rather than continuously varying the spacecraft attitude to manage angular momentum, the controllers can be configured to keep the spacecraft in a specified orientation. In this section, several control laws for holding attitude are designed, and applied in simulations. Attitude hold without management of angular momentum of flywheels or CMGs is the subject of Sec. 4.6.1, the addition of flywheel momentum management is taken up in Sec. 4.6.2, and attitude hold by means of thrusters is discussed in Sec. 4.6.3. Finally, a comparison of the amount of propellant required by various operational techniques is presented in Sec. 4.6.4. In the interest of simplicity, only the pseudo-inverse steering law is exercised in performing these simulations, and flywheel rotor damping is not present.

### 4.6.1 Attitude Hold without Momentum Management

The LQR theory is applied here to the problem of holding a specified attitude without regard for the angular momentum possessed by flywheels or CMGs. The regulated states are

$$\{x\} = [ \theta_1^*, \theta_2^*, \theta_3^*, u_1^*, u_2^*, u_3^*, \int \theta_1^* dt^*, \int \theta_2^* dt^*, \int \theta_3^* dt^* ]^T \quad (4.16)$$

and the weighting matrices  $[Q]$  and  $[R]$  contain associated values presented in Sec. 4.1. The matrices  $[A]$ ,  $[Q]$ , and  $[B]$  are dimensioned  $9 \times 9$ ,  $9 \times 9$ , and  $9 \times 6$ , respectively, in accordance with the number of regulated state variables for this control scheme. Figure 4.19 shows the eigenvalues of the matrix  $[A] - [B][K]$ , or the closed-loop poles of the system. The diagonal lines mark the points at which a damping ratio of  $1/\sqrt{2}$  is obtained. The transpose of the  $6 \times 9$  gain matrix  $[K]$  associated with these poles is given in Eq. (4.17).

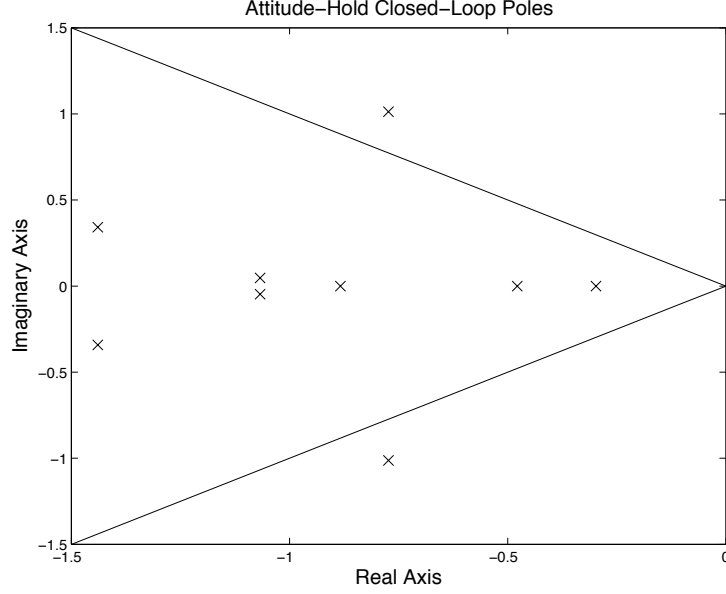


Figure 4.19: Attitude-Hold Closed-Loop Poles

$$[K]^T = \begin{bmatrix} -0.0000 & -2.8176 & 0.0000 & -0.0000 & -2.8176 & 0.0000 \\ -0.7053 & 0.0000 & -0.7346 & -0.7053 & 0.0000 & -0.7346 \\ -2.4708 & -0.0000 & -0.0587 & -2.4708 & -0.0000 & -0.0587 \\ -1.5429 & -0.0000 & -0.1458 & -1.5429 & -0.0000 & -0.1458 \\ -0.0000 & -1.6786 & 0.0000 & -0.0000 & -1.6786 & 0.0000 \\ -0.3632 & 0.0000 & -0.8886 & -0.3632 & 0.0000 & -0.8886 \\ 0.0000 & -0.5235 & 0.0000 & 0.0000 & -0.5235 & 0.0000 \\ 0.3190 & 0.0000 & -0.1908 & 0.3190 & 0.0000 & -0.1908 \\ -0.3012 & 0.0000 & -0.2021 & -0.3012 & 0.0000 & -0.2021 \end{bmatrix} \quad (4.17)$$

The simulation results presented in Figs. 4.20–4.24 are obtained with this control law, together with the initial values of the state variables employed in Sec. 4.5. The commanded attitude for this simulation is  $\theta_1^* = \theta_2^* = \theta_3^* = 0$ ; hence, a small-angle reorientation is necessary at first to align the spacecraft with the commanded attitude. Following this, the control law counteracts the disturbance torques to maintain that attitude until actuator saturation.

A time history of the orientation of  $B$  in  $L$ , described with a body-three, 2-3-1 sequence, is shown in the upper plot of Fig. 4.20; the solid curve is used for  $\theta_1$  (pitch), the dashed curve for  $\theta_2$  (yaw), and the dash-dot curve for  $\theta_3$  (roll). The lower plot of Fig. 4.20 illustrates the behavior of  $u_1$ ,  $u_2$ , and  $u_3$ , shown with solid, dotted, and dashed curves respectively. These results show the response due to the difference between the initial attitude and the commanded attitude. The attitude response reaches steady-state after roughly 1.5 orbits.

Figure 4.21 displays the magnitude of momentum of the CMGs and flywheels in the upper and lower plots, respectively. Once again, the CMGs and flywheels are weighted evenly in the control law design, and as a result the momentum time histories are the same. The secular growth in the CMG and flywheel momentum is a consequence of the commanded attitude not being equal to the torque equilibrium attitude.

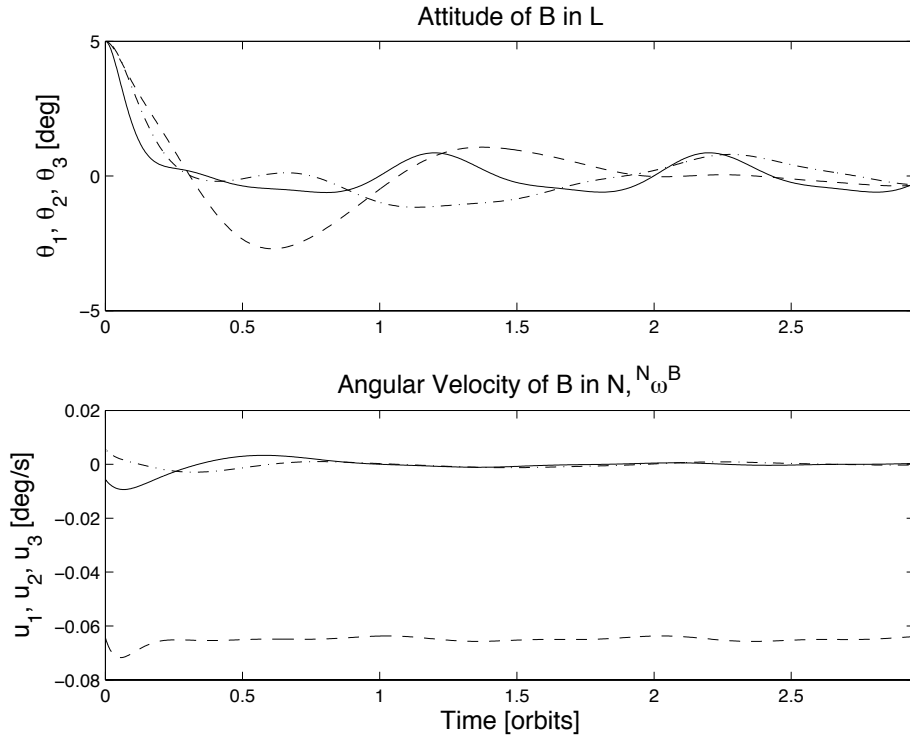


Figure 4.20: Attitude, Angular Velocity

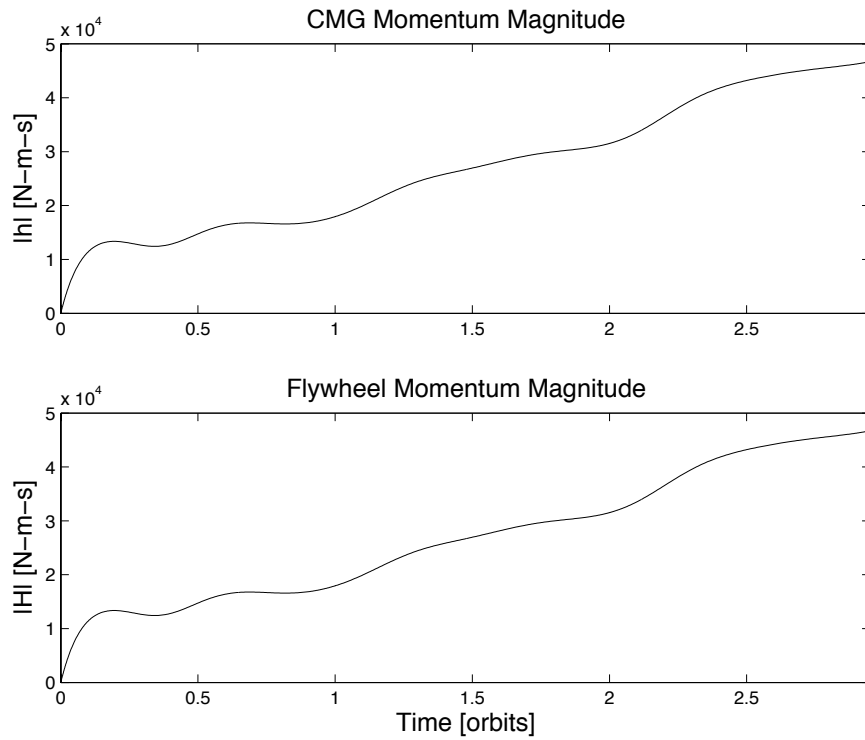


Figure 4.21: Resultant Momentum Magnitude

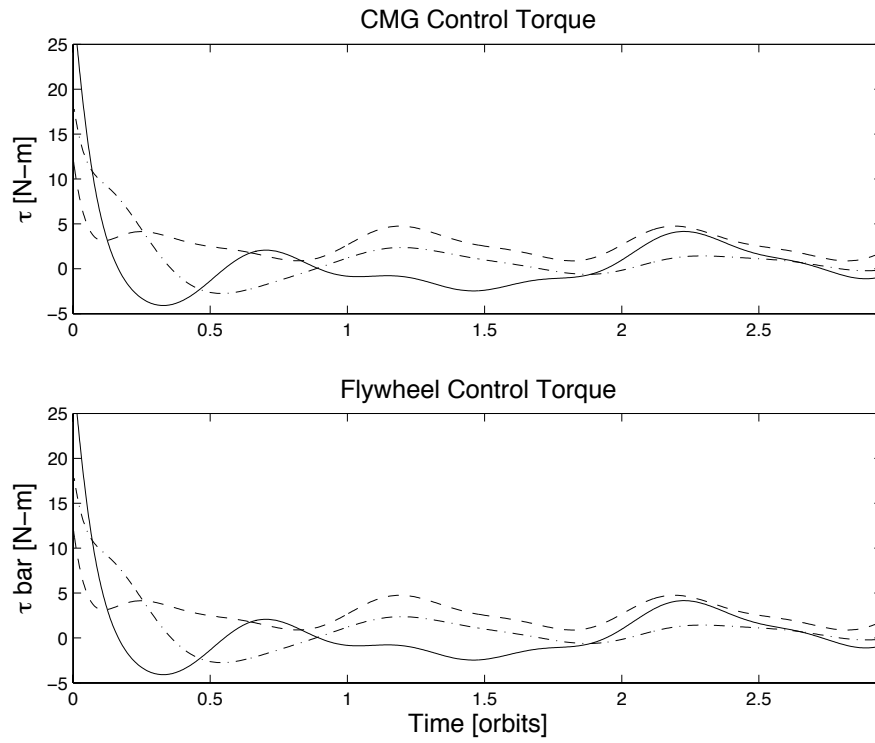


Figure 4.22: Control Torques

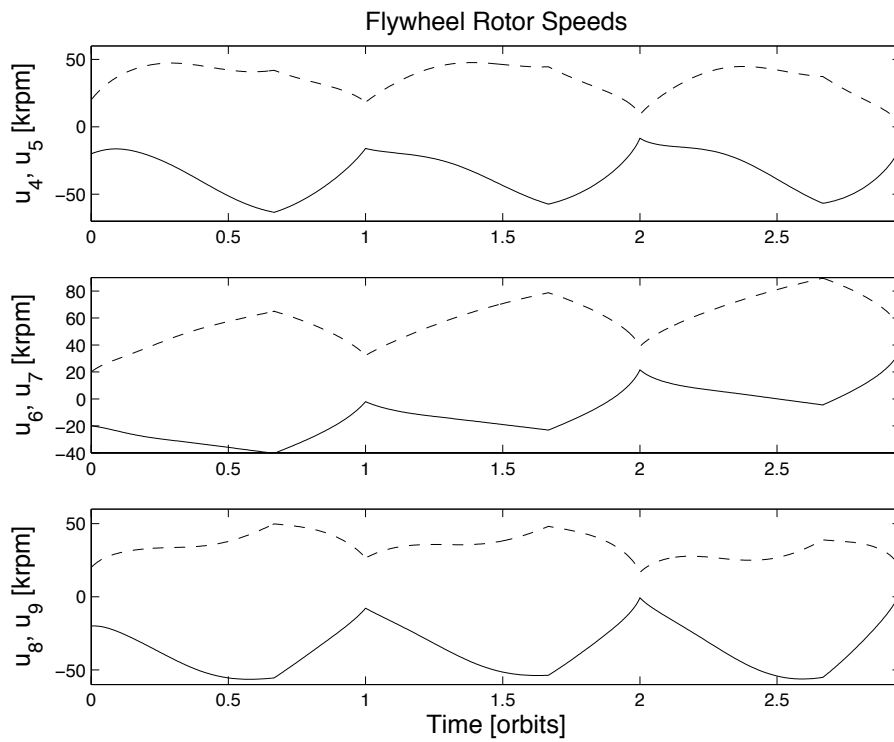


Figure 4.23: Flywheel Angular Speeds

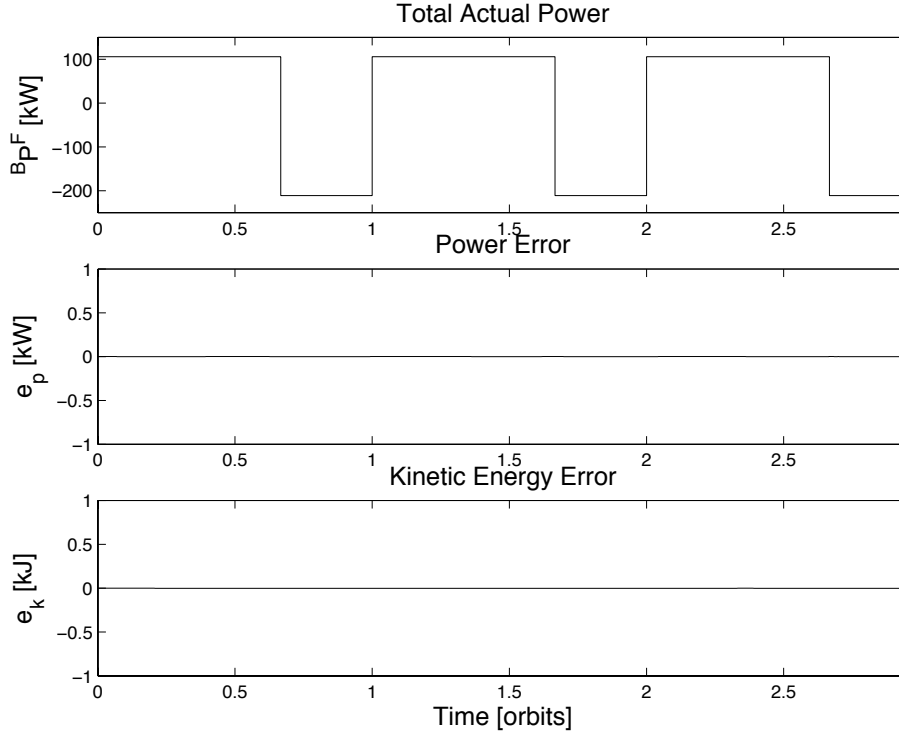


Figure 4.24: Power, Power Error, Kinetic Energy Error

Figure 4.22 shows the time histories of the CMG and flywheel control torques required to hold the attitude specified for this simulation. In each case, the torque component in the direction of  $\hat{\mathbf{b}}_1$  is depicted with a solid curve, and those for  $\hat{\mathbf{b}}_2$  and  $\hat{\mathbf{b}}_3$  are indicated with dashed and dash-dot curves, respectively. It is apparent in this plot that the flywheel and CMG control torques are the same, which is to be expected because they are weighted evenly in the control law. In the steady-state, the control torques obtained with the TEA-seeking controller (see Fig. 4.5) are similar in magnitude to those observed here; however, a key difference is the presence of offsets or biases in the control torques for both types of actuator, caused by constant terms in the aerodynamic and gravity gradient disturbance torques. This offset exists for all three components of the control torque, leading to the secular momentum build up in the actuators; however it is most obvious in the  $\hat{\mathbf{b}}_2$  direction.

Figure 4.23 displays the angular speeds of the 6 flywheel rotors relative to  $B$ . Speeds of the pair whose spin axes are parallel to  $\hat{\mathbf{b}}_1$  are contained in the upper plot, with  $u_4$  represented by the solid curve, and  $u_5$  indicated by the dashed. Speeds of the pairs whose spin axes are parallel to  $\hat{\mathbf{b}}_2$  and  $\hat{\mathbf{b}}_3$  are shown in the middle and lower plots, respectively. The behavior illustrated in this plot is clearly not acceptable; the maximum speed is exceeded quickly as the flywheels store momentum. The rotor speeds in each pair gradually approach each other in order to produce the maximum amount of torque in one direction, which is needed to counter the secular external torque acting on the spacecraft. Just before the end of the third orbit, all flywheel pairs reach the same angular speeds, causing a singularity in the steering law that prevents the required power from being supplied, and thus the simulation is stopped at this point. Prior to this event, the power requirements and attitude control requirements are met simultaneously by the flywheel rotors, as is evident from Fig. 4.24.

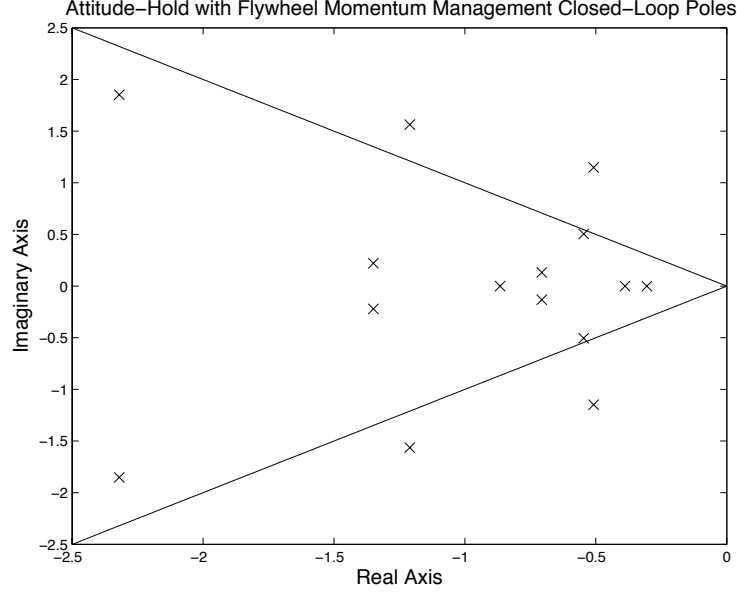


Figure 4.25: Attitude-Hold Closed-Loop Poles, with Flywheel Momentum Management

#### 4.6.2 Attitude Hold with Flywheel Momentum Management

In order to prevent the angular speeds of the flywheel pairs from becoming equal and causing a singularity in the steering law that renders the system incapable of providing the required power to the spacecraft, the control law may be reformulated by adding flywheel angular momenta and their integrals to the set of regulated state variables. Hence,

$$\{x\} = [\theta_1^*, \theta_2^*, \theta_3^*, u_1^*, \dots, H_1^*, \dots, \int H_1^* dt^*, \dots, \int \theta_1^* dt^*, \dots]^T \quad (4.18)$$

In a sense, this configuration is a hybrid of the TEA-seeking and attitude-hold control laws, in which the CMGs are used to store momentum, and flywheels and CMGs both provide an attitude control torque. At the same time, the flywheel momentum feedback ensures that the angular speeds remain in the desired range of operation. The poles of the closed-loop system are shown in Fig. 4.25. The transpose of the  $6 \times 15$  gain matrix  $[K]$  associated with these poles is given in Eq. (4.19).

$$[K]^T = \begin{bmatrix} 0.0000 & -8.2728 & -0.0000 & 0.0000 & -7.0146 & -0.0000 \\ -0.6427 & -0.0000 & -1.9619 & -0.3762 & -0.0000 & -1.4324 \\ -4.5821 & 0.0000 & -0.6899 & -2.9227 & -0.0000 & -0.5904 \\ -2.5466 & 0.0000 & -0.2657 & -1.4013 & -0.0000 & -0.3135 \\ 0.0000 & -3.4046 & -0.0000 & 0.0000 & -2.2261 & 0.0000 \\ -0.3607 & -0.0000 & -1.8298 & -0.2380 & -0.0000 & -0.9712 \\ -1.1454 & 0.0000 & -0.0904 & 0.7325 & -0.0000 & -0.2230 \\ 0.0000 & -1.1785 & 0.0000 & 0.0000 & 0.9679 & 0.0000 \\ 0.0649 & -0.0000 & -0.8586 & -0.1152 & -0.0000 & 0.7623 \\ -0.3763 & 0.0000 & -0.4183 & 0.3446 & -0.0000 & 0.2878 \\ -0.0000 & -0.5997 & 0.0000 & 0.0000 & 0.5007 & -0.0000 \\ 0.5133 & 0.0000 & -0.2593 & -0.4069 & 0.0000 & 0.4765 \\ 0.0000 & -3.4646 & -0.0000 & 0.0000 & -4.1502 & -0.0000 \\ 0.6967 & -0.0000 & -0.4564 & 0.5354 & -0.0000 & -0.4644 \\ -0.3477 & -0.0000 & -0.5374 & -0.7276 & -0.0000 & -0.4741 \end{bmatrix} \quad (4.19)$$

The attitude response produced with this control law is shown in Fig. 4.26, and is quite similar to the behavior obtained without flywheel momentum feedback, presented in Fig. 4.20.

In contrast to the unacceptable motion exhibited in Fig. 4.23, the angular speeds of the flywheel pairs shown in Fig. 4.27 remain well separated and within the stated limits as a consequence of flywheel momentum feedback, thereby avoiding singularities while providing attitude control torque and power management simultaneously.

Figure 4.28 shows the magnitude of CMG momentum in the upper plot, and the magnitude of flywheel momentum in the lower plot. The flywheel momentum remains small, apart from initial transients, due to the momentum feedback terms in the control law. The CMG momentum, however, grows without bound because the commanded attitude differs from the torque equilibrium attitude. The CMG momentum magnitude slope resulting from this control law configuration is essentially double that of Fig. 4.21 because the flywheels no longer aid the CMGs in storing the secular momentum.

Figure 4.29 displays the control torque required to maintain the commanded attitude while simultaneously managing the flywheel momentum. Not surprisingly, the CMG control torque is larger than the flywheel control torque, and it is apparent upon comparing the plots that the CMGs are providing the torque required to null the effect of the constant terms in the disturbance torque, judging by the non-zero offsets. This offset results in the secular momentum buildup in the CMGs. The flywheels do not assist in cancelling the constant terms, but do aid the CMGs in overcoming the periodic terms in the disturbance resulting from aerodynamic and gravity torque. As in the previous example without flywheel momentum feedback, the offset is most apparent in the  $\hat{\mathbf{b}}_2$  direction.

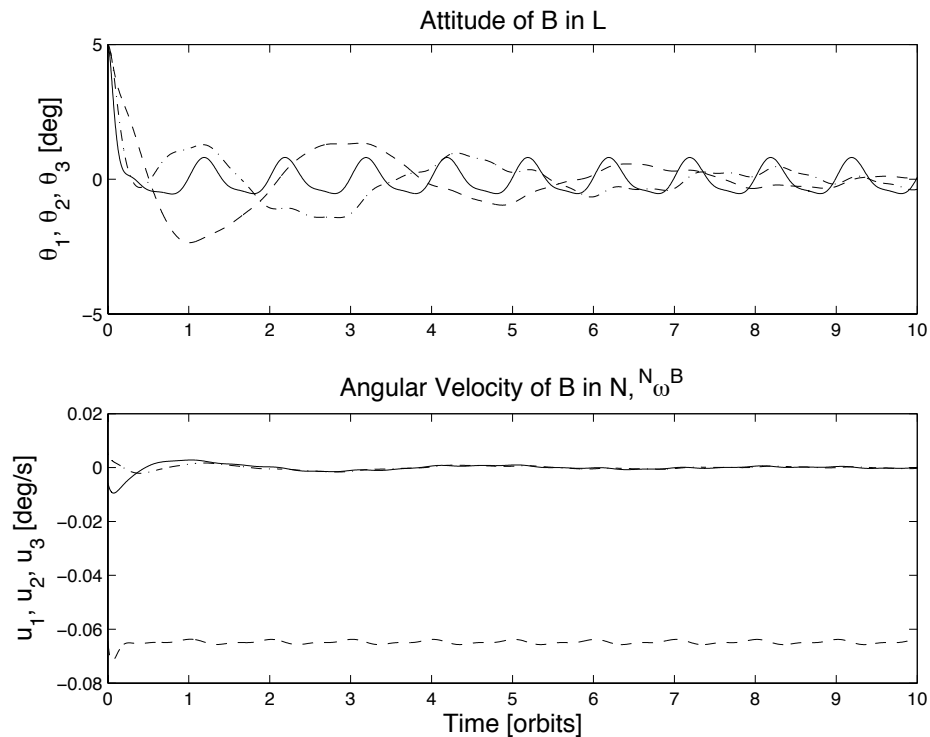


Figure 4.26: Attitude, Angular Velocity

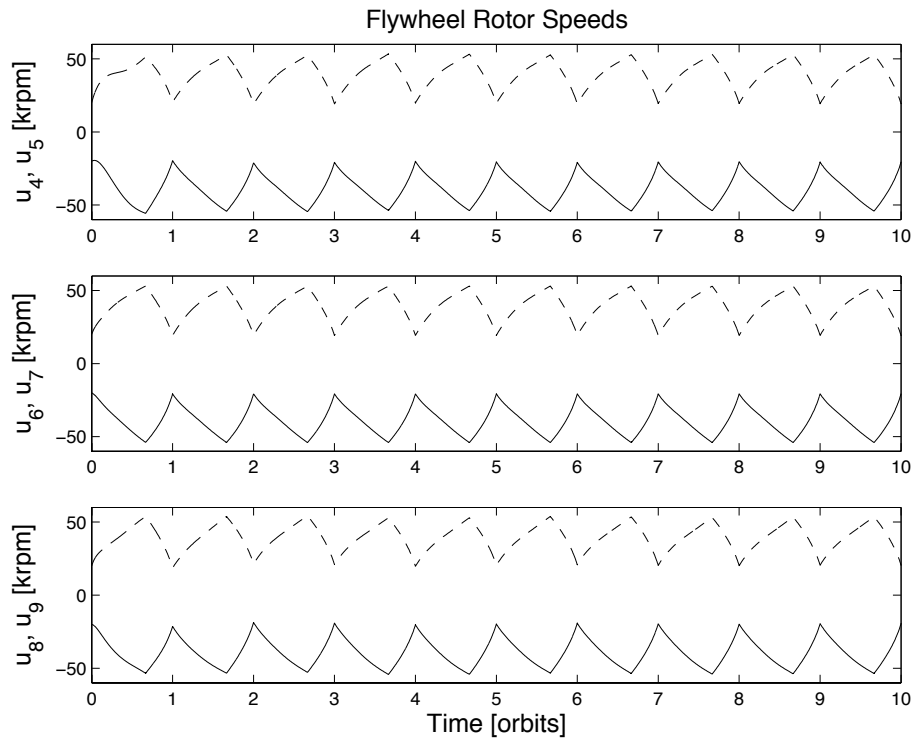


Figure 4.27: Flywheel Angular Speeds

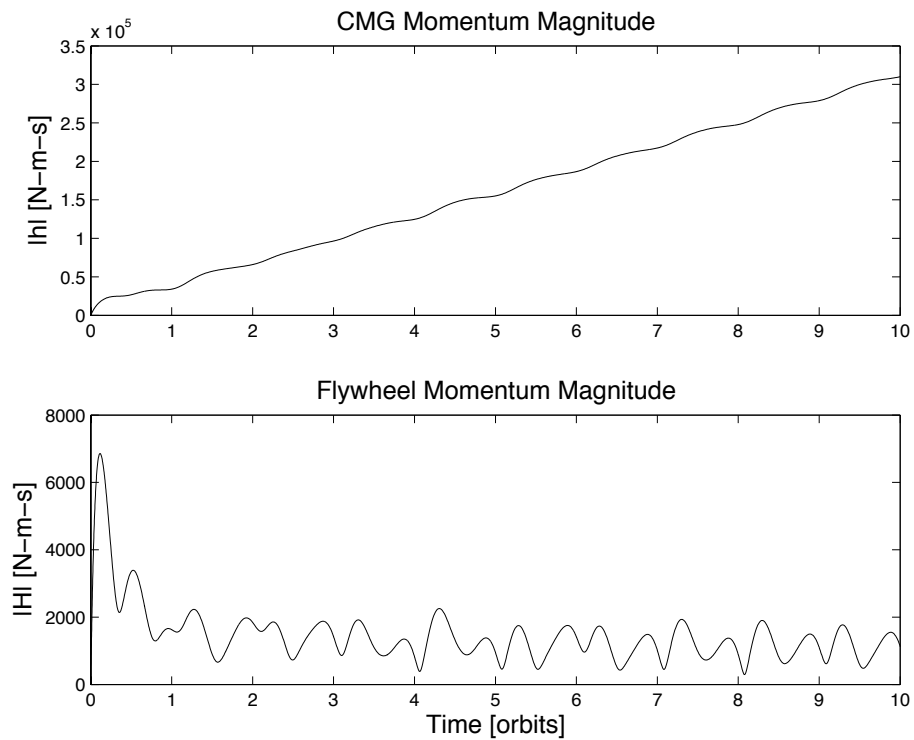


Figure 4.28: Resultant Momentum Magnitude

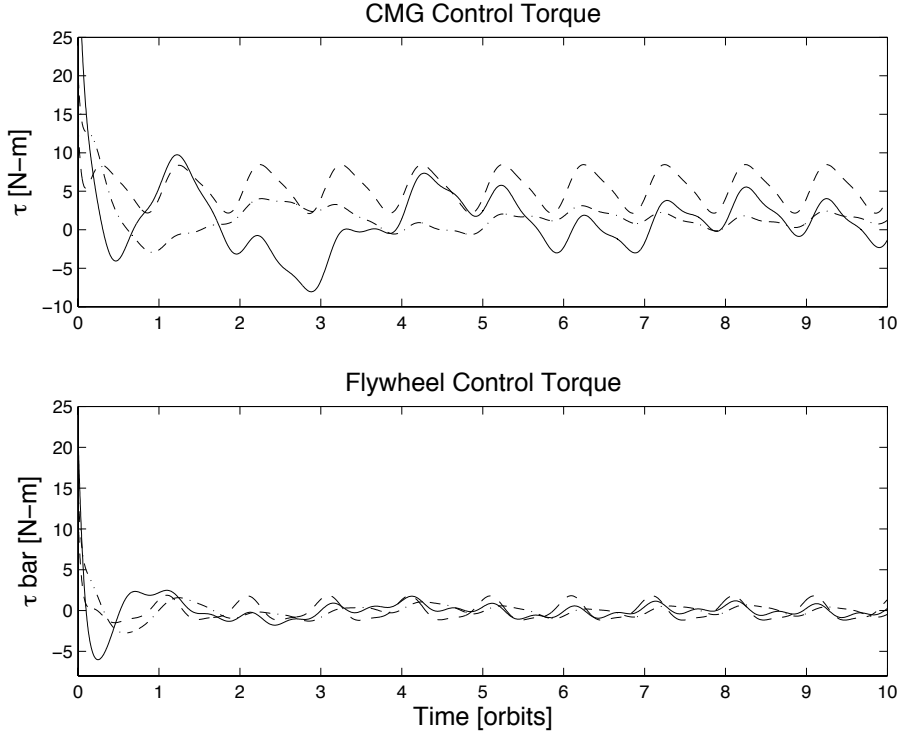


Figure 4.29: Control Torques

### 4.6.3 Attitude Hold with Thrusters

As shown in Secs. 4.6.1 and 4.6.2, holding a specified attitude other than the torque equilibrium attitude results in saturation of the momentum exchange devices. At that point some other means of controlling the attitude of the spacecraft is required; reaction control system (RCS) thrusters are typically used to provide the necessary attitude control torques.

Attitude control thrusters are naturally discrete actuators, typically with a constant thrust magnitude and direction, and a variable thrust duration. The control laws developed for the CMGs and flywheels are continuous, therefore certain modifications must be made if thrusters are to be used. This implementation may be accomplished by specifying a thruster cycle time and holding the attitude control torque constant over this interval. The control system then determines the thruster on-time required to impart the same change in angular momentum to the spacecraft as the continuous control law demands. This objective may be accomplished optimally by choosing the thrusters in order to minimize the expenditure of propellant. As the thrusters operate with a certain minimum duration, and a maximum duration given by the cycle time, the discrete thruster torque may not always match the required continuous torque, typically for extremely small or extremely large torque commands.

A minimum-fuel jet selection algorithm of this nature has been implemented using the thrust levels and directions, and jet locations given in Ref. [27], with a cycle time of 1 s. Since the flywheel system is only providing the power requirements, the flywheel angular speeds will remain in counter-rotation, as shown in Chap. 3, and an angular momentum feedback term is not required in this case. Therefore, the regulated state variables for this flight mode are given by Eq. (4.16), which results in the same state feedback gain matrix obtained in Sec. 4.6.1.

Figure 4.30 shows the attitude response of this system, using the same initial conditions as the

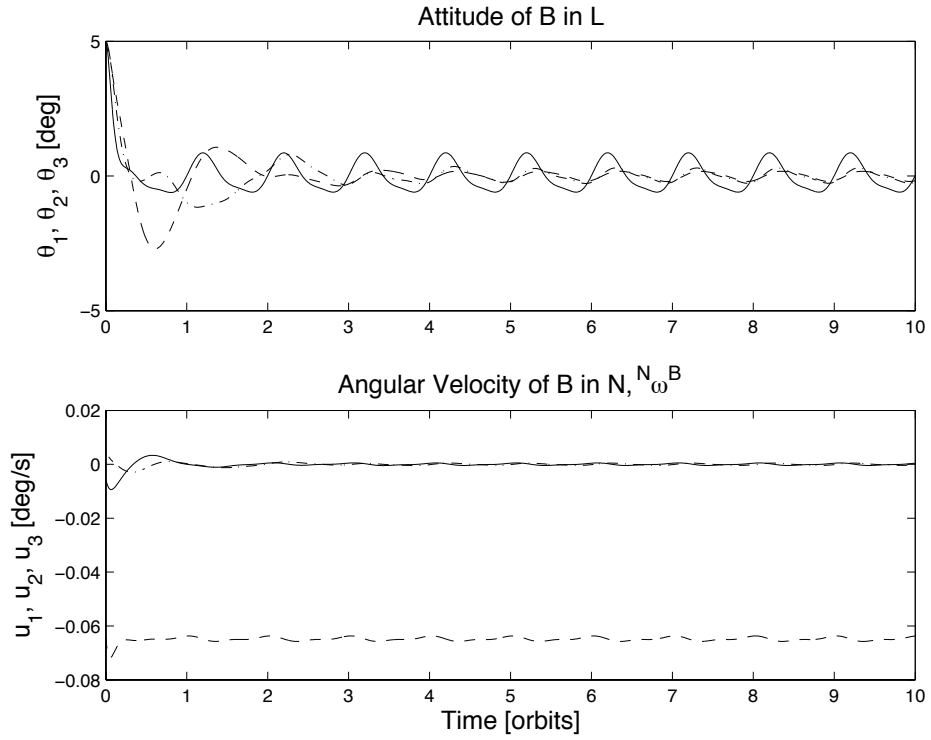


Figure 4.30: Attitude, Angular Velocity, with Thrusters

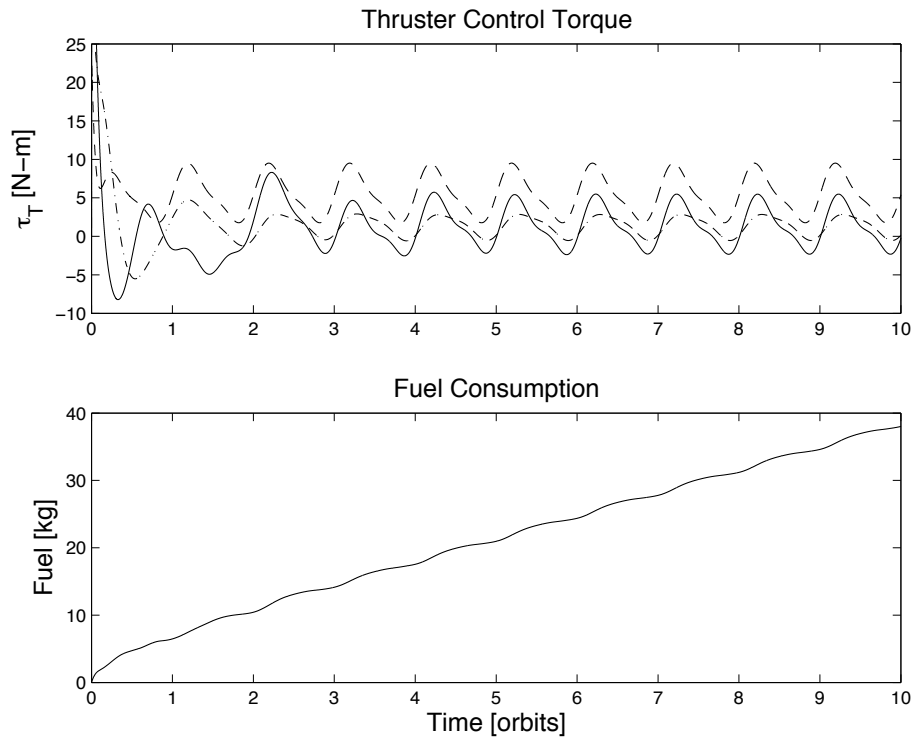


Figure 4.31: Control Torque, Fuel Consumption

previous examples, where the attitude control torques are provided by the thrusters rather than the CMGs or flywheels. The solid, dashed, and dash-dot lines represent the pitch, yaw and roll angles in the upper plot, and the generalized speeds  $u_1$ ,  $u_2$ , and  $u_3$  in the lower plot, respectively.

The applied attitude control torque,  $\tau_T$ , is shown in the upper plot of Fig. 4.31. Propellant is consumed at a rate of approximately 3.8 kg/orbit, as seen in the lower plot.

#### 4.6.4 Fuel Savings for Attitude-Hold Command

Several control laws have been developed for using CMGs, flywheels, and thrusters to control the attitude of a spacecraft while simultaneously providing the required power. Holding a specified attitude other than the torque equilibrium attitude leads to saturation of the momentum exchange devices that provide the necessary attitude control torque without the benefit of momentum feedback. RCS thrusters must then maintain the attitude until commanded to do otherwise (upon completion of a resupply docking, for example). Using the flywheels to aid the CMGs in controlling attitude may relieve some of the momentum burden which in turn will delay the saturation of these devices, thus reducing the propellant costs for holding a specified attitude for a certain period of time. Here we explore and quantify the potential fuel savings to be had in this manner.

To quantify the propellant saving, the attitude of the spacecraft is held at  $\theta_1^* = \theta_2^* = \theta_3^* = 0$  for a period of one orbit, which is a typical scenario for rendezvous and docking procedures. In order to compare directly these results with material published in Ref. [28] regarding fuel costs for docking procedures, the inertia matrix of that report is used here. Specifically,

$$\left[ I^{S/S^*} \right] = 1.36 \times \begin{bmatrix} 94340560.0 & 2316853.0 & 5685949.0 \\ 2316853.0 & 79186536.0 & 992227.0 \\ 5685949.0 & 992227.0 & 147831360.0 \end{bmatrix} \text{ kg-m}^2 \quad (4.20)$$

The CMG saturation level is defined in Refs. [27] and [28] as 2,720 N-m-s (2,000 ft-lb<sub>f</sub>-s). In this simulation the attitude angles and angular velocity of  $B$  relative to  $L$  all have initial values of zero, whereas those of the flywheel angular speeds and CMG momentum are the same as in previous examples.

Figure 4.32 shows the fuel consumption resulting from application of the various control laws. The solid curve indicates the propellant expended when using the attitude-hold control law for which RCS thrusters are the sole actuators. This control method requires a propellant mass of 4.21 kg to maintain the specified attitude for one orbit, which is comparable to the value of 4.7 kg obtained with a simulation of higher fidelity as reported on p. 17 of Ref. [28] for Stage 16A.

The dashed line indicates the fuel consumption when the CMGs are used initially to provide the attitude control torques, until they saturate at 557 s, after which the RCS thrusters are used to hold the specified attitude for the remainder of the orbit. This requires 3.97 kg of propellant. Note that in this control configuration, the flywheels are only used to provide the required power and not to provide any control torques. Since the flywheels never saturate, they may be able to return the spacecraft to a TEA at the end of 1 orbit, and the CMGs can then desaturate themselves without the use of additional propellant.

The dash-dot line displays the results of using the CMGs and flywheels to provide attitude control torques, with the benefit of flywheel momentum feedback. In this configuration, the CMG saturation is delayed slightly and occurs at 636 s. At that point the RCS thrusters are required to expend propellant in order to counteract the constant disturbance torques. The flywheels, however, are prevented from saturating by the momentum feedback portion of the control law, and are therefore available to aid the RCS thrusters in counteracting the periodic portion of the

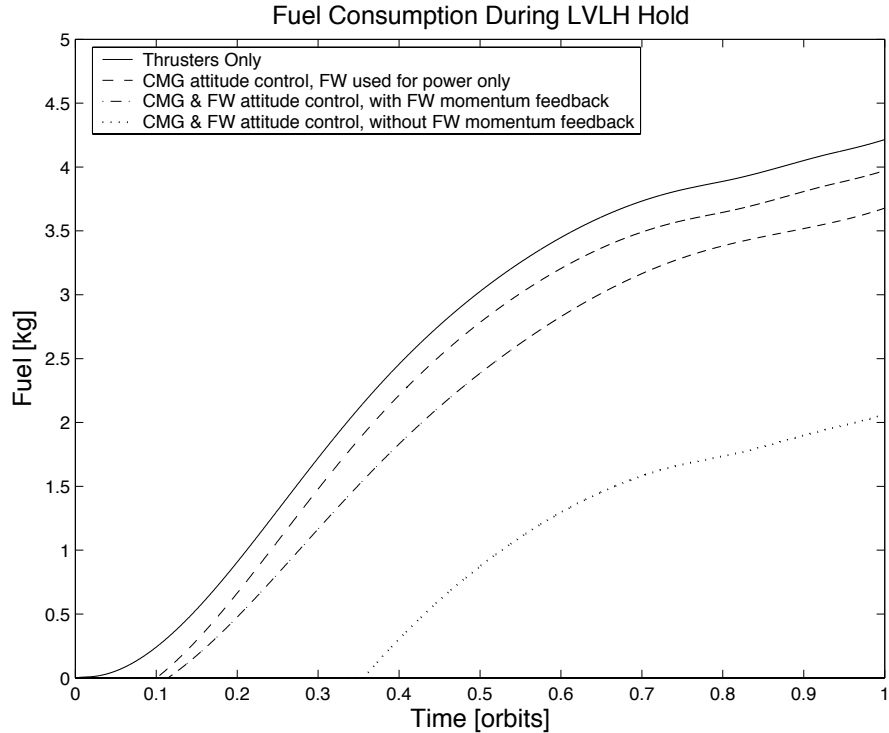


Figure 4.32: Fuel Consumption

disturbance torques, thus decreasing the propellant consumption even further. This method of maintaining the orientation of the spacecraft for one orbit results in an expenditure of 3.68 kg of fuel. The flywheels never saturate and therefore may be able to seek TEA at the end of 1 orbit, allowing the CMGs to desaturate themselves without the intervention of the RCS.

The dotted line displays the result of removing the flywheel momentum feedback, so that the flywheels are used to store momentum along with the CMGs. This control mode results in a significant delay of CMG saturation until 813 s. Subsequently, the flywheels continue to store momentum until the maximum angular speeds of 60,000 rpm are reached after 1,997 s. The RCS thrusters are then used to provide the required attitude control torques. This configuration results in a significant amount of propellant savings, requiring only 2.06 kg of fuel; however, as the flywheels become saturated they can no longer store additional energy, and the power management task cannot be performed. This is clearly not an acceptable result unless the docking task can be completed prior to the flywheel saturation, in which case the maneuver can be completed without expending propellant. Because the CMG saturation level is set to 2,720 N-m-s for this analysis, there is in fact a great deal of CMG momentum available at the end of 1 orbit; this may be enough to return the spacecraft to TEA and allow the CMGs to desaturate themselves without propellant expenditure.

The results of the simulation performed to generate the dash-dot curve in Fig. 4.32 are shown in Figs. 4.33–4.37. Figure 4.33 illustrates the time histories of the attitude angles and inertial angular velocity of the spacecraft; disturbance torques lead the spacecraft on small excursions away from the initial, desired conditions.

The flywheel angular speeds are seen in Fig. 4.34. It is clear that flywheel momentum feedback in the control law prevents rotor speed saturation and singularity in the steering law.

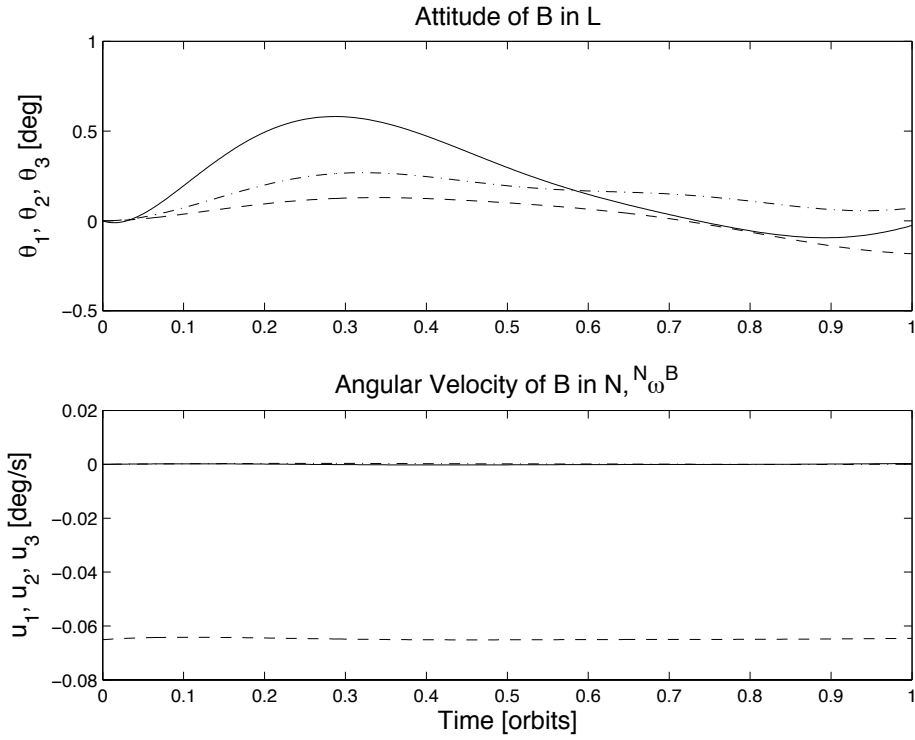


Figure 4.33: Attitude, Angular Velocity

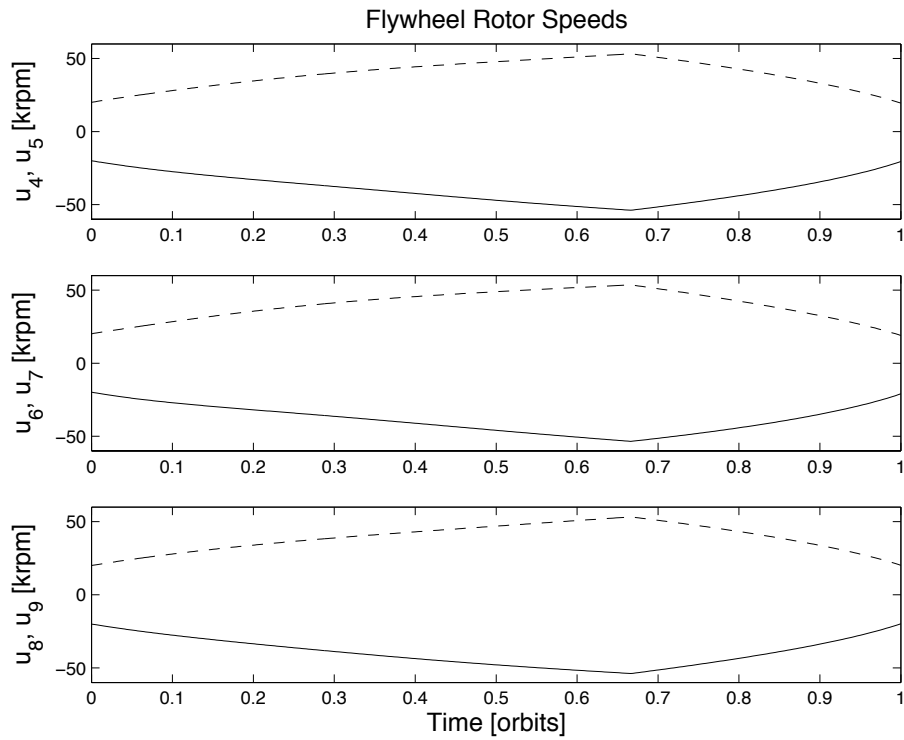


Figure 4.34: Flywheel Angular Speeds

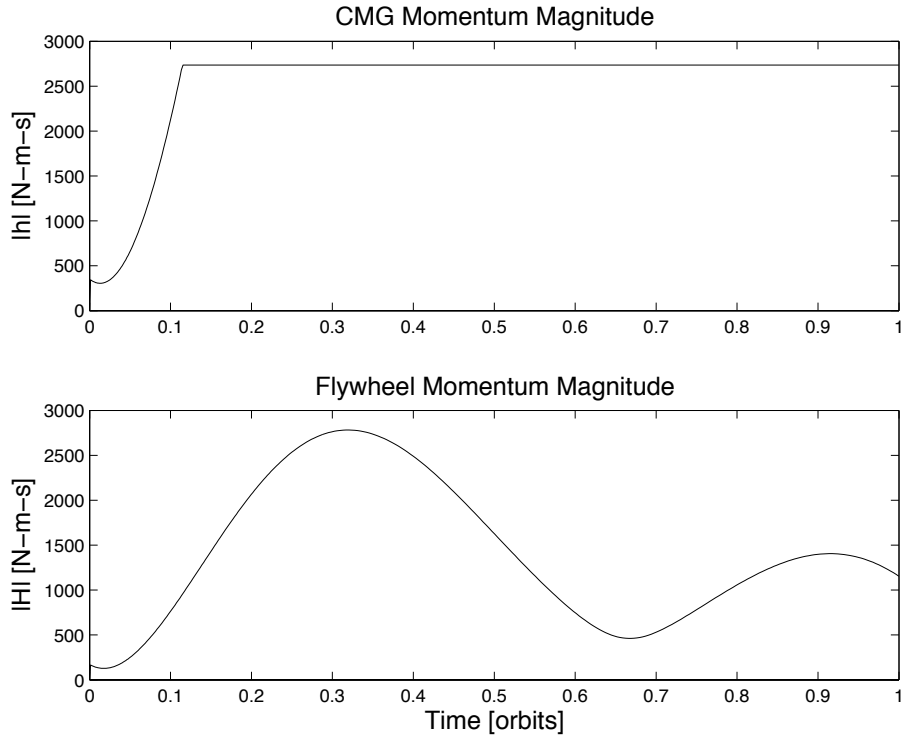


Figure 4.35: Resultant Momentum Magnitude

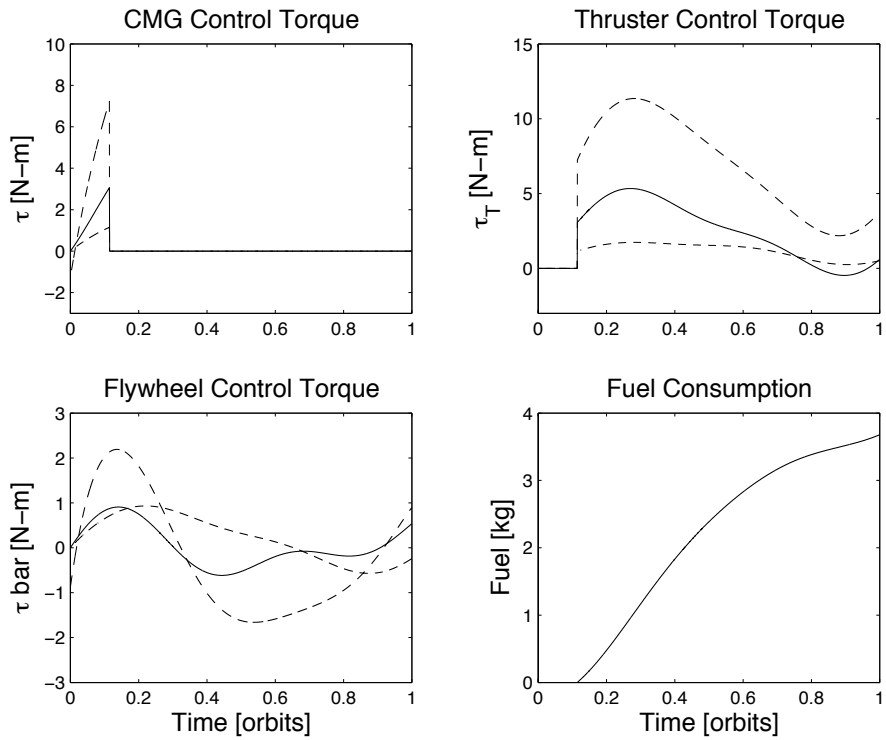


Figure 4.36: Control Torques

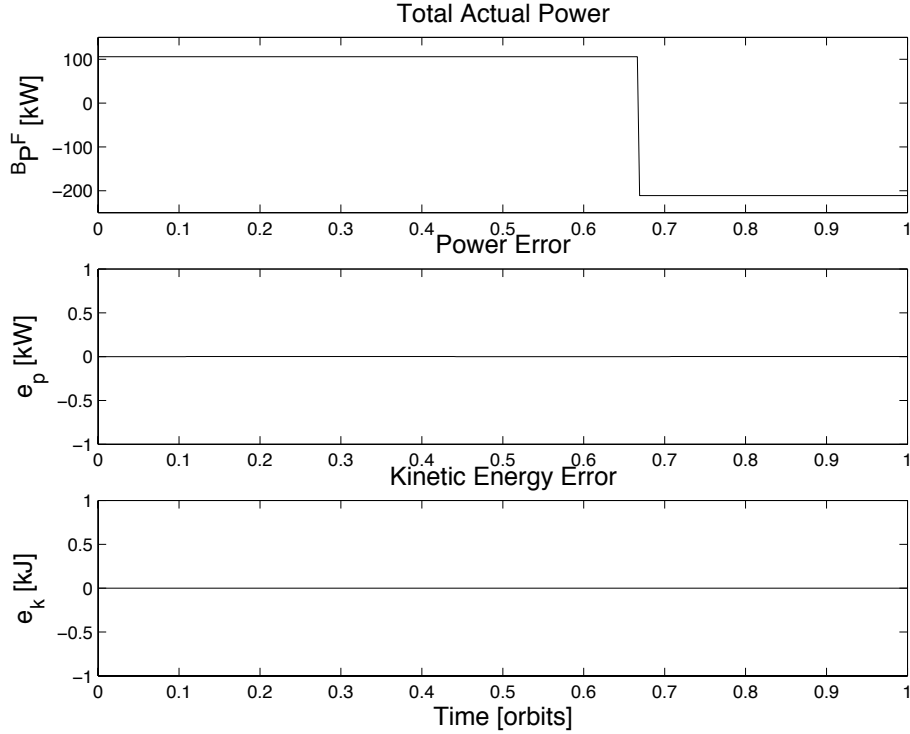


Figure 4.37: Power, Power Error, Kinetic Energy Error

The magnitude of CMG and flywheel momentum is plotted in the upper and lower curves in Fig. 4.35, respectively. This plot displays the buildup of momentum and eventual saturation of the CMGs. Following saturation, the CMGs are no longer used to generate attitude control torques, and therefore the magnitude of the momentum remains constant. The CMG attitude control torques are then provided by the RCS thrusters, aided by those torques produced with the flywheel rotors.

Figure 4.36 shows the time histories of the attitude control torques provided by the various actuators used in this simulation. The upper left plot contains the CMG control torque, which naturally goes to zero upon reaching the momentum saturation point. The RCS thrusters are then used to generate the required control torque, as shown in the upper right plot, which requires the consumption of propellant shown in the lower right plot. Flywheels are used to provide attitude control torque throughout the entire simulation; this torque is displayed in the lower left plot of Fig. 4.36. The flywheels are used also to generate the required power profile, which is tracked without error as shown in Fig. 4.37.

The foregoing results demonstrate that in one orbit approximately 0.3 kg of propellant may be saved by using the flywheels to aid the CMGs in producing attitude control torques. Over 0.5 kg of propellant may be saved by using the combined CMG, flywheel, and RCS control law instead of relying solely upon the RCS thrusters.

The simulation results shown here are for undamped flywheel rotors. Damping does inhibit the ability of the flywheels to provide the required power, as shown previously, but this effect is overcome by using the kinetic energy error feedback method. The damping does not, however, alter the fuel consumption results appreciably in the case we have studied.

## Chapter 5

# Nonlinear Controllers

The material of Chapter 4 deals with the control of attitude that is intended to be fixed, or nearly so, in a local-vertical-local-horizontal reference frame; it is therefore entirely reasonable to design and employ control laws based upon equations of motion linearized about such a condition, and expect them to perform well as long as attitude excursions remain small. The linear equations obtained previously provide a poor description of motion accompanying large-angle reorientations or slew maneuvers, hence, a nonlinear control design is required for such maneuvers. The purpose of the current chapter is to present first the design of an appropriate law, and then some results of its numerical exercise.

Development of a globally asymptotically stable algorithm for reorientation is sketched out in Sec. 5.1. The approach adopted permits the imposition of state and control constraints similar to those obtained with the LQR technique by appropriate choices of the weighting matrices  $[Q]$  and  $[R]$ . Section 5.2 contains results of a simulation in which the law directs CMGs to control attitude, while the only task of the flywheels is to furnish the required power. Consequences of allowing the CMGs to be assisted by the flywheels without and with the benefit of flywheel momentum feedback are reported in Secs. 5.3 and 5.4, respectively.

### 5.1 Global Asymptotically Stable Reorientation

The development and exercise of a controller for performing large-angle reorientation maneuvers is described in Refs. [29] and [30]. The controller is based upon feedback linearization and Lyapunov stability theory, and satisfies specified limits on slew rate and control torque.

One of the motions that can be controlled by the algorithm is a change in the orientation of a rigid body  $B$  from one attitude fixed in any reference frame  $L$ , to another, where  $L$  moves in a Newtonian reference frame  $N$ . The angular velocities of  $B$  and  $L$  in  $N$  are related by Eq. (2.91),

$${}^N\boldsymbol{\omega}^B = {}^N\boldsymbol{\omega}^L + {}^L\boldsymbol{\omega}^B \quad (5.1)$$

and the dynamical equations governing the rotational motion of  $B$  in  $N$  can be expressed as

$$\begin{aligned} \underline{\mathbf{I}}^{B/B^*} \cdot \frac{{}^B d}{{}^B dt} {}^L\boldsymbol{\omega}^B = \mathbf{u} - ({}^N\boldsymbol{\omega}^L + {}^L\boldsymbol{\omega}^B) \times \underline{\mathbf{I}}^{B/B^*} \cdot ({}^N\boldsymbol{\omega}^L + {}^L\boldsymbol{\omega}^B) \\ - \underline{\mathbf{I}}^{B/B^*} \cdot \left( \frac{{}^N d}{{}^N dt} {}^N\boldsymbol{\omega}^L - {}^L\boldsymbol{\omega}^B \times {}^N\boldsymbol{\omega}^L \right) \end{aligned} \quad (5.2)$$

where  $\underline{\mathbf{I}}^{B/B^*}$  denotes the central inertia dyadic of  $B$ . The vector  $\mathbf{u}$  represents the moment about  $B^*$ , the mass center of  $B$ , of forces applied to  $B$  with the intent of controlling its rotational motion;

$\mathbf{u}$  is referred to simply as the control torque. With some manipulation, this relationship can be deduced from Eqs. (2.28) after setting  $\rho = 0$  and letting  $\mathbf{u}$  play the part of  $\mathbf{M}$ , or one may refer to Eqs. (44) in Ref. [30]. It is worth noting that, unlike Eqs. (2.112)–(2.114) used to design the linear control laws, this relationship does not account for the presence of gravitational moment.

During a large-angle reorientation it becomes possible for the second angle of an Euler angle sequence to take on a value of  $\pm\pi/2$ , leading to singular relationships between the time derivatives of the angles and angular velocity measure numbers, as can be seen in Appendix II of Ref. [16]. No such singularities occur in kinematical differential equations for quaternion elements, hence it is preferable to use them as kinematic variables instead of Euler angles, even though the later serve adequately for the linear controllers discussed in Chap. 4.

Euler's theorem on rotation states that every change in relative orientation of two bodies or reference frames  $L$  and  $B$  can be produced by means of a simple rotation of  $B$  in  $L$ . Quaternion elements  $q_1, q_2, q_3,$  and  $q_4$  are defined in terms of a unit vector  $\boldsymbol{\lambda}$  fixed in  $L$  and  $B$  throughout a simple rotation having an angular displacement of  $\theta$ . Referring to Eqs. (1.3.1)–(1.3.3) of Ref. [16],

$$q_1 \triangleq \lambda_1 \sin \frac{\theta}{2}, \quad q_2 \triangleq \lambda_2 \sin \frac{\theta}{2}, \quad q_3 \triangleq \lambda_3 \sin \frac{\theta}{2}, \quad q_4 \triangleq \cos \frac{\theta}{2} \quad (5.3)$$

where  $\lambda_1, \lambda_2,$  and  $\lambda_3$  are the dot products

$$\lambda_i \triangleq \boldsymbol{\lambda} \cdot \hat{\mathbf{i}}_i = \boldsymbol{\lambda} \cdot \hat{\mathbf{b}}_i \quad (i = 1, 2, 3) \quad (5.4)$$

of  $\boldsymbol{\lambda}$  with  $\hat{\mathbf{i}}_1, \hat{\mathbf{i}}_2, \hat{\mathbf{i}}_3$  and  $\hat{\mathbf{b}}_1, \hat{\mathbf{b}}_2, \hat{\mathbf{b}}_3,$  dextral sets of orthogonal unit vectors fixed in  $L$  and  $B$  respectively, with  $\hat{\mathbf{i}}_i = \hat{\mathbf{b}}_i$  ( $i = 1, 2, 3$ ) prior to the rotation. The quaternion elements are not independent of each other, for they must obey the relationship

$$q_1^2 + q_2^2 + q_3^2 + q_4^2 = 1 \quad (5.5)$$

We have occasion in what follows to make use of the Euler vector  $\mathbf{q}$  defined as

$$\mathbf{q} \triangleq \boldsymbol{\lambda} \sin \frac{\theta}{2} \quad (5.6)$$

Kinematical differential equations for the quaternion can be expressed as in Eqs. (1.13.2) and (1.13.3) of Ref. [16],

$$\frac{{}^B d}{dt} \mathbf{q} = \frac{1}{2} (q_4 {}^L \boldsymbol{\omega}^B + \mathbf{q} \times {}^L \boldsymbol{\omega}^B) \quad (5.7)$$

$$\dot{q}_4 = -\frac{1}{2} {}^L \boldsymbol{\omega}^B \cdot \mathbf{q} \quad (5.8)$$

The control torque  $\mathbf{u}$  derived in Refs. [29] and [30] takes the form

$$\begin{aligned} \mathbf{u} = & ({}^N \boldsymbol{\omega}^L + {}^L \boldsymbol{\omega}^B) \times \underline{\mathbf{I}}^{B/B^*} \cdot ({}^N \boldsymbol{\omega}^L + {}^L \boldsymbol{\omega}^B) + \underline{\mathbf{I}}^{B/B^*} \cdot \left( \frac{{}^N d}{dt} {}^N \boldsymbol{\omega}^L - {}^L \boldsymbol{\omega}^B \times {}^N \boldsymbol{\omega}^L \right) \\ & - \underline{\mathbf{I}}^{B/B^*} \cdot [k(t)\mathbf{q} + c({}^L \boldsymbol{\omega}^B, \mathbf{q}, q_4, t) {}^L \boldsymbol{\omega}^B] \end{aligned} \quad (5.9)$$

where the terms on the first line of the right hand member are required for feedback linearization, and the second line represents feedback of the quaternion and the angular velocity of  $B$  relative to  $L$ . Thus, the dynamical equations of motion are reduced to the form

$$\frac{{}^B d}{dt} {}^L \boldsymbol{\omega}^B = -k(t)\mathbf{q} - c({}^L \boldsymbol{\omega}^B, \mathbf{q}, q_4, t) {}^L \boldsymbol{\omega}^B \quad (5.10)$$

Global asymptotic stability is guaranteed for the dynamical system described by Eqs. (5.2), (5.7), and (5.8), and subject to the control torque  $\mathbf{u}$  given by Eq. (5.9), when the scalar gain functions  $k(t)$  and  $c({}^L\boldsymbol{\omega}^B, \mathbf{q}, q_4, t)$  satisfy a set of conditions set forth in Ref. [29]. By asymptotic stability, we mean the magnitudes of  ${}^L\boldsymbol{\omega}^B$  and  $\mathbf{q}$  are always driven to zero, and the scalar  $q_4$  always approaches  $\pm 1$ . Furthermore, satisfaction of a slew rate limit  $\bar{\Omega}$

$${}^L\boldsymbol{\omega}^B \cdot {}^L\boldsymbol{\omega}^B \leq \bar{\Omega}^2 \quad t \geq 0 \quad (5.11)$$

is guaranteed when  $k$  and  $c$  meet additional conditions identified in Ref. [29]. A control constraint  $\bar{u}$

$$\mathbf{u} \cdot \mathbf{u} \leq \bar{u}^2 \quad t \geq 0 \quad (5.12)$$

is also satisfied when explicit gain functions  $k$  and  $c$  are constructed according to the specifications given in Ref. [30].

As indicated in Ref. [30], design of the control law requires the analyst to specify the parameters  $\underline{c}$ , the minimum value of the gain  $c$ , and  $\bar{k}$ , the maximum value of gain  $k$ . A heuristic method is proposed to override the slew rate limit  $\bar{\Omega}$  with a smaller value in order to ensure that the magnitude of  $\mathbf{u}$  remains less than or equal to  $\bar{u}$ . This is done in Ref. [30] with the aid of two additional parameters,  $p_2$  and  $p_3$ , where a value of 0.5 is recommended for each. A nonlinear controller is constructed with the numerical values of these parameters reported in Table 5.1.

Table 5.1: Nonlinear Controller Parameters

Parameter	Value
$\underline{c}$	$10^{-8} \text{ s}^{-1}$
$\bar{k}$	$1 \text{ s}^{-2}$
$p_2$	0.5
$p_3$	0.5

The remainder of this chapter contains simulation results obtained by exercising this control law, where the role of the generic  $L$  in the foregoing development is played by the local-vertical-local horizontal reference frame described in Sec. 2.4. In all cases the initial attitude of  $B$  in  $L$  is given by  $\theta_1(t_0) = 50^\circ$  (pitch),  $\theta_2(t_0) = 50^\circ$  (yaw), and  $\theta_3(t_0) = 50^\circ$  (roll), and the attitude specified for the conclusion of the reorientation is  $\theta_1 = \theta_2 = \theta_3 = 0^\circ$ . The initial and final values of the angular velocity  ${}^L\boldsymbol{\omega}^B$  are of course  $\mathbf{0}$ . Rotor spin speeds at the beginning are  $u_4(t_0) = u_6(t_0) = u_8(t_0) = -20,000$  rpm, and  $u_5(t_0) = u_7(t_0) = u_9(t_0) = 20,000$  rpm. Initial values of CMG momentum measure numbers are  $h_1(t_0) = h_2(t_0) = h_3(t_0) = 0$ . As before, changes in the mass distribution of the spacecraft are ignored; central principal moments of inertia are obtained from the moments and products given in Eq. 4.3, and  $\hat{\mathbf{b}}_1$ ,  $\hat{\mathbf{b}}_2$ , and  $\hat{\mathbf{b}}_3$  are taken to be parallel to central principal axes of inertia of  $S$ . The history of aerodynamic torque prescribed by Eq. 4.4 is appropriate when the attitude of this ISS configuration remains in the vicinity of TEA, but not when slew maneuvers are performed; therefore, no aerodynamic torque is applied in these simulations. As is the case in Chap. 4, gravitational moment is applied to the spacecraft in the simulation; since it is not included in Eq. (5.2), it presents an unmodeled disturbance to the controller.

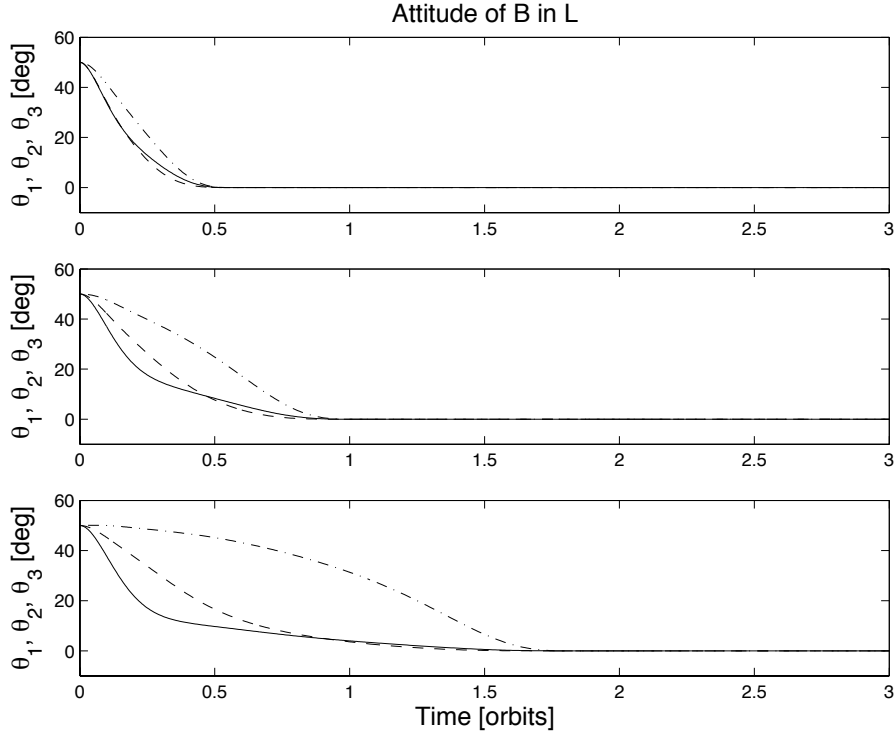


Figure 5.1: Attitude

## 5.2 Large-Angle Reorientation with CMGs

Exploration of the performance of the nonlinear controller begins with attitude control performed solely by CMGs, while the flywheels provide the required power profile. Three values of the control torque limit  $\bar{u}$  are considered: 1000 N-m, 500 N-m, and 350 N-m. A slew rate limit  $\bar{\Omega}$ , specified as 0.35 deg/s, is automatically reduced by the aforementioned heuristic method for each value of  $\bar{u}$ , yielding 0.085 deg/s, 0.052 deg/s, and 0.039 deg/s, respectively. The upper, middle, and lower plots of Figs. 5.1–5.5 contain results associated with the high, middle, and low values of  $\bar{u}$ .

A time history of the orientation of  $B$  in  $L$  appears in Fig. 5.1; the solid curve is used for  $\theta_1$  (pitch), the dashed curve for  $\theta_2$  (yaw), and the dash-dot curve for  $\theta_3$  (roll). Simulations performed with values of  $\bar{u}$  below 300 N-m give poor results (not shown), because the controller is not given the authority to perform the feedback linearization. Naturally, as the control torque limit is decreased, the time to perform the maneuver is increased.

Figure 5.2 shows the behavior of inertial angular velocity measure numbers  $u_1$ ,  $u_2$ , and  $u_3$ , presented with solid, dashed, and dash-dot curves respectively.

Time histories of the CMG control torque corresponding to the three values of  $\bar{u}$  are recorded in Fig. 5.3, where  $\tau_1$ ,  $\tau_2$ , and  $\tau_3$  [having the same meanings as in Eqs. (2.93)–(2.95)] are displayed with solid, dashed, and dash-dot curves respectively. The associated control gains  $k$  and  $c$  are shown as functions of time in Fig. 5.4. This plot shows that the gains increase with time, until the maximum value of  $k$  is reached, and then the gains are held constant. Note that a decrease in the torque limit postpones the time at which the gains reach a maximum.

the time at which the maximum gains are reached increases as the torque limit is decreased.

Figure 5.5 displays the magnitudes of CMG momentum for the three levels of the control torque constraint. In each case it can be seen that the momentum capacity of the four ISS CMGs (18,981

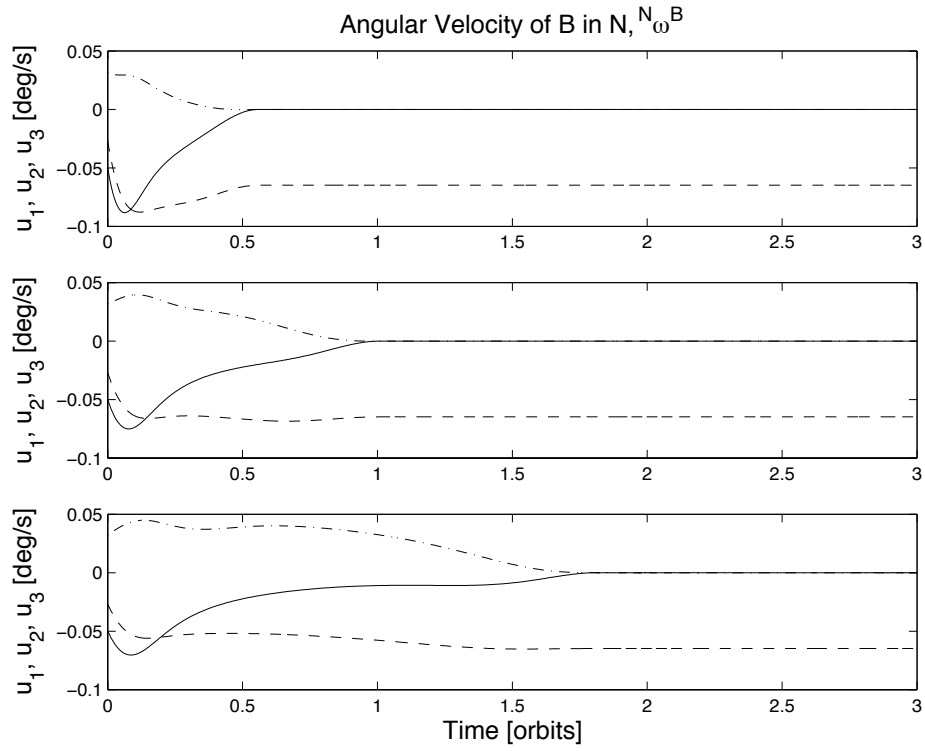


Figure 5.2: Angular Velocity

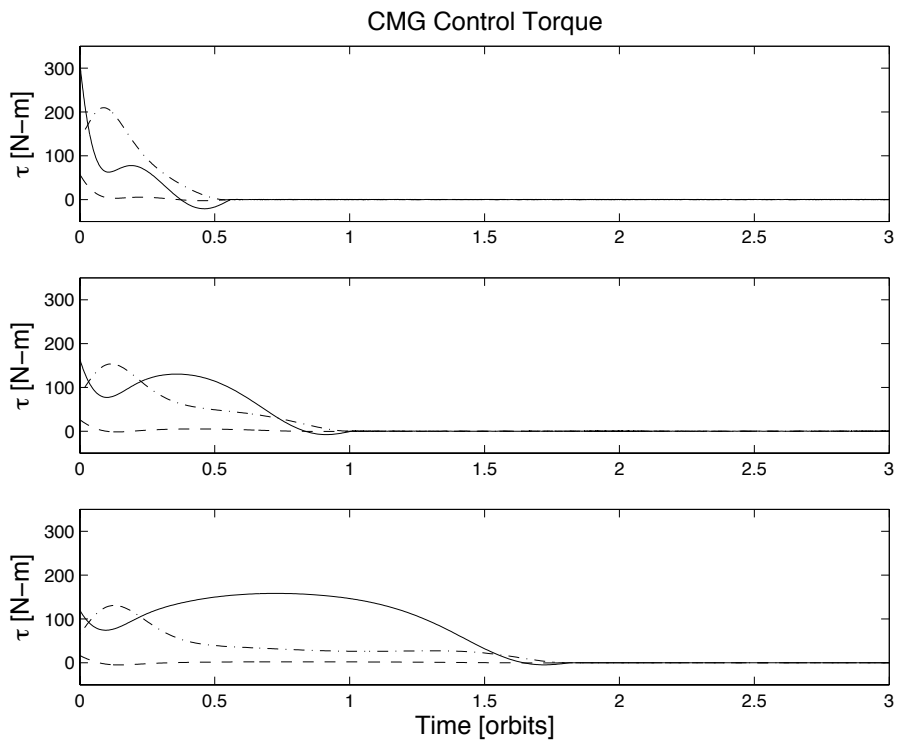


Figure 5.3: Control Torques

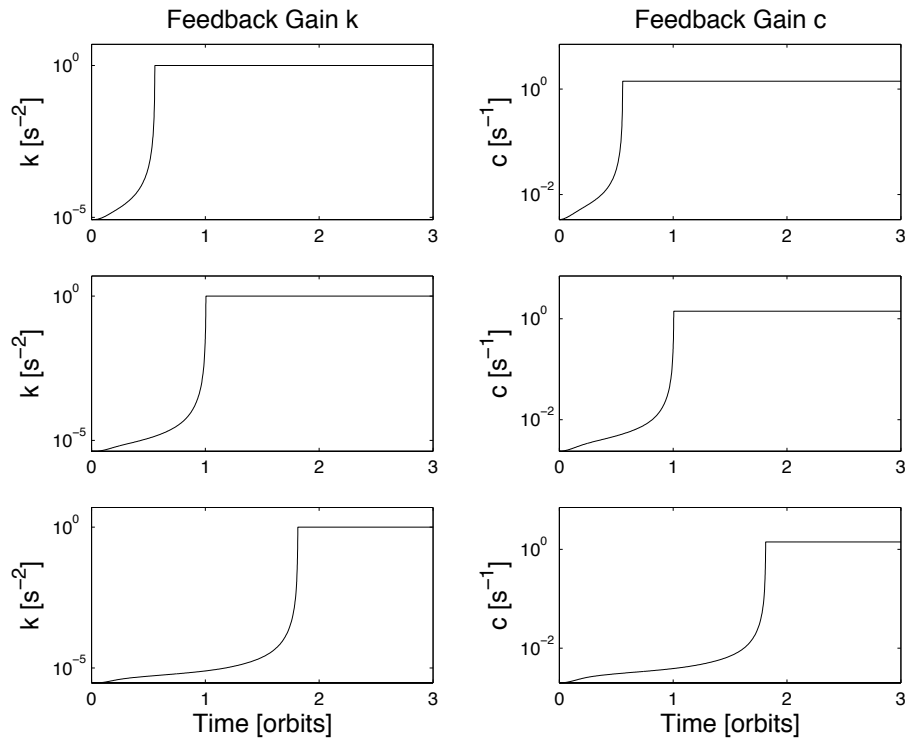


Figure 5.4: Control Gains

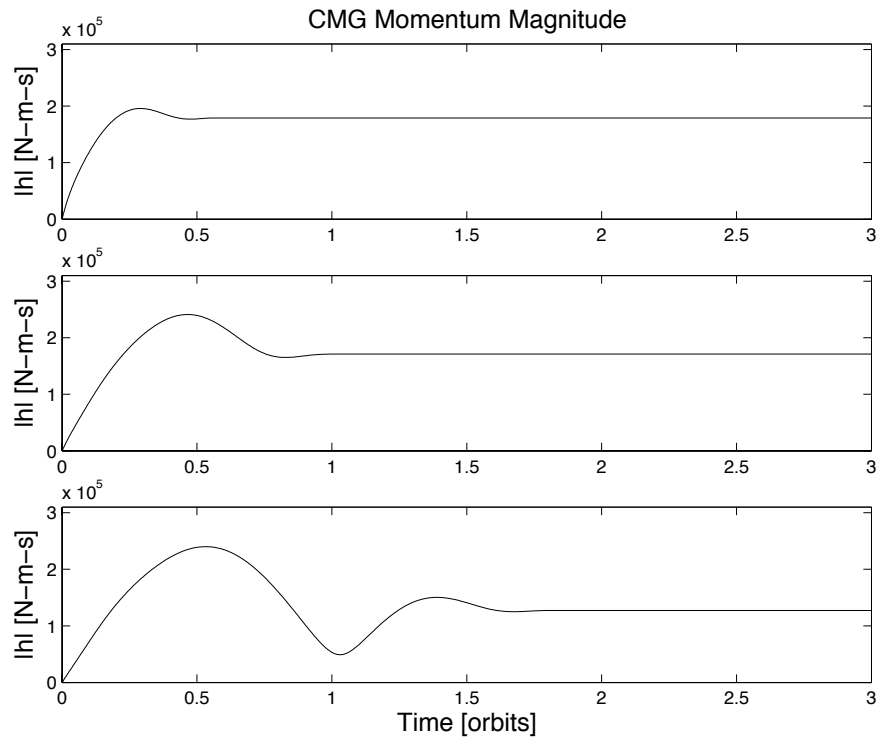


Figure 5.5: Resultant Momentum Magnitude

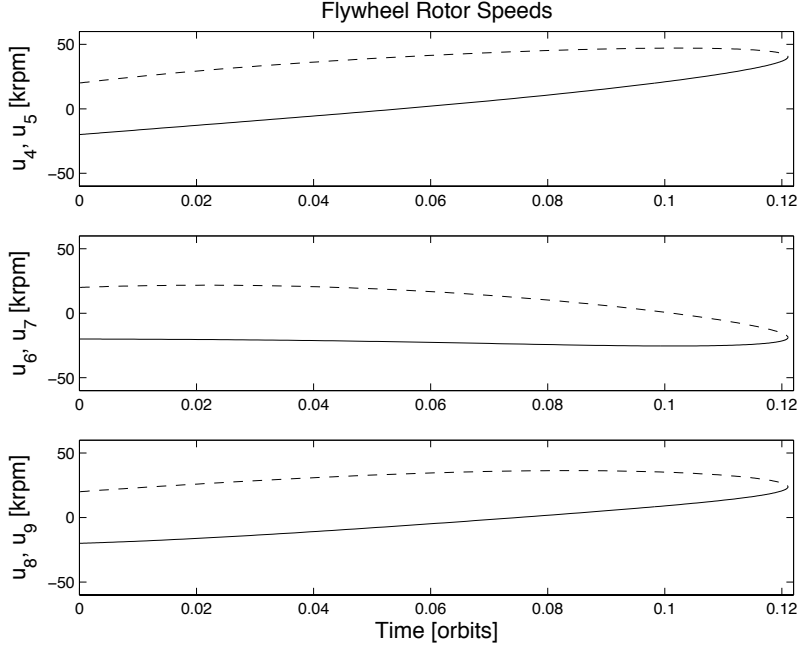


Figure 5.6: Flywheel Angular Speeds

N-m-s) is exceeded in less than one tenth of an orbit; as is well known, the CMGs are not adequate for performing large-angle reorientations or controlling the ISS at attitudes that differ significantly from a TEA.

### 5.3 Large-Angle Reorientation with CMGs and Flywheels

It stands to reason that matters can be improved, but only slightly, by allowing the flywheels and CMGs to share equally the burden of controlling attitude during a large-angle reorientation. This division of labor is accomplished by assigning half the nonlinear control torque  $\mathbf{u}$  to each type of actuator,

$$\boldsymbol{\tau} = \bar{\boldsymbol{\tau}} = \mathbf{u}/2 \quad (5.13)$$

The flywheels, of course, perform their duty of providing the required power as long as possible.

Figure 5.6 shows the flywheel angular speeds associated with this control law configuration and  $\bar{u} = 500$  N-m. After slightly more than one tenth of an orbit, the rotor speeds in each flywheel pair become identical, causing a singularity in the steering law and preventing the required power from being supplied to the spacecraft. This state of affairs results from a lack of flywheel momentum feedback, as discussed in Sec. 4.6.1.

### 5.4 Large-Angle Reorientation with CMGs, Flywheels, and Flywheel Momentum Feedback

A simple way of making up for the lacuna in feedback is to augment the control with the product of flywheel momentum and integrals of momentum, and their corresponding LQR gains, an approach

similar to that taken in Sec. 4.6.2.

$$\begin{pmatrix} \tau \cdot \hat{\mathbf{b}}_1 \\ \tau \cdot \hat{\mathbf{b}}_2 \\ \tau \cdot \hat{\mathbf{b}}_3 \\ \bar{\tau} \cdot \hat{\mathbf{b}}_1 \\ \bar{\tau} \cdot \hat{\mathbf{b}}_2 \\ \bar{\tau} \cdot \hat{\mathbf{b}}_3 \end{pmatrix} = \frac{1}{2} \begin{pmatrix} \mathbf{u} \cdot \hat{\mathbf{b}}_1 \\ \mathbf{u} \cdot \hat{\mathbf{b}}_2 \\ \mathbf{u} \cdot \hat{\mathbf{b}}_3 \\ \mathbf{u} \cdot \hat{\mathbf{b}}_1 \\ \mathbf{u} \cdot \hat{\mathbf{b}}_2 \\ \mathbf{u} \cdot \hat{\mathbf{b}}_3 \end{pmatrix} - [K] \{x\} \quad (5.14)$$

where  $\{x\} = [H_1^*, H_2^*, H_3^*, \int H_1^* dt^*, \int H_2^* dt^*, \int H_3^* dt^*]^T$ , and  $[K]$  is the LQR state feedback gain matrix associated with  $\{x\}$ . Application of this control law, with  $\bar{u} = 500$  N-m, to the reorientation maneuver gives rise to the results shown in Figs. 5.7–5.12.

Time histories of the attitude and angular velocity of  $B$  in  $L$  are contained in Fig. 5.7, and the response is similar to what appears in the middle plots of Figs. 5.1 and 5.2.

After inspection of the flywheel angular speeds plotted in Fig. 5.8, it is apparent that the steering law singularity has been avoided. In the steady state, the rotor speeds are similar to those illustrated in Fig. 4.27.

The magnitudes of CMG and flywheel angular momenta are shown in Fig. 5.9. It is clear that the CMGs store the bulk of the momentum required to change the spacecraft's orientation; unfortunately, the ISS CMGs would saturate less than one tenth of an orbit after the maneuver begins. After an initial period of transient behavior, flywheel momentum is kept near zero.

Figures 5.10–5.11 show the control torques and nonlinear feedback gains, respectively. The CMG and flywheel control torques begin with the same initial values; however, their time histories are significantly different because the flywheel control torques are used to manage the flywheel angular momentum as well as assist the CMGs in providing the attitude control torques for the large-angle reorientation. The flywheels provide the required power profile, as demonstrated in Fig. 5.12.

Augmenting the nonlinear control law as described in Eq. (5.14), and using the LQR gains obtained in Sec. 4.6.2, constitutes an ad-hoc approach at best; nevertheless, good performance is exhibited when conducting large-scale reorientations in  $L$ . The large amount of angular momentum required for such maneuvers, together with a capacity of current ISS CMGs that is limited even when supplemented with a significant flywheel energy storage system, dictates the use of RCS thrusters rather than momentum exchange devices.

Stability properties of the augmented controller, formed by adding momentum feedback to the feedback linearization, have not been studied to date; this is a subject for future research.

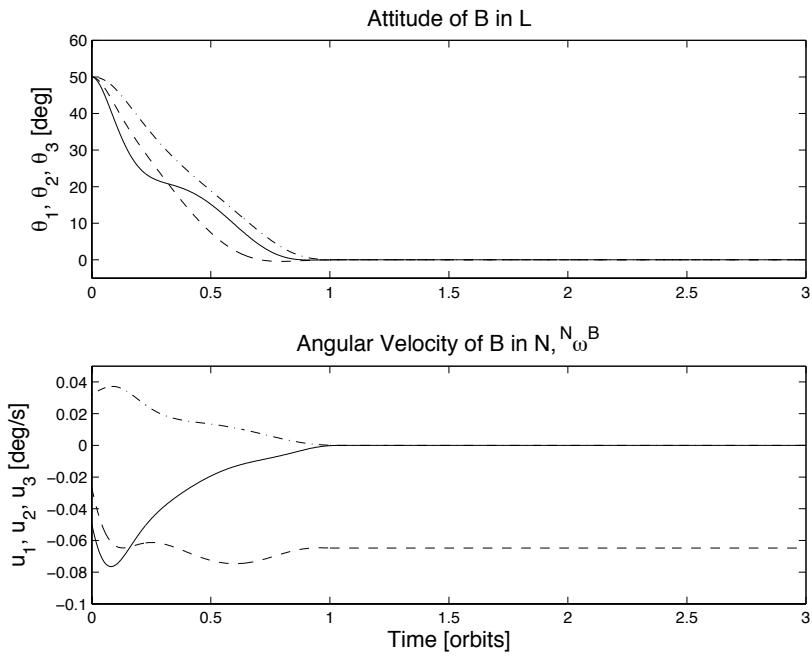


Figure 5.7: Attitude, Angular Velocity

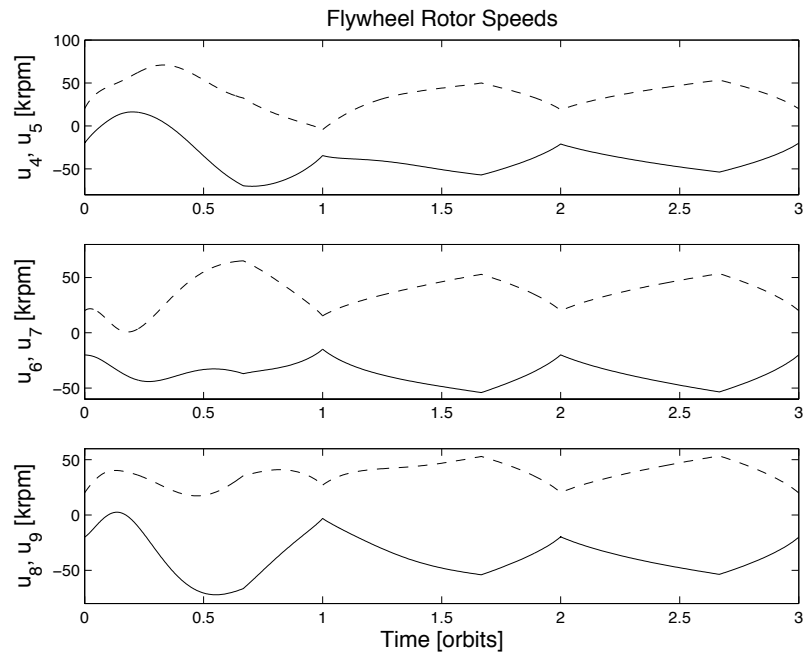


Figure 5.8: Flywheel Angular Speeds

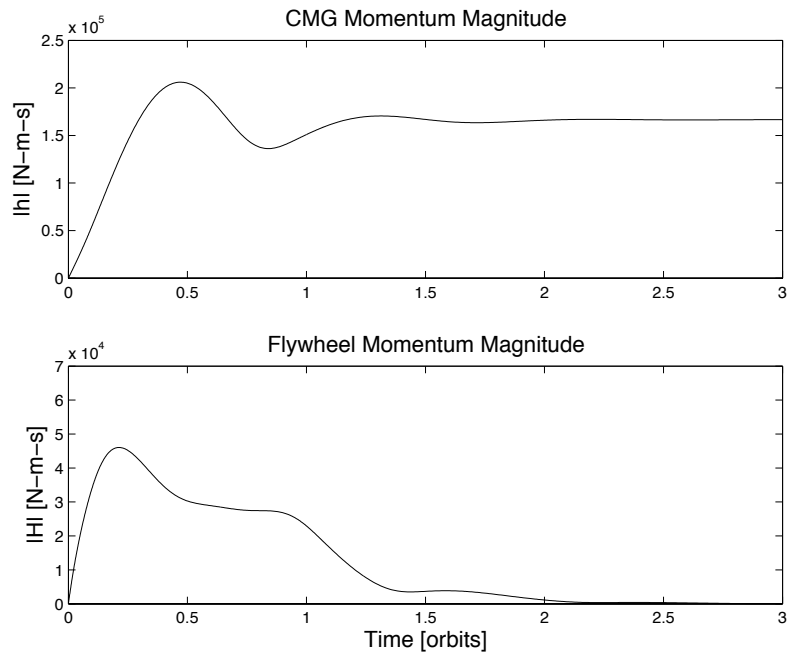


Figure 5.9: Resultant Momentum Magnitude

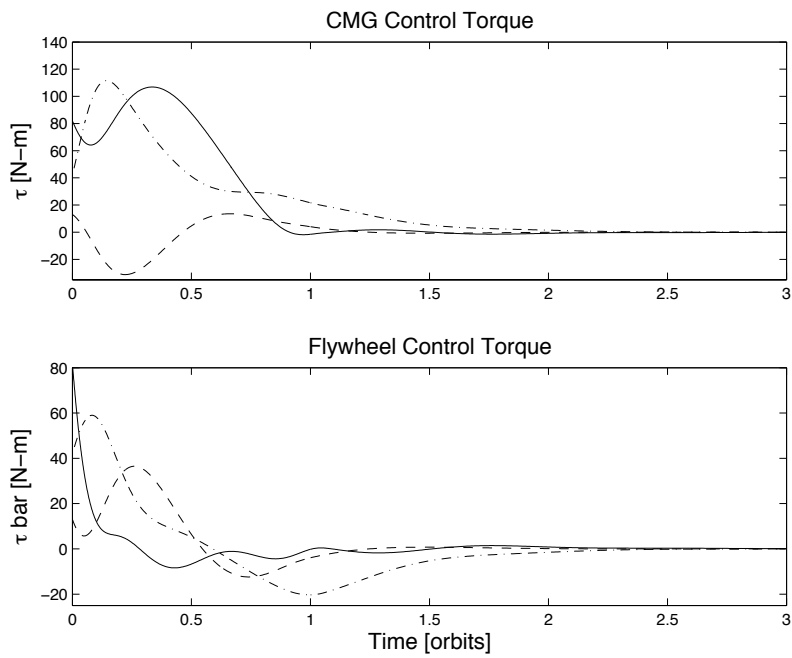


Figure 5.10: Control Torques

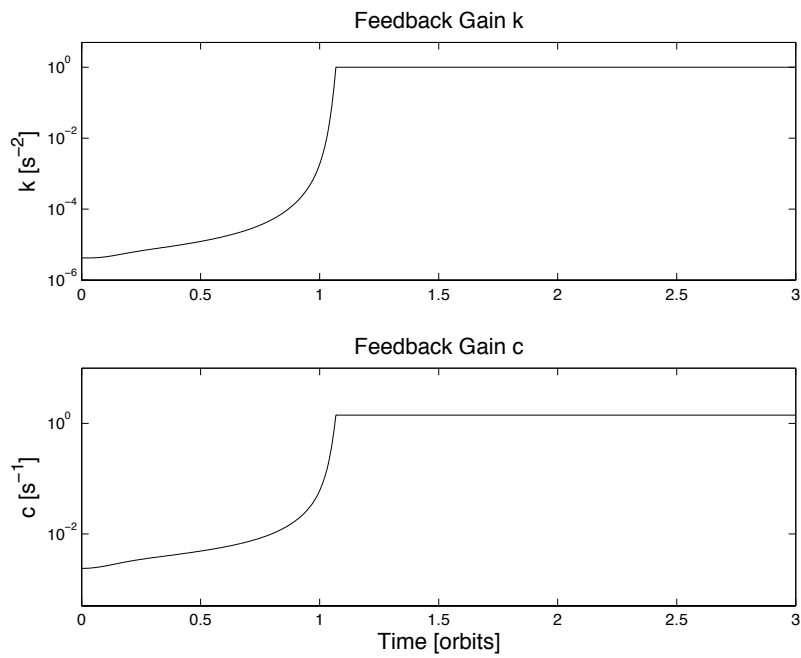


Figure 5.11: Control Gains

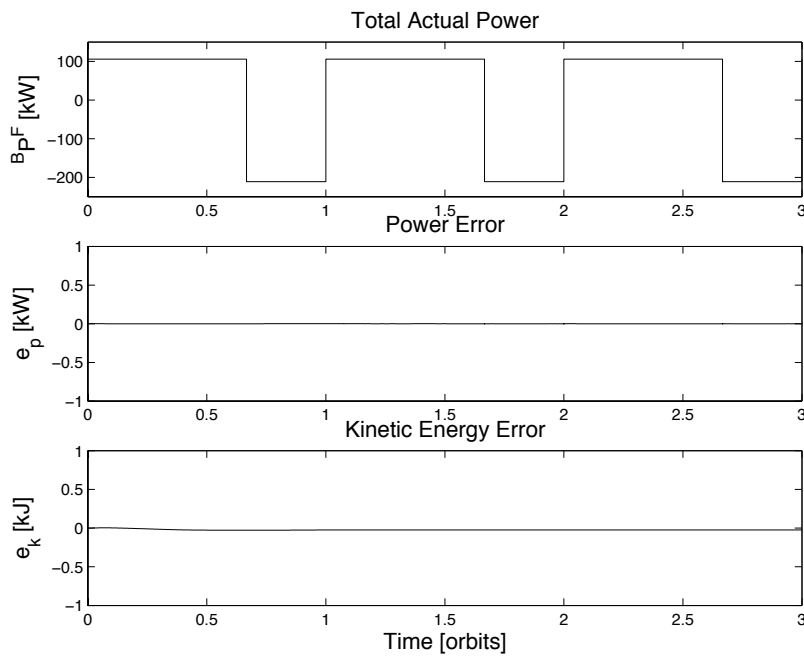


Figure 5.12: Power, Power Error, and Kinetic Energy Error

## Chapter 6

# Summary of Results

The purpose of this research is to obtain algorithms for simultaneous control of the orientation of an Earth-pointing spacecraft, the energy stored by counter-rotating flywheels, and the angular momentum of the flywheels and control moment gyroscopes (CMGs) used together as an integrated set of actuators for attitude control. Three important classes of motion relative to a local-vertical-local-horizontal reference frame  $L$  are examined. The first involves maintaining a torque equilibrium attitude (TEA), in which angular momentum of the actuators remains small and cyclic. In the second, attitude is held fixed, resulting in secular growth in angular momentum and eventual saturation of the momentum exchange devices. The third consists of a large-angle reorientation from one attitude, fixed in  $L$ , to another.

In order to construct control laws and evaluate their performance with numerical simulations, dynamical equations of motion for a multibody spacecraft containing flywheels and CMGs are derived using Kane's method, and expressed in vector-dyadic form. Each device is modeled as a rigid axisymmetric rotor; the spin axis of a flywheel is regarded as fixed in the spacecraft, whereas the spin axis of a CMG is not. The equations are nonlinear, and completely general with regard to the number and orientation of flywheel rotors, and the number of CMG rotors and gimbals. A set of twelve scalar equations is obtained by applying the generic relationships to the special case of a complex gyrostator consisting of a base body and three pairs of flywheels mounted in orthogonal directions. Existing literature contains equations for describing motion of a spacecraft with CMGs; they are shown to follow from the generic ones under two reasonable assumptions, namely that gimbal speeds are much less than the rotor spin speed, and reorientation of CMG rotors (and gimbals) does not significantly redistribute system mass. The exact equations for the complex gyrostator, and the approximate relationships associated with CMGs are combined to form approximate equations for a spacecraft with flywheels and CMGs, and subsequently linearized and nondimensionalized in preparation for design of linear control laws.

We develop two steering laws whose purpose is to determine the flywheel motor torques necessary to meet the attitude control and power management requirements simultaneously. The first of these involves formation of a pseudo-inverse to solve an underdetermined system of equations by minimizing the sum of the squares of flywheel motor torques, whereas the second divides the power requirements evenly among the three pairs of rotors, resulting in a uniquely determined solution.

Several laws are designed with the Linear Quadratic Regulator technique to control the first two types of motion described heretofore, seeking and maintaining TEA, and holding an attitude fixed. Controller performance is illustrated through numerical simulations involving the International Space Station (ISS). Energy storage is shown to be affected adversely by damping of the flywheel rotors, which must be expected under realistic conditions, but the problem is eliminated by feedback

of the error in flywheel rotational kinetic energy. A law that holds attitude without managing the angular momentum of flywheels or CMGs soon leads to undesirable flywheel rotor speeds and associated singularities in the steering laws, a situation that is rectified by the inclusion of flywheel momentum management. In order to continue holding attitude after the CMGs become saturated, we formulate a control law that uses reaction control system (RCS) thrusters and minimum-fuel jet selection logic. Thrusters, CMGs, and flywheels are used in various combinations to hold attitude for one orbit, and a significant reduction in propellant expenditure is possible when flywheels aid the CMGs.

The third type of motion is addressed by the construction of nonlinear control laws for performing large-angle reorientation maneuvers with CMGs and flywheels. An ad-hoc scheme for managing the flywheel angular momentum is proposed, similar in effect to what is obtained with linear control laws. This method performs well; however, proof of stability is a topic for further investigation. These large-angle maneuvers require a significant amount of momentum storage and as a result, RCS thrusters are required to provide the bulk of the necessary control torque.

One topic of future research that may be valuable is the study of controller performance in the face of imperfect knowledge of spacecraft inertia properties, or flywheel rotor pairs whose axial moments of inertia are not identical. Inclusion of a pre-filter would allow the control laws to estimate these parameters from attitude response, and compensate for any significant changes in the mass distribution of the spacecraft over time. Another topic with possible merit is exploration of the best way to apportion the control torque between the flywheels and CMGs; an adaptive feature for distributing the workload unequally could be preferable to the practice of sharing it equally. Future spacecraft are likely to rely solely on flywheels, rather than a mixture of flywheels and CMGs, and the control laws developed here are easily applied to this special case.

The promising results demonstrated here for control of power, momentum, and attitude of Earth-pointing spacecraft suggest that it would be worthwhile to examine the very important class of inertially oriented spacecraft.

# References

- [1] Christopher, D. A., and Beach, R., “Flywheel Technology Development Program for Aerospace Applications,” *IEEE Aerospace and Electronic Systems Magazine*, Vol. 13, Issue 6, June, 1998, pp. 9–14.
- [2] Advanced Cross-Enterprise Technology Development for NASA Missions, Research Announcement 99-OSS-05, Office of Space Science, Nov. 26, 1999.
- [3] Notti, J. E., Cormack, A., and Klein, W. J., “Integrated Power/Attitude Control System (IPACS),” AIAA Paper No. 74-921, Mechanics and Control of Flight Conference, Anaheim, CA, Aug. 5–9, 1974.
- [4] Oglevie, R. E., “Wheel Configurations for Combined Energy Storage and Attitude Control Systems,” AIAA Paper No. 85-1989, Guidance, Navigation and Control Conference, Snowmass, CO, Aug. 19–21, 1985, pp. 788–798.
- [5] Roithmayr, C. M., “International Space Station Attitude Motion Associated With Flywheel Energy Storage,” *Proceedings of the Space Technology and Applications International Forum*, Albuquerque, NM, Jan. 30–Feb. 3, 2000, pp. 454–459.
- [6] Wie, B., et al., “New Approach to Attitude/Momentum Control for the Space Station,” *Journal of Guidance Control, and Dynamics*, Vol. 12, No. 5, 1989, pp. 714–722.
- [7] Harduvel, J. T., “Continuous Momentum Management of Earth-Oriented Spacecraft,” *Journal of Guidance Control, and Dynamics*, Vol. 15, No. 6, 1992, pp. 1417–1426.
- [8] Kennel, H. F., *Steering Law for Parallel Mounted Double-Gimbaled Control Moment Gyros—Revision A*, NASA TM-82390, Jan. 1981.
- [9] Hall, C. D., “High Speed Flywheels for Integrated Energy Storage and Attitude Control,” *Proceedings of the 1997 American Control Conference*, Albuquerque, NM, June 4–6, 1997, Vol. 3, pp. 1894–1898.
- [10] Tsiotras, P., Shen, H., and Hall, C. D., “Satellite Attitude Control and Power Tracking with Energy/Momentum Wheels,” *Journal of Guidance Control, and Dynamics*, Vol. 24, No. 1, 2001, pp. 23–34.
- [11] Costic, B. T., et al., “Energy Management and Attitude Control Strategies using Flywheels,” *Proceedings of the 40th IEEE Conference on Decision and Control*, Orlando, FL, December 2001.
- [12] Fausz, J. L., and Richie, D. J., “Flywheel Simultaneous Attitude Control and Energy Storage Using a VSCMG Configuration,” *Proceedings of the 2000 IEEE International Conference on Control Applications*, Anchorage, AK, Sept. 2000, pp. 991–995.

- [13] Richie, D. J., Tsiotras, P., and Fausz, J. L., “Simultaneous Attitude Control and Energy Storage Using VSCMGs— Theory and Simulation,” *Proceedings of the 2001 American Control Conference*, Arlington, VA, June 25–27, 2001, Vol. 5, pp. 3973–3979.
- [14] Yoon, H., and Tsiotras, P., “Spacecraft Adaptive Attitude and Power Tracking with Variable Speed Control Moment Gyroscopes,” *Journal of Guidance, Control and Dynamics*, Vol. 25, No. 6, 2002, pp. 1081–1090.
- [15] Varatharajoo, R., and Fasoulas, S., “Methodology for the Development of Combined Energy and Attitude Control Systems for Satellites,” *Aerospace Science and Technology*, Vol. 6, No. 4, 2002, pp. 303–311.
- [16] Kane, T. R., Likins, P. W., and Levinson, D. A., *Spacecraft Dynamics*, McGraw-Hill, New York, 1983.
- [17] Kane, T. R., and Levinson, D. A., *Dynamics: Theory and Applications*, McGraw-Hill, New York, 1985.
- [18] Mitiguy, P. C., and Reckdahl, K. J., “Efficient Dynamical Equations for Gyrostats,” *Journal of Guidance, Control, and Dynamics*, Vol. 24, No. 6, 2001, pp. 1144–1156.
- [19] Hughes, P. C., *Spacecraft Attitude Dynamics*, John Wiley & Sons, Inc., New York, 1986.
- [20] Rheinforth, M. H., and Carroll, S. N., *Space Station Rotational Equations of Motion*, NASA Technical Paper 2511, Marshall Space Flight Center, 1985.
- [21] Dobrinskaya, J., *International Space Station Guidance, Navigation, and Control Training Manual*, TD9705, Mission Operations Directorate, Space Flight Training Division, National Aeronautics and Space Administration, Lyndon B. Johnson Space Center, Houston, Texas, December 19, 1997.
- [22] Roithmayr, C. M., *International Space Station Attitude Control and Energy Storage Experiment: Effects of Flywheel Torque*, NASA TM-1999-209100, NASA Langley Research Center, Hampton, VA, February, 1999.
- [23] Lay, D. C., *Linear Algebra and its Applications*, Addison-Wesley, Reading, MA, 1994.
- [24] Bryson, A. E., and Ho, Y-C., *Applied Optimal Control*, Hemisphere Publishing Corporation, New York, NY, 1975.
- [25] Rose, D., *International Space Station Familiarization*, TD9702A, Mission Operations Directorate, Space Flight Training Division, National Aeronautics and Space Administration, Lyndon B. Johnson Space Center, Houston, Texas, July 31, 1998.
- [26] Sunkel, J. W., and Shieh, L. S., “Optimal Momentum Controller for the Space Station,” *Journal of Guidance Control, and Dynamics*, Vol. 12, No. 4, 1990, pp. 659–668.
- [27] Guidance, Navigation and Control Design Guidelines and Assumptions, GN&C/P 97-001 Rev. B, National Aeronautics and Space Administration, Lyndon B. Johnson Space Center, Houston, Texas, March 31, 1997.
- [28] Geissler, W. H., “DAC 8 TDS 8.21.1-03 Attitude Control Analysis (Rigid Body) for Baseline Configuration,” GN&C FSED-00-020, Lockheed Martin Space Operations, Houston, Texas, March 14, 2000.

- [29] Seywald, H., et al., “Stability Analysis for Constrained Principal Axis Slew Maneuvers,” *The Journal of the Astronautical Sciences*, Vol. 47, Nos. 3/4, 1999, pp. 239–258.
- [30] Seywald, H., “Globally Asymptotically Stable Reorientation Controller with Control Constraint and Slew Rate Limit,” *The Journal of the Astronautical Sciences*, Vol. 48, No. 1, 2000, pp. 45–67.

# REPORT DOCUMENTATION PAGE

*Form Approved*  
OMB No. 0704-0188

Public reporting burden for this collection of information is estimated to average 1 hour per response, including the time for reviewing instructions, searching existing data sources, gathering and maintaining the data needed, and completing and reviewing the collection of information. Send comments regarding this burden estimate or any other aspect of this collection of information, including suggestions for reducing this burden, to Washington Headquarters Services, Directorate for Information Operations and Reports, 1215 Jefferson Davis Highway, Suite 1204, Arlington, VA 22202-4302, and to the Office of Management and Budget, Paperwork Reduction Project (0704-0188), Washington, DC 20503.

<b>1. AGENCY USE ONLY (Leave blank)</b>		<b>2. REPORT DATE</b> April 2003	<b>3. REPORT TYPE AND DATES COVERED</b> Technical Publication	
<b>4. TITLE AND SUBTITLE</b> Dynamics and Control of Attitude, Power, and Momentum for a Spacecraft Using Flywheels and Control Moment Gyroscopes			<b>5. FUNDING NUMBERS</b> 706-25-02-33	
<b>6. AUTHOR(S)</b> Carlos M. Roithmayr, Christopher D. Karlgaard, Renjith R. Kumar, Hans Seywald, and David M. Bose				
<b>7. PERFORMING ORGANIZATION NAME(S) AND ADDRESS(ES)</b> NASA Langley Research Center Hampton, VA 23681-2199			<b>8. PERFORMING ORGANIZATION REPORT NUMBER</b> L-18277	
<b>9. SPONSORING/MONITORING AGENCY NAME(S) AND ADDRESS(ES)</b> National Aeronautics and Space Administration Washington, DC 20546-0001			<b>10. SPONSORING/MONITORING AGENCY REPORT NUMBER</b> NASA/TP-2003-212178	
<b>11. SUPPLEMENTARY NOTES</b> Roithmayr: Langley Research Center, Hampton, Virginia; Karlgaard, Kumar, Seywald, and Bose: Analytical Mechanics Associates, Inc., Hampton, Virginia				
<b>12a. DISTRIBUTION/AVAILABILITY STATEMENT</b> Unclassified-Unlimited Subject Category 18                      Distribution: Standard Availability: NASA CASI (301) 621-0390			<b>12b. DISTRIBUTION CODE</b>	
<b>13. ABSTRACT (Maximum 200 words)</b> Several laws are designed for simultaneous control of the orientation of an Earth-pointing spacecraft, the energy stored by counter-rotating flywheels, and the angular momentum of the flywheels and control moment gyroscopes used together as an integrated set of actuators for attitude control. General, nonlinear equations of motion are presented in vector-dyadic form, and used to obtain approximate expressions which are then linearized in preparation for design of control laws that include feedback of flywheel kinetic energy error as a means of compensating for damping exerted by rotor bearings. Two flywheel "steering laws" are developed such that torque commanded by an attitude control law is achieved while energy is stored or discharged at the required rate. Using the International Space Station as an example, numerical simulations are performed to demonstrate control about a torque equilibrium attitude, and illustrate the benefits of kinetic energy error feedback. Control laws for attitude hold are also developed, and used to show the amount of propellant that can be saved when flywheels assist the CMGs. Nonlinear control laws for large-angle slew maneuvers perform well, but excessive momentum is required to reorient a vehicle like the International Space Station.				
<b>14. SUBJECT TERMS</b> Flywheels, Control Moment Gyroscopes, Attitude Control, Earth-pointing Spacecraft, Energy Storage, Integrated Power and Attitude Control System (IPACS), Equations of Motion, Gyrostat, Flywheel Steering Law, Linear Quadratic Regulator (LQR), Nonlinear Control Law, Attitude Slew Maneuver			<b>15. NUMBER OF PAGES</b> 87	
			<b>16. PRICE CODE</b>	
<b>17. SECURITY CLASSIFICATION OF REPORT</b> Unclassified	<b>18. SECURITY CLASSIFICATION OF THIS PAGE</b> Unclassified	<b>19. SECURITY CLASSIFICATION OF ABSTRACT</b> Unclassified	<b>20. LIMITATION OF ABSTRACT</b>	